Enhancer-AAVs allow genetic access to oligodendrocytes and diverse populations of astrocytes across species

Authors: John K. Mich[1*], Smrithi Sunil[2], Nelson Johansen[1], Refugio A. Martinez[1], Jiatai Liu[1], Bryan B. Gore[1], Joseph T. Mahoney[1], Mckaila Leytze[1], Yoav Ben-Simon[1], Darren Bertagnolli[1], Ravi Bhowmik[1], Yemeserach Bishaw[1], Krissy Brouner[1], Jazmin Campos[1], Ryan Canfield[4], Tamara Casper[1], Nicholas P. Donadio[1], Nadezhda I. Dotson[1], Tom Egdorf[1], Amanda Gary[1], Shane Gibson[4], Jeff Goldy[1], Erin L. Groce[1], Kenta M. Hagihara[2], Daniel Hirschstein[1], Han Hou[2], Will D. Laird[1], Elizabeth Liang[1], Luke V. Loftus[1], Nicholas Lusk[1], Jocelin Malone[1], Naomi X. Martin[1], Deja Monet[1], Josh S. Nagra[1], Dakota Newman[1], Nhan-Kiet Ngo[1], Paul A. Olsen[1], Victoria Omstead[1], Ximena Opitz-Araya[1], Aaron Oster[1], Christina A. Pom[1], Lydia Potekhina[1], Melissa Reding[1], Christine Rimorin[1], Augustin Ruiz[1], Adriana E. Sedeño-Cortés[5], Nadiya V. Shapovalova[1], Michael Taormina[1], Naz Taskin[1], Michael Tieu[1], Nasmil J. Valera Cuevas[1], Sharon W. Way[1], Natalie Weed[1], Vonn Wright[1], Zizhen Yao[1], Thomas Zhou[1], Delissa A. McMillen[1], Michael Kunst[1], Medea McGraw[1], Bargavi Thyagarajan[1], Jack Waters[1], Trygve E. Bakken[1], Nick Dee[1], Shenqin Yao[1], Kimberly A. Smith[1], Karel Svoboda[2], Kaspar Podgorski[2], Yoshiko Kojima[3,6], Greg D. Horwitz[4,6], Hongkui Zeng[1], Tanya L. Daigle[1], Ed S. Lein[1,7,8], Bosiljka Tasic[1], Jonathan T. Ting[1,4,6], Boaz P. Levi[1*]

Author Affiliations:
1 Allen Institute for Brain Science, Seattle WA, USA.
2 Allen Institute for Neural Dynamics, Seattle WA, USA.
3 Department of Otolaryngology Head and Neck Surgery, University of Washington, Seattle, WA, USA.
4 Department of Neurobiology and Biophysics, University of Washington, Seattle, WA, USA.
5 Division of Medical Genetics, University of Washington, Seattle, WA, USA.
6 Washington National Primate Research Center, University of Washington, Seattle, WA, USA.
7 Department of Neurological Surgery, Univ. of Washington, Seattle WA.
8 Department of Laboratory Medicine and Pathology, Univ. of Washington, Seattle WA
* Corresponding authors boazl@alleninstitute.org and johnmi@alleninstitute.org

Abstract: Proper brain function requires the assembly and function of diverse populations of neurons and glia. Single cell gene expression studies have mostly focused on characterization of neuronal cell diversity; however, recent studies have also revealed substantial diversity of glial cells, particularly astrocytes. To better understand glial cell types and their roles in neurobiology, we built a new suite of adeno-associated viral (AAV)-based genetic tools to enable genetic access to astrocytes and oligodendrocytes. These oligodendrocyte and astrocyte enhancer-AAVs are highly specific (usually > 95% cell type specificity) with variable expression levels, and the astrocyte enhancer-AAVs show multiple distinct expression patterns reflecting the spatial distribution of astrocyte cell types. To provide the best glial-specific functional tools, several enhancer-AAVs were: optimized for higher expression levels, shown to be functional and specific in rat and macaque, shown to maintain specific activity across transgenes and in epilepsy where traditional promoters changed activity, and used to drive functional transgenes in astrocytes including Cre recombinase and acetylcholine-responsive sensor iAChSnFR. The astrocyte-specific iAChSnFR revealed a clear reward-dependent acetylcholine response in astrocytes of the nucleus accumbens during reinforcement learning. Together, this collection of glial enhancer-AAVs will enable characterization of astrocyte and oligodendrocyte populations and their roles across species, disease states, and behavioral epochs.

Introduction

Glial cell types play critical roles in CNS development, function, and homeostasis[1,2]. Astrocytes provide trophic support for neurons[3,4], coordinate regional wiring patterns[5], respond to and regulate neurotransmission[6,7], and drive repair or pathology after traumatic injury[8–10]. Oligodendrocytes form myelin sheaths[11], strengthen circuits[12], secrete critical neurotrophic factors[13], and contribute to pathologic disease progression[14,15]. Transcriptomic characterization of glial cells has revealed an array of astrocyte and oligodendrocyte cell types, often with pronounced regional signatures[16–18]. Furthermore, species-specific features have been described[19], although the functional significance of these differences is unknown. Glial cell types have also been shown to play critical roles in CNS diseases ranging from epilepsy[20] to neurodegenerative diseases[21] to cancer[22,23]. To understand how glia differ between cell types, regions, species, and disease states, a set of tools is needed to grant targeted genetic access to these specific populations across species.

Adeno-associated virus (AAV) vectors are exceptionally useful tools for somatic transgenesis across mammalian species including human[24–29]. Short enhancer or promoter regulatory elements work effectively in AAV expression cassettes to drive cell-type selective gene expression in the brain or other organs. Recent work has shown that selective AAVs can be rationally designed by using enhancers identified from epigenetic datasets that are selectively active and fit in an AAV vector[30–40]. Enhancer-AAVs were recently developed to target different populations of excitatory and inhibitory neurons in the brain, and some enhancers have shown successful targeting of glial cell populations as well[35,41–43]. However, the field largely relies on glial promoters that have some undesirable characteristics, most notably loss of specificity or change in strength in different contexts as seen for astrocytic *GFAP* promoter fragments[44–46]. Furthermore, single cell genomics studies have revealed region-specific astrocyte cell types for which no current tools are available[16–18].

Here we present characterization of a collection of enhancer-AAVs that selectively target astrocytes and oligodendrocytes. Twenty-five astrocyte and 21 oligodendrocyte enhancer AAVs were identified from mouse and human neocortical epigenetic data that produced reporter expression that was highly specific for the intended populations, often labeling more than half of the intended cells in the area, and with a wide range of expression strengths. Multiple astrocyte-targeting vectors exhibited distinct CNS region-specific expression patterns, whereas oligodendrocyte-selective vectors generally drove expression throughout the entire CNS. Several enhancer-AAVs maintained selective expression for astrocytes or oligodendrocytes across rat and macaque, across epileptic disease status, and even for difficult transgenes. Lastly, several astrocyte tools were adapted to drive expression of functional transgenes like Cre or the detection of neurotransmitters to reveal the role of astrocytes in neurobiology. We used astrocyte-selective AAV expressing iAChSnFR[47] to measure the dynamics of acetylcholine in astrocytes of the nucleus accumbens during reinforcement learning. This collection of tools opens up new opportunities for selective labeling and functional interrogation of glial cell types across species and disease states, and could have translational applications via AAV-based therapeutics[48–50].

Results

Generation of astrocyte- and oligodendrocyte-specific enhancer-AAVs. We identified putative enhancers specific for astrocytes and oligodendrocytes from single cell/single nucleus assay for transposase-accessible chromatin (sc/snATAC-seq[33,34]) and single nucleus methyl-cytosine sequencing (snmC-seq) studies from neocortex[51–54]. Thousands of astrocyte- and oligodendrocyte-selective scATAC-seq peaks were identified previously in both human middle temporal gyrus (MTG) and mouse primary visual cortex (VISp), averaging approximately 300-600 bp in size (**Figure 1A**). Additional ATAC-seq datasets confirmed these peaks[55,56]. Generally, astrocyte and oligodendrocyte candidate enhancers were accessible in non-neuronal cells but not in neuronal cells across the human forebrain[33,55] (**Figure 1—figure supplement 1A-F**), and in the corresponding astrocyte or oligodendrocyte subclasses across the mouse forebrain without strong cell type preferences[56] (**Figure 1—figure supplement 1G-L**).

We used three strategies to identify putative enhancers for testing: “high specificity”, “high strength”, and “marker gene” (**Figure 1B-E**). The “high specificity” nomination criteria (gold square or star icons) required enhancers and their orthologs to show accessibility specifically for both mouse and human astrocytes or oligodendrocytes but not other cell types[33,34]. In addition, we required that these putative enhancers not be detected in demethylated genomic regions in both mouse and human neuron populations[52]. Some “high specificity” enhancers also showed specific demethylation in bulk human and mouse glial cells[51] (marked by gold star icons). “High strength” putative enhancers were selected on the basis of strong astrocyte-specific peaks using only mouse scATAC-seq data[34], with strength measured by accessibility read count within peaks. Finally, “marker gene” putative enhancers showed specific and strong accessibility near known astrocyte- and oligodendrocyte-specific marker genes.

We tested putative enhancer function in AAV vectors upstream of a minimal promoter driving the reporter SYFP2 and evaluated expression throughout the mouse brain after systemic administration of PHP.eB-serotyped AAVs. Enhancer-AAVs that showed anticipated reporter expression, were further evaluated for specificity, completeness of expression, and cross-species activity (**Figure 1C** and **Table S1**). All three strategies were effective, with approximately half of the candidates for both cell types yielding astrocyte or oligodendrocyte-specific expression patterns during primary screening (**Figure 1D**, **E**), which were confirmed on-target by immunohistochemistry (IHC) and/or scRNA-seq (see figures below). Some of these vectors were also characterized in parallel large-scale efforts[35], all raw data from which are available online at https://portal.brain-map.org/genetic-tools/genetic-tools-atlas, and the full set of experimental mice described below are summarized in **Table S2**.

A collection of astrocyte-specific enhancer-AAVs. We screened 50 candidate astrocyte-specific enhancer-AAVs, and 25 (50%) of them labeled astrocytes specifically with SYFP2 expression (**Figure 2—figure supplement 1**). Astrocyte-specific enhancer-AAVs showed a range of expression strengths and patterns (**Figure 2A-O**) and vectors were categorized based on their labeling as: “Most of the CNS”, “Regional”, “Scattered”, “Weak” and “Mixed specificities”. “Most of the CNS” astrocyte enhancer-AAVs, including AiE0380h and the human *GFAP* promoter (GfaABC1D[57]), labeled cells with astrocyte morphology in both brain and spinal cord (SpC, **Figure 2A-B**, **G-H**). Other examples in this category include AiE0387m, AiE0390h, AiE0390m, and the synthetic element ProB12[41] (**Figure 2—figure**

125 **supplement 1**). “Regional” astrocyte enhancer-AAVs showed regionally restricted expression, such as
126 AiE0385m that labeled astrocytes primarily in the telencephalon (**Figure 2C**, **F, Figure 2—figure**
127 **supplement 1**). Other "Regional” enhancer-AAVs labeled astrocytes in subcortical domains but not in
128 the telencephalon, such as AiE0381h and AiE2160m (**Figure 2—figure supplement 1**); while
129 AiE0375m only labeled Bergmann glia, specialized astrocytes in the cerebellar cortex (CBX, **Figure 2—**
130 **figure supplement 1**). Interestingly, enhancers AiE2120m and AiE2160m labeled astrocytes in nearly
131 mutually exclusive regions (**Figure 2—figure supplement 2**). “Scattered” enhancer-AAVs labeled
132 astrocytes strongly but sparsely in most brain regions. These enhancer-AAVs include AiE0374m and its
133 ortholog AiE0374h (**Figure 2—figure supplement 1**). Enhancer-AAVs labeled as “Weak” gave
134 astrocyte-specific patterns with low expression of SYFP (e.g., AiE0373m and AiE0386m, **Figure 2—**
135 **figure supplement 1**). Last, we designated several enhancer-AAVs as “Mixed specificities” because
136 they labeled astrocytes and neurons. For example, AiE2118m labels many astrocytes strongly and
137 specifically within the telencephalon, but also labels neurons strongly in non-telencephalic structures
138 like midbrain (MB), deep cerebellar nuclei (CBN), and globus pallidus, external segment (GPe) (**Figure**
139 **2—figure supplement 1**).

140 We quantified the specificity of many of these astrocyte-specific enhancer-AAVs using multiple
141 independent techniques. First, we characterized SYFP2-expressing cells with immunohistochemistry
142 (IHC) for Sox9, a marker of astrocytes throughout the brain[58] (**Figure 2G-O**). Many of the astrocyte-
143 specific enhancer-AAV vectors show high specificity, which we define as >80% specificity for the target
144 cell population[33]. Astrocyte-specific enhancer-AAVs are usually >95% specific, and often >99% specific
145 in VISp for Sox9-expressing astrocytes (**Figure 2P**). Second, we also observed high specificity when
146 we isolated single SYFP2+ cells by flow cytometry and profiled them by scRNA-seq (**Figure 2P**).
147 Additionally, we assessed completeness of astrocyte labeling using IHC, and we observed that vectors
148 scored as “Most of CNS” often label >50% of astrocytes in VISp, but “Weak” or “Scattered” vectors
149 labeled many fewer astrocytes (**Figure 2P**). “Regional” vectors showed differing completeness across
150 brain regions as expected (**Figure 2P**). Whole-brain serial two-photon tomography (STPT) of mouse
151 brain transduced with astrocyte-specific enhancer-AAVs demonstrated distinct astrocyte morphologies
152 in multiple brain regions (**Figure 2Q**). Thus, this collection of astrocyte-specific enhancer-AAVs are
153 diverse with regard to the density of labeled cells, expression strength, and regionalization.

154 *A collection of oligodendrocyte-specific enhancer-AAVs.* We screened 43 candidate oligodendrocyte
155 enhancers, of which 21 (49%) gave oligodendrocyte-specific expression patterns (**Figure 3—figure**
156 **supplement 1**). Unlike the astrocyte collection, the oligodendrocyte enhancer-AAVs all produced
157 similar expression patterns throughout the gray matter and white matter tracts without any obvious
158 regional specificity (**Figure 3A-F**). Oligodendrocyte-specific enhancer-AAV vectors ranged in
159 expression from strong (for example AiE0410m, **Figure 3A**, AiE0641m, AiE0395h, and AiE0396h), to
160 moderate (for example AiE0409h, **Figure 3B**, and the Myelin Basic Protein (*MBP*) promoter[25,59], **Figure**
161 **3—figure supplement 1**), to weak (for example AiE0400h, **Figure 3C**). These vectors also labeled
162 oligodendrocytes throughout the spinal cord (**Figure 3D-F**). We confirmed molecular oligodendrocyte
163 characteristics of the vector-labeled cells by co-staining with CC1, a marker of oligodendrocytes[60],
164 which showed most vectors were highly specific across multiple brain regions (**Figure 3G-O**).
165 Quantification by immunohistochemistry and scRNA-seq on sorted SYFP2-expressing cells showed

166 >99% specificity and >45% completeness of labeling in VISp for multiple vectors (**Figure 3P**). STPT
167 demonstrated myelinating oligodendrocyte morphologies in multiple parts of mouse brain (**Figure 3Q**).
168 This collection of oligodendrocyte-specific enhancer-AAV vectors shows a diversity of expression
169 strengths, but appears to label a homogeneous population of oligodendrocytes.

170 *Transcriptomic identities of astrocytes and oligodendrocytes.* To investigate distinctions among
171 enhancer-AAV-transduced cells, we performed SMARTerV4 scRNA-seq on sorted SYFP2-expressing
172 cells. We characterized 2040 cells from 47 mice injected with 31 different enhancer-AAVs (1-2 mice per
173 enhancer-AAV). After removing low-quality single-cell transcriptomes and cells not expressing the
174 SYFP2 transcript, we focused the analysis on 1946 high-quality single cells. Astrocytes and
175 oligodendrocytes separated in the UMAP space, as did astrocytes sorted from the distinct brain regions
176 including VISp, midbrain/hindbrain (MB/HB), and CBX (**Figure 4A**). The molecular distinctions among
177 regional astrocyte populations agree with findings from recent whole-brain atlases[18]. Indeed, mapping
178 to a whole-brain taxonomic atlas indicates that, with high confidence, VISp-profiled astrocytes are
179 predominantly mapped to the *Gja1*- and *Gfap*-expressing cluster "5112 Astro-TE NN_3"[18], whereas
180 MB/HB-profiled astrocytes marked by AiE0381h and AiE2160m mapped primarily to the *Gja1*- and *Agt*-
181 expressing cluster "5109 Astro-NT NN_2"[18]. Likewise, the CBX-profiled Bergmann glia astrocytes
182 mapped primarily to cluster identity "5102 Bergmann NN" as expected (**Figure 4B-D**). In contrast,
183 labeled oligodendrocytes largely mapped to *Cldn11*- and *Mog*-expressing and most abundant
184 oligodendrocyte cluster "5158 MOL NN"[18] regardless of the enhancer used to label them (**Figure 4E**),
185 confirming that oligodendrocyte enhancer-AAVs label a largely homogeneous population of
186 oligodendrocytes.

187 To understand the molecular regulation of these astrocyte and oligodendrocyte-selective enhancer-
188 AAVs, we performed de novo motif detection on a collection of specific and strong astrocyte and
189 oligodendrocyte enhancers (n = 15 each) using MEME-CHIP[61]. This analysis yielded one motif
190 occurring in the majority of enhancers in each set (**Figure 4F**, **G**). Thes motifs had strong enrichments
191 as measured by MEME-CHIP E-values less than 0.01, corresponding to the expected number of
192 equally sized motifs of same or greater log likelihood ratio occurring in a set of random sequences of
193 equal nucleotide content. We mapped these motifs against known transcription factor (TF) motif
194 databases[62–64], which revealed top matches to the Zic family consensus motifs for astrocytes (JASPAR
195 accession numbers MA0697.2, MA1628.1, and MA1629.1; average of these three shown) and the Sox
196 family motif for oligodendrocytes (JASPAR accession number MA0442.1 [Sox10 shown], and also
197 Uniprobe accession numbers UP00030.1 and UP00062.1; **Figure 4F**, **G**). These analyses suggest that
198 Zic and Sox family transcription factors might be key determinants of astrocyte versus oligodendrocyte
199 identity in the CNS[65–68], confirming the results of independent analysis of these sequences[36]. Moreover,
200 Zic and Sox gene family members were differentially expressed between the profiled astrocytes and
201 oligodendrocytes (*Zic5* 32-fold mean difference, *Sox10* 455-fold mean difference, $p < 1e-16$ each;
202 **Figure 4H**). These results suggest Zic5 and Sox10 each play key roles in determining specificity of
203 these glial enhancer-AAVs.

204 *Regional expression correlates with astrocyte cell type distribution.* Using STPT imaging, we observed
205 astrocyte-specific enhancer-AAVs to have two distinct expression patterns within the basal ganglia
206 circuit. Several enhancer-AAVs showed elevated expression in astrocytes of the dorsolateral striatum

207 and depletion in the globus pallidus (GP; **Figure 4I-K**), and several other enhancer-AAVs drove
208 stronger transgene expression in astrocytes in the GP compared with those of the lateral striatum
209 (**Figure 4L-N, Figure 2—figure supplement 2**). To determine if these enhancer-AAV expression
210 patterns correspond to transcriptomically defined astrocyte cell types, we evaluated the spatial
211 distributions of all astrocyte cell types in the Allen Brain Cell Whole Mouse Brain taxonomy[18].
212 Interestingly, two closely related astrocyte cell types were strongly enriched in the dorsolateral striatum
213 and cortex ("5112 Astro-TE NN_3" and "5113 Astro-TE NN_3"), while another was strongly enriched in
214 the GP ("5109 Astro-NT NN_2"), demarcating the same boundaries observed with the collection of
215 astrocyte enhancer-AAVs (**Figure 4O-R**).

216 *Measuring and optimizing enhancer strength.* In some cases, enhancer-AAVs might not drive sufficient
217 levels of a transgene to functionally affect the target cell. We sought to boost the expression levels of
218 some enhancers by assembling concatemers of "core" sequences. These core sequences are
219 responsible for the selective expression patterns and are often found in the central third of the original
220 enhancer region identified by snATAC-seq[33] (that is, ~100-200 bp core from ~300-600 bp original
221 enhancer, **Figure 5A**). We observed that concatenation of the core can substantially increase
222 expression from the original enhancer, such as AiE0387m concatenated to AiE0387m_3xC1 (**Figure**
223 **5B**, **C**), AiE0390h concatenated to AiE0390h_3xC2 (**Figure 5D**, **E**), or AiE0390m concatenated to
224 AiE0390m_3xC2 (**Figure 5F**, **G**) while retaining similar expression patterns (**Figure 5H-J**) and cell type
225 specificity (**Figure 5K**). However, concatenation sometimes resulted in a less dramatic effect on
226 expression, (e.g., AiE0410m_3xC and AiE0641m_3xC; **Figure 3—figure supplement 1**).

227 We established single-cell measurements of reporter expression to compare enhancer strengths. We
228 found that single-cell reporter fluorescence by flow cytometry correlated with vector read counts from
229 SMARTerV4 scRNA-seq for both astrocytes and oligodendrocytes (astrocyte Pearson correlation
230 coefficient = 0.63, $p < 0.001$; oligodendrocyte Pearson correlation coefficient = 0.53, $p < 0.05$; **Figure**
231 **5L**, **M**, **Figure 5—figure supplement 1**). These measurements revealed that several concatenated
232 enhancer-AAVs, including AiE0390m_3xC2 and AiE0390h_3xC2, drove the strongest expression
233 among the vectors we have tested (**Figure 5L**), consistent with the microscopy results (**Figure 5B-J**).
234 Conversely, MB/HB (AiE0381h and AiE2160m) and Bergmann glia (AiE0375m) astrocyte enhancers
235 have among the weakest expression levels we have tested (**Figure 5L**), likely a consequence of
236 selecting glial enhancers from cortical accessibility datasets.

237 *Enhancers can yield more robust specific expression across transgenes than classic promoters*.
238 Previously it was demonstrated that the human *GFAP* promoter (GfaABC1D[57]) can change specificity
239 from astrocytes to neurons over time when driving certain difficult transgene cargos including NeuroD1-
240 mCherry fusion protein[44]. Accordingly we tested whether astrocyte-specific enhancers might be more
241 robust to transgenes than *GFAP* promoter. As demonstrated previously, we found that at seventeen
242 days post transduction, *GFAP*-driven NeuroD1-mCherry is expressed predominantly in NeuN+ neurons
243 in primary visual cortex (VISp, 90 ± 2% of labeled cells, mean ± standard deviation), unlike *GFAP*-
244 driven SYFP2 which is expressed with high Sox9+ astrocyte specificity (98 ± 2% of labeled cells,
245 **Figure 6A-B**, $p < 0.001$, see also **Figure 2**). In sharp contrast an optimized astrocyte-specific
246 enhancer, AiE0390m_3xC2 maintains high levels of astrocyte specificity whether driving SYFP2 (100 ±
247 0% of labeled cells) or NeuroD1-mCherry (95 ± 4% of labeled cells, **Figure 6A-B**, $p < 1e-7$, see also

248 **Figure 5K**). These results suggest that optimized astrocyte-specific enhancers may provide more
249 predictable expression for certain transgenes, and confirm the previous results that astrocytic NeuroD1-
250 mCherry expression alone is insufficient to drive astrocyte transdifferentiation to neurons[44].

251 *Predictability of enhancer-AAV expression across tissues and disease states.* Recent work suggests
252 that AAV-mediated transduction and high transgene expression in organs such as the liver and dorsal
253 root ganglia is associated with toxicity[29,69]. We tested if we could predict off-target activity from
254 enhancer accessibility profiles in a human body-wide epigenetic dataset[70]. Different astrocyte-specific
255 enhancers showed either moderate or low accessibility across many body organs (**Figure 7A**), since
256 this was not a factor in their selection for testing. We assessed off-target transgene expression in liver
257 after intravenous delivery since PHP.eB capsid transduces the liver[71]. We observed that astrocyte
258 enhancers with moderate levels of accessibility in liver (AiE0381h, AiE0371m, AiE0371h, and
259 AiE0386m) expressed SYFP2 in many hepatocytes, whereas the enhancers with little or no liver
260 accessibility (AiE0387m, AiE0375m, AiE0390h, and AiE0390m) expressed SYFP2 in many fewer
261 hepatocytes ($p < 0.001$, **Figure 7B-C**), demonstrating strong predictability of enhancer expression
262 profiles in off-target tissues. In contrast, the *GFAP* promoter can drive bright expression in few
263 hepatocytes, which is not predictable from any epigenetic or transcriptomic atlases.

264 *GFAP* expression can change expression in the context of disease or injury[9], and the synthetic *GFAP*
265 promoter can change specificity when delivering different transgenes[44–46], suggesting this might be a
266 poor tool for genetic access to astrocytes in disease. We compared *GFAP* promoter and one of the
267 best enhancer-AAVs (AiE0390m) in *Scn1a*$^{+/-}$ Dravet syndrome model mice since they have strong
268 epilepsy-associated reactive astrogliosis[72]. We injected SYFP2-expressing enhancer-AAVs into these
269 mice prior to the Dravet syndrome critical period of high susceptibility to seizures and mortality at P21
270 and analyzed tissues at P42 (**Figure 8A**). Significant hippocampal gliosis was seen in Dravet syndrome
271 model mice, revealed by elevated endogenous GFAP immunoreactivity in all hippocampal layers
272 (**Figure 8B**). Concomitant with this gliosis, the *GFAP* promoter-driven AAV reporter changed its
273 expression pattern. Normally, this promoter drives moderate levels of astrocyte-specific reporter
274 expression. However, in the Dravet mice experiencing epilepsy, expression strength in astrocytes was
275 considerably elevated, and ectopic expression was observed in many dentate gyrus granule cell
276 neurons (DGCs, 12 ± 6% of DGCs labeled, $p < 0.01$, **Figure 8B, C**). In sharp contrast, the AiE0390m
277 enhancer-AAV vector maintains astrocyte specificity at moderate levels despite the profound reactive
278 gliosis in these diseased animals (0 ± 0% of DGCs labeled, **Figure 8B, C**).

279 *Astrocyte specific sensing of cholinergic signals in the nucleus accumbens during behavior.* We next
280 asked whether the vectors would drive sufficient expression to obtain functional signals in a cell-type
281 specific manner. We created a vector driving astrocyte-specific expression of the acetylcholine indicator
282 iAChSnFR[47] (**Figure 9A,B**), to detect extracellular acetylcholine fluctuations in the nucleus accumbens
283 (NAc) in an awake and behaving animal using fiber photometry. After stereotaxic injection, we
284 implanted optical fibers above the injection site to perform fiber photometry. We trained mice to perform
285 a dynamic foraging reinforcement learning task while we recorded photometry signals to assess bulk
286 acetylcholine fluctuations in the NAc. In the task, water-restricted mice chose freely between two lick
287 ports for a water reward after an auditory cue. Reward probabilities of the two lick ports were changed
288 in a block-design manner, which resulted in both rewarded and unrewarded trials (**Figure 9C**). During

these trials, the astrocyte-specific iAChSnFR vector drove sufficient expression to observe fluorescence intensity fluctuations (**Figure 9D**) which can be seen to differ during individual rewarded and unrewarded licks (**Figure 9D**, bottom left). Both rewarded and unrewarded trials showed an increase in fluorescent signal at the time of choice, followed by a deviation in signal depending on whether the trial was rewarded (**Figure 9E**). Astrocyte acetylcholine signals decreased more in rewarded trials than in unrewarded trials (**Figure 9E**). In summary, these results indicate that glial-selective enhancer-AAVs can be applied to measure functional acetylcholine dynamics in the NAc.

Astrocyte- and oligodendrocyte-specific AAV-Cre vectors. AAVs that can selectively drive Cre recombinases are valuable tools for mouse genetics since the AAV can be delivered somatically for cell type-specific recombination of floxed alleles. We used some of the best astrocyte- and oligodendrocyte-specific enhancers to express an attenuated R297T mutant Cre recombinase in *Ai14* reporter mice[73,74] (**Figure 10A**). AiE0390m_3xC2-driven Cre vector drove astrocyte-specific recombination in many parts of mouse brain, including specific (95 ± 3%) and complete (98 ± 1%) labeling in VISp gray matter astrocytes (**Figure 10B-D**). Similarly, an AiE0410m-driven Cre vector also incorporating three miR126 binding sites to prevent unwanted endothelial cell recombination[75] drove oligodendrocyte-specific recombination in many parts of mouse brain, including specific (97 ± 3%) and complete (81 ± 0.1%) labeling in VISp gray matter oligodendrocytes (**Figure 10E-G**). Additional vectors utilizing AiE0390m and AiE0387m also showed specific and complete astrocyte labeling in VISp (**Figure 10H-I**). These tools may permit fine interrogation of the roles of astrocyte and oligodendrocyte gene expression in brain biology.

Cross-species genetic access to astrocytes and oligodendrocytes. We tested whether several glial-selective enhancer-AAV vectors could maintain specific expression across species. We first tested conservation in neonatal rats after ICV administration (**Figure 11A**). We observed that an optimized AiE0390m_3xC2 vector containing 4X2C miRNA binding sites to prevent any unwanted expression in excitatory neurons[76] labeled rat cortical astrocytes with high specificity (98% specific, **Figure 11B**, **C**). We also found that an AiE0641m-driven AAV vector labeled rat cortical oligodendrocytes with high specificity (91% specific, **Figure 11D**). Note that astrocyte labeling completeness and spread to caudal brain structures could not be assessed since ICV administered virus resulted in uneven spread. Thus, some vectors identified in the mouse screen maintained specificity in rats after ICV injection into neonates, consistent with the results from other enhancer-AAV collections[38].

We extended these cross-species tests to primate, using multisite intraparenchymal injections into *Macaca nemestrina* (pig-tailed macaque, **Figure 11E**). We administered AiE0410m AAV vector into motor (MO) cortex and observed cell morphologies of myelinating oligodendrocytes throughout the cortical column (**Figure 11F-G**). Interestingly, we also observed SYFP2-expressing cells with a different morphology: one to three processes that spiral around stretches of tubular structures approximately 15-20 microns in diameter often running perpendicular to the cortical pial surface (**Figure 11H**). These tubular structures have not yet been defined and were not observed in mouse or rat testing, but both morphological types of SYFP2-expressing cells co-expressed the oligodendrocyte marker *SOX10* by mFISH with high specificity (94%, **Figure 11I**).

328 We also injected the somatosensory cortex (SS) with the astrocyte-specific AiE0390m AAV vector and
329 observed many SYFP2-expressing cells with astrocyte morphology throughout the cortical column
330 (**Figure 11J**; note a small number of large layer 5 pyramidal neurons labeled as well, which we did not
331 observe in mouse testing). SYFP2-expressing astrocytes co-expressed GFAP either in parenchyma
332 (**Figure 11K**) or in apposition to a large blood vessel (**Figure 11L**), and some showed fibrous
333 morphology in white matter (**Figure 11—figure supplement 1**). Enhancer-AAV-labeled astrocytes also
334 expressed the astrocyte-specific transcript *FGFR3* with high specificity (92%) and about half of the
335 *FGFR3+* gray matter astrocytes were labeled through the whole cortical depth near the injection site
336 (51%) (**Figure 11M**). In an additional animal we also tested AiE0390m_3xC2 vector containing 4X2C
337 miRNA binding sites in MO, and we observed 99% specificity for SOX9+ astrocytes and no layer 5
338 pyramidal neuron labeling (**Figure 11N-O**), and a final injection into a third animal also confirmed 98%
339 specificity of AiE0390h-driven vector for SOX9+ astrocytes in SS (**Figure 11P-Q**). These studies
340 suggest that enhancer-AAV vectors can provide specific and dependable genetic access to astrocytes
341 and oligodendrocytes across multiple species and reveal morphological glial features not observed in
342 the mouse.

343

344

Discussion

Flexible and dependable tools to target glial cell populations will be essential to understand their diverse roles in brain biology. Here we report a collection of astrocyte- and oligodendrocyte-specific enhancers that can be used in AAV vectors and applied across species. Most of these enhancer-AAVs generated highly specific labeling of astrocytes or oligodendrocytes, and often substantial completeness of labeling. Detailed characterization revealed the enhancers showed a range of expression strengths, and the astrocyte enhancers frequently exhibited regional enrichment and differences in labeling densities. We demonstrate that this enhancer-AAV toolset can be applied: 1) across species in mouse, rat and macaque, 2) in epileptic mice where gliosis is occurring without losing specificity, and 3) to deliver Cre selectively to many astrocytes and oligodendrocytes, 4) irrespective of transgene delivered, and 5) to measure circuit dynamics with a neurotransmitter sensor *in vivo*. As a result, these glial enhancer-AAVs will be useful for interrogating the roles of these glial cell types in health and disease.

Lesson learned from screening. Several lessons were learned through the process of screening for astrocyte and oligodendrocyte enhancer-AAVs. First, multiple selection criteria can identify strong glial enhancer-AAVs. Excellent functional enhancers were derived from genome-wide peak selection across mouse and human datasets of distinct epigenetic modalities, peak selection from one mouse dataset based on peak strength, or peak selection only near marker genes. Second, screening one enhancer-AAV at a time can be efficient for the identification of useful enhancer-AAVs. Nearly half of the candidate enhancers proved to be specific for the targeted type, and this created a large and diverse library of new enhancer-AAVs that labeled astrocytes or oligodendrocytes in different ways. Third, while enhancers were identified from neocortex at the subclass level, brain-wide patterns match well to whole brain cell gene expression atlas patterns[18]. Specifically, AAV-labeled oligodendrocytes appear homogeneous across the brain, while astrocytes show prominent regional enrichments and differences in cell density. Fourth, body-wide specificity of enhancer-AAV expression can be predicted based on body-wide epigenetic datasets[70]. Thus, off-target expression can be predicted and limited during the enhancer selection process, and enhancers can be identified that label different cell types throughout the body. These attributes will make enhancer-AAVs a valuable tool for precision gene therapy where only the cell population of interest is expressing the therapeutic transgene.

Enhancer-AAVs show diverse expression patterns. We tested a large collection of astrocyte-selective enhancer-AAVs and saw a diversity of expression patterns. Some astrocyte enhancer-AAVs predominantly labeled in telencephalic structures, some in MB/HB structures, and others showed sparse “Scattered” but uniform expression. Within the forebrain, we also observed multiple enhancer-AAVs that showed mutually exclusive enriched or depleted expression in dorsolateral striatum or the globus pallidus. These regional differences were reflected by region-specific astrocyte transcriptomic profiles in agreement with recent results[18]. The GPe astrocytes express high levels of GABA uptake gene *Slc6a11*[16,77,78] while striatal and cortical (but not GPe) astrocytes express high levels of glutamate uptake gene *Slc1a2*[16,78,79]. This suggests that the astrocytes help selectively maintain glutamate or GABA tone depending on the local neurotransmitter balance. The functional roles of astrocytes in different brain regions will require additional experiments that this collection of enhancer-AAVs may

385 facilitate. Similarly, it is not yet clear what produces “Scattered” astrocyte reporter expression, and the
386 answer will await future experiments.

387 *Enhancer-AAVs can be optimized to improve vector function.* Achieving functional levels of transgene
388 expression is critical for applying enhancer-AAV tools to learn new biology and deliver gene therapies.
389 We show that two astrocyte enhancers could be optimized through generation of a triple concatenated
390 core to produce significantly higher levels of transgene expression without sacrificing astrocyte
391 specificity. One such optimized tool was used to detect acetylcholine activity in the NAc. The NAc has
392 been implicated in reward-related reinforcement learning and receives inputs from dopaminergic and
393 serotonergic neurons, in addition to local cholinergic signaling[80–83]. We used enhancer-AAVs to deliver
394 the acetylcholine indicator iAChSnFR to astrocytes within the NAc, and measured dynamics with fiber
395 photometry. This experiment showed that the astrocyte enhancer AiE0390m_3xC2 maintained faithful
396 astrocyte specificity after direct injection into NAc and expressed sufficient iAChSnFR for sensing of
397 acetylcholine in live awake animals. It also showed that iAChSnFR expressed by astrocytes could
398 readily detect acetylcholine dynamics in NAc, and that astrocytes are a good cellular compartment for
399 the sensor.

400 Different optimization efforts enabled the generation of a functional Cre-AAV that was specific for
401 astrocytes in most parts of the brain. Cre recombinases can lose specificity when expressed from
402 enhancer-AAVs, possibly due to low-level expression of this potent enzyme[30]. We were able to
403 successfully generate an astrocyte-selective Cre AAV using an attenuated Cre recombinase with the
404 R297T mutation[73,74], in combination with the AiE0390m_3xC2 enhancer. As a result we produced a
405 highly specific somatic astrocyte Cre. Similarly we were able to produce a highly specific
406 oligodendrocyte Cre AAV using the AiE0410m enhancer along with miR126 binding sites. We
407 anticipate these vectors may unlock many types of functional experiments dissecting the roles of these
408 important glial cell populations.

409 *Enhancers-AAVs can be identified that have conserved specificity from mouse to macaque.* Some
410 astrocyte and oligodendrocyte enhancer-AAVs are active and selective across species from mouse
411 through macaque. This property will allow these tools to be applied somatically in multiple organisms
412 besides mice. Testing enhancers in macaques revealed interesting morphological differences
413 compared to mouse. Abundant mature oligodendrocytes with large dendritic arbors were labeled in
414 both mouse and primate tissues with AiE0410m, but this enhancer-AAV also labeled *SOX10*+ cells
415 wrapping around radial tubes (presumably blood vessels) in primate but not mouse. Also, the astrocyte
416 enhancer AiE0390m labeled abundant protoplasmic astrocytes in the gray matter in mouse and
417 macaque, but also labeled several large fibrous astrocytes that were not observed in the mouse
418 experiments. The ability to function across species and label cells that are not obviously represented in
419 mouse tissue, makes this collection of enhancer-AAVs a powerful toolset to better understand new
420 biology. It also makes a compelling case that some of these enhancer-AAVs could be suitable for use
421 in human gene therapy where astrocyte or oligodendrocyte expression selectivity is required.

422 *Enhancer-AAVs can be cell state-independent.* AAVs that drive expression using promoters can cause
423 gene expression changes in a state dependent fashion. We showed that the *GFAP* promoter changed
424 expression strength and specificity in the context of epilepsy-induced gliosis using an *Scn1a*

425 haploinsufficiency model. This is not surprising since the *GFAP* gene is known to change in response to
426 disease and injury[8,9]. Additionally, *GFAP* promoter-driven expression changed specificity from
427 astrocytes to neurons with the difficult transgene NeuroD1-mCherry, as seen in other reports[44].
428 Enhancer-AAVs utilizing AiE0390m, on the other hand, did not show a change of expression in either
429 epileptic gliosis conditions or due to differing transgenes. This could be due to the enhancer being
430 selected based on core cell type identity, and most properties of cell types have not been seen to
431 change character dramatically in the context of disease[20,84,85]. Enhancers can be selected that do not
432 change activity during development, aging, or disease, in a similar way to avoid selecting enhancers
433 predicted to have activity in off-target tissues. As epigenetic datasets are expanding to cover these
434 axes of disease, development, and aging, it is becoming feasible to select only putative enhancers with
435 the desired activity profiles.

436 *Conclusion.* We have characterized a large collection of enhancer-AAV vectors for targeting astrocytes
437 and oligodendrocytes. These vectors will provide researchers with the ability to mark and manipulate
438 these critical cell types in a variety of species, genetic backgrounds, ages, and disease contexts, and
439 could also enable delivery of therapeutics. Combined with other recently discovered AAV-based
440 tools[25,26,31–38,40,43,71], this glial-targeting toolbox will help to advance the understanding of the roles of
441 glial cell types in brain biology, make the complex cellular anatomy of the brain more experimentally
442 tractable, and advance the development of AAV-based therapeutics for human CNS disorders.

443

Methods

Epigenetic analysis and enhancer nomination. We identified candidate astrocyte- and oligodendrocyte-specific enhancers from cortical epigenetic datasets. We used the following datasets: human middle temporal gyrus snATAC-seq[33], mouse primary visual cortex scATAC-seq[34], human frontal cortex snmC-seq[52], mouse frontal cortex snmC-seq[52], human frontal cortex bulk mC-seq[51], and mouse frontal cortex bulk mC-seq[51]. A single cell glial snmC-seq dataset[53,54] became available only after initial identification of most of the enhancers described in this study. From the single nucleus/cell ATAC-seq datasets, we aggregated reads according to cell subclass as in the references, and then called peaks using Homer findPeaks (http://homer.ucsd.edu/homer/) with the -region flag, yielding typically tens of thousands of peaks per subclass, sized approximately 300-600 bp, as previously described[33]. To find differentially methylated regions (DMRs) we either used the published regions by Luo et al. 2017 in Extended Data Tables 5 and 6[52], and aggregated by subclass and then to all neurons using bedtools merge (https://bedtools.readthedocs.io/en/latest/). Alternatively for bulk non-neuronal DMRs we used methylpy DMRfind with minimum differentially methylated sites set to 1 on the dataset of Lister 2013, as previously described[33,52]. To convert mouse and human peak or DMR regions to each other's genomic coordinates for direct intersectional analysis, we used liftOver (https://genome.ucsc.edu/cgi-bin/hgLiftOver) with minMatch parameter set to 0.6. All peak regions described in this manuscript successfully liftOver from human to mouse, and vice-versa, except AiE0733m which does not have an obvious human ortholog via liftOver.

To automatically identify peaks and DMRs genome-wide that are astrocyte- or oligodendrocyte-specific within each dataset, we used a series of bedtools intersectBed (https://bedtools.readthedocs.io/en/latest/) operations to filter for regions that are only detected in astrocytes or oligodendrocytes. For the "high specificity" criteria, we found peaks that were specifically detected in both human and mouse cortical astrocytes/oligodendrocytes[33,34], but did not overlap DMRs from either human or mouse neurons of any subclass[52], and these candidate enhancers are marked by gold square icons in **Figure 1**. These criteria yielded a set of 87 candidate astrocyte-specific enhancers and 112 candidate oligodendrocyte-specific enhancers, and the top 17 (Astrocyte) or 16 (Oligodendrocyte) candidate enhancers were chosen from this list as ranked by Homer findPeaks score. Homer findPeaks score is a measure of peak significance relative to local background, not peak strength. Additionally, a small number of these "high specificity" criteria candidate enhancers also overlapped with DMRs from both human and mouse non-neuronal cells[51] (3 Astrocyte and 4 Oligodendrocyte), and these are marked by gold star icons in **Figure 1** and **Figure 1—figure supplement 1**.

For the "high strength" criteria we found peaks that were specifically detectable in cortical astrocytes, using mouse scATAC-seq data only[34], and agnostic to detection in human and methylation datasets. This analysis yielded 2119 (astrocyte) and 3940 (oligodendrocyte) candidate enhancers, which were ranked by read counts within the region, and the top 7 candidate enhancers for astrocytes from this list were chosen. This ranking led to nomination of peaks that are overall stronger and longer, and these candidate enhancers are marked with a purple triangle in **Figure 1B**, but accessibility profiles were not always conserved in human tissue, as shown in **Figure 1—figure supplement 1A,C**.

484 Some candidate enhancers were identified manually in the vicinity of known astrocyte or
485 oligodendrocyte marker genes by visual inspection of ATAC-seq read pileups on UCSC browser
486 (marked as "*M*" for Marker genes in **Figure 1B**). Methylation data was not visualized in this manual
487 nomination process. Importantly we found that both automatic and manual approaches can identify
488 peaks with high strength and specificity, as shown in **Figure 1D-E**.

489 Additionally, enhancer AiE2160m was initially identified as a candidate enhancer for pericytes in cortex
490 using the data of Graybuck et al.[34], but it was found in the course of this study to instead label
491 mid/hindbrain astrocytes.

492 To model enhancer screening results as a generalized linear model, we confined analysis to 50
493 screened enhancers where we observed a clear yes/no screening result for both itself and its cross-
494 species ortholog. These candidate enhancers were AiE0371, 372, 373, 375, 377, 379, 380, 382, 383,
495 384, 388, 393, 394, 398, 399, 401, 406, 407, 408, 374, 376, 390, 395, 409, and 410, both the m and h
496 orthologs for each. For each of these genomic regions we calculated candidate enhancer strength
497 (read CPM within either astrocytes or oligodendrocytes), candidate enhancer specificity (defined as the
498 proportion of astrocyte or oligodendrocyte enhancer strength relative to the summed strength in all
499 populations, using the data of Mich et al. or Graybuck and Daigle et al.[33,34]), candidate enhancer length
500 in base pairs, region-segmented PhyloP using the previous method[33], and tabulated whether each
501 candidate enhancer's partner ortholog worked (binary yes [1] or no [0]). We fit a logistic generalized
502 linear model of testing results from these predictors using glm() in R with the following command:

503 `glm( Screen_result_01 ~ Length + PhyloP + Specificity + Strength_cpm +`
504 `Ortholog_result_01, family=binomial(link='logit'), data = data)`

505 The significance of each coefficient to predict the screening result was determined from the coefficients
506 of the model, using the data as provided in **Table S1**. Although high peak specificity and strength were
507 important criteria for candidate enhancer identification, these metrics each had little predictive power to
508 explain success or failure of screening collection testing as evidenced by coefficients of fit to a logistic
509 linear model (**Table S1**; strength z-value = 1.43, p = 0.15; specificity [defined as proportional strength
510 within target cell subclass] z-value = -1.20, p = 0.23), similar to enhancer length (z-value = -0.13, p =
511 0.89), enhancer sequence conservation measured by PhyloP (z-value = 0.87, p = 0.38), and the
512 presence of a functional ortholog in testing (z-value = 1.77, p = 0.077), which suggests that there are
513 additional undiscovered elements that determine successes versus failures in AAV-based enhancer
514 screening. Overall, the null deviance was 67.3 on 49 degrees of freedom, and the residual deviance
515 was 57.7 on 44 degrees of freedom, again indicating little power of these features to predict the
516 screening results.

517 *Cloning and packaging enhancer-AAVs.* With candidate enhancers chosen, we next found their
518 predicted DNA sequence from genomic reference sequence using Bioconductor package Bsgenome[86].
519 We extracted the sequence and padded 50 bp to each side of the enhancer to provide room for forward
520 and reverse primer binding sites that capture the entire enhancer. From these padded sequences, we
521 used automatic primer design in Geneious to identify primer pairs within the 50 bp pads to specifically
522 amplify each enhancer, and append a constant 5' homology arm to each enhancer for automatic
523 Gibson assembly into reporter-AAV plasmid. We amplified the regions from C57Bl/6 tail snip DNA or

524 from human male genomic DNA (Promega catalog # G1471) using FastPhusion 2x Master Mix
525 (Thermo Fisher catalog # F548L), and >90% of the PCR reactions were successful on the first try. In
526 some cases we redesigned primers to attempt a second amplification.

527 We cloned into reporter backbone CN1244 (Addgene plasmid #163493) using the sites MluI/SacI and
528 the 5' primer homology arms F: TTCCTGCGGCCGCACGCGT and R:
529 GACTTTTATGCCCAGCCCGAGCTC, using Infusion kit (Takara catalog # 638949). For some
530 enhancers we instead cloned into a next generation reporter vector backbone that includes a SYFP2-
531 P2A-3xFLAG-H2B reporter for detection of cytosolic SYFP2 and nuclear FLAG for simultaneous
532 expression analysis and snRNA-seq, using the same cut sites and homology arms (see **Table S1**). We
533 transformed infusion reactions into Mix N' Go (Zymo Research catalog # T3001) chemically competent
534 Stbl3 E. coli (Thermo Fisher catalog # C737303) and selected on 100 µg/mL carbenicillin plates. We
535 cultured individual clones at 32 C, verified them by Sanger sequencing, maxiprepped them with 100
536 µg/mL ampicillin, and saved them as frozen glycerol stocks at -80°C.

537 We used maxiprep DNA for packaging into PHP.eB AAV particles. For routine enhancer-AAV screening
538 by intravenous delivery in mouse we generated small-scale crude AAV preps by transfecting 15 µg
539 maxiprep enhancer-reporter DNA,15 µg PHP.eB cap plasmid, and 30 µg pHelper plasmid into one 15-
540 cm dish of confluent HEK-293T cells using PEI-Max (Polysciences Inc. catalog # 24765-1). After
541 transfection the next day we changed the medium to 1% FBS, and after 5 days the cells and
542 supernatant were collected, freeze-thawed 3x to release AAV particles, treated with benzonase (1 µL)
543 for 1 hr to degrade free DNA, then clarified (3000g 10min) and then concentrated to approximately 150
544 µL by using an Amicon Ultra-15 centrifugal filter unit at 5000g for 30-60 min (NMWL 100 kDa, Sigma
545 #Z740210-24EA), yielding a titer of approximately 3-5 E13 genome copies (gc)/mL. For large-scale
546 gradient preps for intraparenchymal injection into macaque or mouse or ICV injection into rat, we
547 transfected 10 15-cm plates of cells, and also purified preps by iodixanol gradient centrifugation. We
548 assessed viral titer for both crude and gradient AAV preps by digital droplet PCR on a BioRad QX200
549 system. All vectors showing specific expression patterns are available through Addgene.

550 *Optimizing enhancer strength through concatemerization*. For some native enhancers that showed
551 specific expression patterns, we sought to boost their expression levels through concatemerization. To
552 concatemerize, we segmented the enhancer (typically approximately 400-600 bp) into approximately
553 thirds with approximately 25 bp of overlaps at the junctions (each a candidate "core" of approximately
554 200 bp), then designed a tandem array of three cores in series (approximately 600 bp). These synthetic
555 tandem array sequences were gene synthesized by Azenta/GeneWiz PRIORITYGene synthesis
556 service with flanking MluI/SacI sites for restriction enzyme digestion and ligation into corresponding
557 sites in CN1244. We then packaged and tested concatemerized PHP.eB enhancer-AAVs as above.

558 *Mice and injections.* All mouse experimentation was approved by Allen Institute Institutional Animal
559 Care and Use Committee (IACUC) as part of protocol #2020-2002. In these studies, we purchased
560 C57Bl/6J mice from The Jackson Laboratory (Stock # 000664). For enhancer screening these C57Bl/6J
561 mice were injected with AAVs in the retro-orbital sinus at age P21 with 5E11 genome copies of
562 AAV/PHP.eB viral vectors with brief isoflurane anesthesia. For enhancer validation studies (IHC) mice
563 were injected the same way but between ages P42 to P56. Tissues from mice were harvested at 3 to 4

564 weeks post injection for analysis, except in the case of the NeuroD1-mCherry experiments (**Figure 1F**)
565 where mice were analyzed at 17 days post injection as previously reported[44], and in the liver
566 experiments (**Figure 6C**) in which 1-2 mice for each vector were analyzed at 3 weeks and 1-2 mice
567 were analyzed at 36 weeks to confirm durability across age. We perfused animals with saline then
568 4%PFA in PBS, and harvested brains or other tissues and post-fixed in 4%PFA overnight, before
569 rinsing and cryoprotecting in 30% sucrose solution before sectioning at 30 micron thickness on sliding
570 microtome with a freezing stage. PFA used in these experiments was prepared by dissolving solid PFA
571 (VWR Chemicals #28794.295) in PBS by heating, which was then stored in frozen aliquots. For
572 enhancer screening we counterstained with DAPI and propidium iodide and mounted in Vectashield
573 Vybrance, and imaged on either a Nikon Ti-Eclipse or Nikon Ti-Eclipse 2 epifluorescent microscope,
574 Olympus FV-3000 confocal microscope, or Leica Aperio slide scanner. In some experiments where
575 noted, we tested enhancer-AAVs after bilateral intracerebroventricular (ICV) injection at age P2 using
576 the technique of Kim et al.[87] These ICV-injected pups were harvested for tissue analysis at age P21.
577 For whole brain imaging of expression pattern, we performed sequential blockface imaging of brains
578 using the TissueCyte 1000 serial two-photon tomography system[88].

579 For testing in Dravet syndrome model mice, 129S1/SvImJ -*Scn1a*$^{em1Dsf/J}$ mice (strain # 034129) were
580 purchased from Jackson Laboratories and bred to C57Bl/6J mice to create *Scn1a*$^{R613X/+}$ pups on a F1
581 hybrid C57Bl/6J:129S1/SvImJ background, and these pups were injected retro-orbitally at P21 with
582 tissue analysis at P42. Additionally, we also tested enhancer-AAV vectors in *CMV-Cre;Scn1a*$^{A1783V/+}$
583 pups on C57Bl/6J background, which were generated from crossing B6(Cg)-*Scn1a*$^{tm1.1Dsf/J}$ male mice
584 (The Jackson Laboratory, strain #:026133) with homozygous CMV-Cre female mice (*B6.C-Tg(CMV-*
585 *cre)1Cgn/J*, The Jackson Laboratory, strain # 006054). Data from both lines appeared similar, so we
586 combined them for analysis.

587 *Mouse immunohistochemistry (IHC).* For IHC and ISH, we transcardially perfused mice with ice-cold 25
588 mL HBSS (Thermo Fisher Scientific # 14175079) containing 0.25 mM EDTA (Thermo Fisher Scientific
589 # AM9260G), followed by 12 mL of ice-cold 4% paraformaldehyde in 1x PBS, freshly prepared from
590 16% PFA (Electron Microscopy Sciences #15710). We dissected brains and other tissues from
591 carcasses and post-fixed them at 4 degrees overnight, and the next morning we rinsed the tissues with
592 fresh PBS, and then transferred to 30% sucrose solution in PBS for cryoprotection. For sectioning on
593 Leica CM3050 cryostat, we then embedded tissues in OCT cryo-compound (Tissue-Tek # 4583) at
594 room temperature at least 3 hours, then froze the blocks on dry ice and stored at -80°C until sectioning
595 at 25 micron thickness. Alternatively, we sectioned half-brains at 25 µm thickness on frozen 30%
596 sucrose solution slabs on a sliding microtome (Leica SM2000R) equipped with freezing stage. Sections
597 were stored at 4 degrees in PBS containing 0.1% sodium azide until analysis. IHC of liver was
598 performed as for brain, focusing on the frontal lobe.

599 For IHC we used the following antibodies: chicken anti-GFP (Aves # GFP-1010, 1/3000), rabbit anti-
600 Sox9 (Cell Signaling clone D8G8H, # 82630S), mouse CC1 antibody (Abcam # ab16794, 1/1000),
601 mouse anti-GFAP (Millipore Sigma clone G-A-5, # G3893, 1/1000), with 5% normal goat serum
602 (Thermo Fisher Scientific # 31872) and 0.1% Triton X-100 (VWR 97062-208) for blocking and
603 permeabilization, and appropriate Alexa Fluor-conjugated secondary antibodies for detection.

604 *Flow cytometry and single cell transcriptomics.* We prepared cell suspensions for flow cytometry and
605 single cell RNA-seq from brain tissue as previously described[89]. Briefly, for flow cytometry, we perfused
606 mice transcardially under anesthesia with ACSF.1. We harvested the brains, embedded in 2% agarose
607 in PBS, then sliced thick 350 micron sections using a compresstome with blockface imaging, then
608 picked the sections containing the region of interest (VISp, or mid- and hindbrain, or cerebellar cortex),
609 and dissected out the regions of interest. We then treated dissected tissues with 30U/mL papain
610 (Worthington LK003176) in ACSF.1 containing 30% trehalose (ACSF.1T) in a dry oven at 35°C for 30
611 minutes. After papain treatment we quenched digestion with ACSF.1T containing 0.2% BSA, triturated
612 sequentially using fire-polished glass pipettes with 600, 300, and 150 micron bores, filtered the
613 released cell suspensions into ACSF.1T containing 1% BSA, centrifuged cells at 100g for 10 min, then
614 resuspended cells in ACSF.1T containing 0.2% BSA and 1 µg/mL DAPI prior to flow cytometry and
615 sorting on a FACSAria III (Becton-Dickinson). SYFP2 reporter brightness was measured as the ratio of
616 positive cell population mean fluorescence intensity, divided by the low mean fluorescence intensity of
617 autofluorescence in non-expressing cells. This measure of reporter brightness is more consistent than
618 positive cell population mean fluorescence intensity alone, due to differences in raw signal across days,
619 cytometers, and cytometer settings.

620 For single cell RNA-seq, we sorted single SYFP2+ cells into tubes and processed them via SMARTer
621 v4 using the workflow described previously[89], on 47 enhancer-AAV-injected mice. In each experiment
622 from one mouse injected with one single enhancer-AAV we sorted and profiled up to 48 cells per
623 experiment, and each measurement was taken from a distinct individual cell. After retroorbital
624 injections, enhancer-AAV SYFP2-expressing cells consisted of on average 7% of the positive brain
625 cells (range 0.1-20.1% of cells, n = 47 experiments). We sequenced single cell-derived SMARTer
626 libraries at 659996 ± 199038 (mean ± standard deviation) reads per library on an Illumina NovaSeq
627 instrument at Broad Institute (Cambridge, MA) or on an Illumina NextSeq instrument at Allen Institute
628 (Seattle, WA). We aligned the libraries to mm10 genome using STAR
629 (https://github.com/alexdobin/STAR), and also aligned them to the synthetic AAV transgene reference
630 construct using bowtie2 (https://bowtie-bio.sourceforge.net/bowtie2/index.shtml). From 2040 initial cells,
631 we excluded from analysis the libraries with poor library quality metrics, consisting of: firstly low-quantity
632 or degraded libraries (judged as less than 65% percentage of cDNA library sized greater than 400 bp,
633 consisting of 71 [3.4%] libraries in this study), and secondly those that lacked AAV transgene-mapping
634 reads (likely mis-sorted events, 23 [1.1%] of remaining libraries). Applying these filtering criteria yielded
635 a dataset for analysis of 1946 high-quality AAV transgene-expressing cells, with alignment rates of 92 ±
636 3% to mm10 genome and 4654 ± 1285 genes detected per cell (mean ± standard deviation). To assess
637 enhancer specificity within the cortex we mapped the high quality transgene-expressing SMARTer cells
638 to the SMARTer-based VISp cellular taxonomy generated by Tasic et al. using bootstrapped
639 hierarchical approximate nearest neighbor mapping[18,89], and quantified the specificity as the percentage
640 of positively sorted cells that mapped to the expected cell subclass (astrocytes or oligodendrocytes). To
641 test for significance of correlation of brightness by flow cytometry with expression levels by scRNA-seq,
642 we calculated Pearson's product-moment correlation coefficient by cor.test() function in R.

643 To understand different characteristics of different regional astrocyte populations we utilized
644 scrattch.mapping (https://github.com/AllenInstitute/scrattch) from the Allen Institute. To accomplish this

645 we first transformed these cells by principal component analysis and performed UMAP dimensionality
646 reduction on the first 40 principal components for visualization using the default scanpy parameters,
647 which clearly separated oligodendrocytes and regional groupings of astrocytes. For clustering
648 astrocytes we subset the dataset to astrocytes only, then identified the top 2000 genes ranked by
649 variance among them, recomputed UMAP projections from these high-variance genes, then performed
650 Leiden clustering[90] which identified VISp, MB/HB, and CBX astrocyte clusters as expected, and finally
651 identified differential genes among them (differential gene expression threshold false discovery rate
652 less than 5% and $\log_2$-fold change greater than 0.5) using scanpy
653 (https://scanpy.readthedocs.io/en/stable/). In doing so we detected two major subgroups of VISp
654 astrocytes that are distinguished by presence or absence of immediate-early gene markers (for
655 example, *Fos*, *Fosl2*, *Nr4a1*, *Irs2*, *Pde10a*, and *Pde7b*). This distinction may be an artifact of the cell
656 dissociation process for scRNA-seq; for the purposes of this study we collapse these cortical astrocyte
657 clusters. In order to understand the different regional characteristics of astrocyte populations we
658 mapped cells to whole brain taxonomy we mapped to the best-correlated mean-aggregated taxonomic
659 cluster from the ABC-WMB atlas[18] with 100 bootstrapped iterations using the top 10% of high-variance
660 genes and omitting a variable number of genes (10-50%) each round. We interpret the frequency of
661 correct mapping rounds as the mapping confidence. We also used CELLxGENE for single cell
662 visualization (https://github.com/chanzuckerberg/cellxgene). Spatial transcriptomic analysis was
663 performed as described in the recent whole brain transcriptomic taxonomy study[18], and cell type
664 location data was visualized using Cirrocumulus
665 (https://cirrocumulus.readthedocs.io/en/latest/index.html).

666 For determination of *Zic5* and *Sox10* differential gene expression between astrocytes and
667 oligodendrocytes, we used two-sided ANOVA on expression measurements from individually profiled
668 cells from all the experiments with no exclusion, and no covariates were tested. Testing for normality by
669 the Shapiro-Wilk test revealed that *Zic5* and *Sox10* expression are not normally distributed (*Zic5* W =
670 0.539, p-value < 2.2e-16; *Sox10* W = 0.958, p-value = 5.1e-16), so we used a non-parametric Wilcoxon
671 rank-sum test. No significance thresholds adjustments were made for multiple comparisons since only
672 one comparison was performed. For the comparison of *Sox10* versus *Zic5* expression (mean counts
673 per million +/- standard deviation, n cells): astrocyte *Zic5* expression 32 ± 71, n = 864; astrocyte *Sox10*
674 expression 0.3 ± 5, n = 864; oligodendrocyte *Zic5* expression 0.6 ± 6, n = 964, oligodendrocyte *Sox10*
675 expression 456 ± 276, n = 964.

676 *Motif analysis.* We performed de novo motif discovery from the sets of astrocyte and oligodendrocyte
677 enhancers that showed specific and strong expression patterns, excluding those enhancers scored as
678 weak. For astrocytes this list consisted of: AiE0375m, AiE0376h, AiE0376m, AiE0377m, AiE0380h,
679 AiE0381h, AiE0385h, AiE0385m, AiE0380h, AiE0390h, AiE0390m, AiE2120m, AiE2122m, AiE2160m,
680 and ProB12. For oligodendrocytes this list consisted of: AiE0361h, AiE0395h, AiE0395m, AiE0396h,
681 AiE0397m, AiE0398h, AiE0400m, AiE0401h, AiE0403h, AiE0407h, AiE0409h, AiE0409m, AiE0410h,
682 AiE0410m, and AiE0641m. We used MEME-CHIP[61] to identify recurrent de novo motifs in these sets of
683 sequences, using the parameter -meme-maxw 12, and comparing to a background set of random
684 sequence with the same nucleotide content. This analysis revealed one strong motif in each set of
685 sequences, as measured by its E-value, which is an estimate of the number of motifs expected by

686 chance to have as strong a log likelihood ratio as itself within the given sequences. These de novo
687 motifs where then mapped to known sequences using TomTom[61] which revealed several possible
688 matches to known motifs at significant p-values, but the strongest motif match (lowest p-value) in each
689 case is shown. In the case of the Zic family transcription factors, for simplicity we averaged together the
690 highly correlated strongest hits in the Zic family (JASPAR accession numbers MA0697.2, MA1628.1,
691 and MA1629.1 covering Zic1, Zic2, and Zic3), since Zic5 itself is not present in databases. In the case
692 of Sox10, the highly correlated Sox family members Sox4 and Sox11 (Uniprobe accession numbers
693 UP00062.1 and UP00030.1) showed slightly stronger motif match p-values than Sox10 (JASPAR
694 accession number MA0442.1), but these were excluded from analysis due to lack of expression in
695 almost all oligodendrocytes as observed by Tasic et al.[89] and in this study.

696 *Enhancer-AAV testing in rat.* The Allen Institute Institutional Animal Care and Use Committee (IACUC)
697 approved the following in vivo testing experiments in rat under protocol 2010. We procured timed-
698 pregnant female Sprague-Dawley rats from Charles River laboratories. We tattooed and injected ice-
699 anesthetized neonatal pups at P1 with 1.5e11 viral genomes of enhancer-AAV virus, diluted with PBS
700 to a total volume of 10 µL, unilaterally into the forebrain lateral ventricle (ICV delivery) with a 31-gauge,
701 4 point, 12º bevel 1 inch needle (custom ordered from Hamilton) and 25 µL capacity removable needle
702 syringe (Hamilton, 7636-01). Between injections we washed the needle and syringe with 100% ethanol,
703 and then nuclease-free water. We targeted the ICV space at 2 mm posterior to bregma, 2 mm lateral to
704 the anterior-posterior midline, and at a depth of 2 mm perpendicular to the surface of the skull. We
705 injected into the ventricle slowly over approximately 30 seconds. After injection, we held the needle in
706 place for approximately 10 seconds to prevent viral leakage, then slowly withdrew the needle at the
707 same relative angle as injection and then placed the animal onto a prewarmed heating pad in a clean
708 cage. We sacrificed pups at 18 days post injection, prior to weaning, and transcardially perfused with
709 1X PBS and then 4% PFA in PBS. We hemisected each brain and cryoprotected in 30% sucrose in
710 deionized water for a minimum of 24 hours before sectioning. We sectioned each brain at 30 µm
711 thickness using a sliding microtome (Leica part number SM2000R) on a leveled mount of Tissue-Tek®
712 O.C.T. Compound, collecting 3 sagittal planes separated by approximately 500 µm. We counterstained
713 sections with 1 µg/mL DAPI and 2.5 µg/mL propidium iodide (Thermo catalog # P1304MP) overnight at
714 4ºC and mounted in Vectashield HardSet Antifade Mounting Medium (Vector Laboratories # H-1400-
715 10) prior to imaging by epifluorescence.

716 *Macaque enhancer-AAV testing. Macaca nemestrina* (pig-tailed macaque) animals were housed and
717 injected at the Washington National Primate Center according to NIH guidelines and as approved by
718 the University of Washington Animal Care and Use Committee under UW IACUC protocol #41-6701.
719 These animals received several intraparenchymal injections under general anesthesia at spatially
720 distinct sites located at least ~1cm apart throughout the brain. During injection, over the course of 10
721 minutes we expelled a total of approximately 1e11 gc iodixanol gradient-purified PHP.eB-packaged
722 viral vectors in a total volume of 5 µL at 10 depths ranging from 200 to 2000 microns deep in the
723 animals. After injection the animal rested for 10 minutes between injections. These numbers are
724 approximate and timing, volume, and depths may be adjusted according to animal anatomy and
725 surgical considerations. The experiments described here result from four injection sites in three *Macaca*

726 *nemestrina* animals (two males, one female). We harvested tissue from these animals after necropsy at
727 38, 47, and 113 days post injection.

728 After locating the injection sites and cutting out tissue blocks about 1-2cm on each side surrounding the
729 injection sites, we fixed these tissue blocks in 4% PFA for 24 hrs. Then we rinsed the blocks with PBS,
730 cut 350 µm thick slices on the sliding microtome, and postfixed the slices in 4% PFA for 2 hours at
731 room temperature (RT), and then washed three times in PBS for 10 min each. For ISH analysis using
732 HCR we transferred slices to 70% EtOH at 4°C for a minimum of 12 hours, and up to 30 days. To stain
733 we first incubated the slices in 8% SDS in PBS at RT for two hours with agitation, then washed the
734 slices at RT with 5X sodium chloride sodium citrate (SSC) for three hours, exchanging with fresh 5X
735 SSC every hour. Next we performed HCR v3.0 using reagents and a modified protocol from Molecular
736 Technologies and Molecular Instruments[91]. We first incubated slices in pre-warmed 30% probe
737 hybridization buffer (30% formamide, 5X sodium chloride sodium citrate (SSC), 9 mM citric acid pH 6.0,
738 0.1% Tween 20, 50 µg/mL heparin, 1X Denhardt's solution, 10% dextran sulfate) at 37°C for 5 min.
739 Then we exchanged hybridization buffer for hybridization buffer containing probes added at a
740 concentration of 2 nM. Molecular Instruments designed the probes using the following accession
741 numbers: SLC17A7 – XM_011768126.1, GAD1 – XM_011744029.1, FGFR3 – XM_011744842.2,
742 SOX10 – XM_011712410.2. Hybridization proceeded overnight at 37°C, and afterwards we washed the
743 tissue thrice with 5X SSC for 10 minutes each (total 30 minutes), then 30% probe wash buffer (30%
744 formamide, 5X SSC, 9 mM citric acid pH 6.0, 0.1% Tween 20, 50 µg/mL heparin) for one hour at 37°C.
745 Then we exchanged probe wash buffer with 5X SSC, then amplification buffer (5X SSC, 0.1% Tween
746 20, 10% dextran sulfate) for 5 min at room temperature. Meanwhile we pooled even and odd
747 amplification hairpins for each of the three genes and snap-cooled them by heating to 95°C for 90
748 seconds then cooling to room temperature for 30 min, and afterwards we added the snap-cooled
749 hairpins to amplification buffer at a final concentration of 60 nM, and finally centrifuged at 18000g for 1
750 minute. Then we incubated tissue slices in amplification solution containing amplification hairpins for 4
751 hours at room temperature, followed by staining in DAPI (10µg/mL in 2X SSC) for 1 hour at room
752 temperature, and finally washing twice for 30 min in 2X SSC at room temperature before imaging. We
753 prepared a fresh aliquot of 67% 2,2'-Thiodiethanol (TDE) solution for use as a clearing and immersion
754 fluid by mixing ≥99% TDE (Sigma-Aldrich) with deionized water to create a 67% TDE solution with a
755 refractive index of 1.46. We transferred slices to 67% TDE and allowed them to equilibrate for at least 1
756 hour at room temperature prior to imaging on a confocal microscope (Olympus FV-3000). For IHC
757 analysis of injected NHP tissue we subsectioned 350 µm thick slices to 30 µm and stained as for
758 mouse tissue.

759 *Stereotaxic injection and fiber implant surgery.* Virus injection and optic fiber implantation surgery was
760 performed in C57BL/6J mice (The Jackson Laboratory, #000664) at around P60. Mice were
761 anesthetized with isoflurane and monitored throughout the surgery using breathing rate and tail pinch.
762 The skin above the skull surface was removed to make room for the fiber implant and headframe. After
763 leveling the skull, a craniotomy was drilled above the injection and fiber coordinates (AP: 1.2 mm, ML: -
764 1.3 mm, DV: 4.1 mm). First, a glass pipette positioned at the injection coordinates was lowered through
765 the craniotomy and virus injection was performed (100 nl, titer: 4e13 gc/mL). Once the injection was
766 complete, the pipette was slowly raised, and the optic fiber probe was positioned at the same AP and

767 ML coordinates as the injection. The tip of the fiber was then lowered to 100 μm above the injection site
768 and glued in place where the base of the fiber ferrule contacts the skull. A custom headframe was then
769 glued to the skull to allow head-fixed behavior and imaging. After surgery, the mouse was returned to
770 the home cage and allowed to recover for at least two weeks prior to start of water restriction for
771 behavior and imaging.

772 *Dynamic foraging reinforcement learning task.* Water-restricted and head-restrained mice were trained
773 to perform a reinforcement learning task where they freely choose between two lick ports that delivered
774 a water reward with nonstationary probabilities. This is a variation on the task described in Bari et al.[92].
775 The base reward probability of both lick ports summed to 0.6 where the probabilities of the two lick
776 ports were selected from two sets of ratios (0.53/0.07, 0.51/0.09). Block lengths that corresponded to
777 each ratio lasted for about 30 trials (min trials per block: 40, max trials per block: 60). Each trial began
778 with an auditory "go cue" that signaled the start of a trial. The mouse was free to choose between the
779 left or right lick port immediately after the "go cue". The trials were separated by a variable inter-trial-
780 interval (range between 1-7 seconds). The data shown in this study was from a two-hour behavior
781 session that consisted of 438 trials (170 rewarded trials).

782 *Fiber photometry and analysis.* Fiber photometry was performed using a commercially available
783 photometry system (Neurophotometrics LLC, FP3002). A 470 nm LED was used to excite the
784 iAChSnFR fluorophore, Venus, and the emitted fluorescence signals were collected using a CMOS
785 camera. The 470 nm excitation was interleaved with a 415 nm LED as an isosbestic control to remove
786 motion artifacts. Bonsai acquisition software was used to record the photometry signals as well as the
787 behavior trigger signals events (go-cue, left and/or right lick choices, reward/no reward) for offline
788 alignment of imaging data to behavioral events. Prior to start of acquisition, an ROI was drawn over the
789 fiber image seen on the camera, and fluorescence intensity within this ROI was averaged for real-time
790 signal visualization and offline analysis. First, the fiber photometry acquisition was started, following
791 which the behavior task was initialized. Photometry signals were analyzed using custom python scripts.
792 First, the fluorescence signal was detrended for photobleaching using a fourth order polynomial
793 function and then corrected for motion using the control signal from the 415 nm excitation using
794 standard photometry analysis techniques[93]. Acetylcholine signal changes were calculated as a change
795 in fluorescence intensity over the mean fluorescence ($\Delta F/F$ as a percentage). The photometry signals
796 were then aligned to behavior events using simultaneously acquired TTL readouts of behavior events
797 (go-cue, left and/or right lick choices, reward/no reward) using a NI USB card. These behavior events
798 were then used to calculate trial averaged traces of rewarded and unrewarded signals.

799

Data Availability:

All AAV viral vector plasmids are freely available for research use at Addgene (addgene.org/). Mouse scRNA-seq generated from this study are available at GEO with the accession number GSE235987 (https://www.ncbi.nlm.nih.gov/geo/). Mouse primary testing data are available at the Allen Genetic Tools Atlas (https://portal.brain-map.org/genetic-tools/genetic-tools-atlas). Serial two photon tomography datasets will be made available through the Brain Imaging Library (https://www.brainimagelibrary.org/). All other data will be made available upon request.

Ethics Declarations:

Competing interests

Several authors including ESL, JTT, JKM, RAM, XOA, BT and BPL are inventors on one PCT stage patent application (PCT_US2021_024525) and one provisional patent covering vectors described in this manuscript. BPL is a scientific advisor for Patch Bioscience.

Acknowledgements

We would like to thank the Washington National Primate Center and staff for animal care, as well as the supporting grant P51OD010425 from the National Institutes of Health to support primate research. The WaNPRC SPF *M. nemestrina* colony is supported by grant U42OD011123 from the NIH Office of Research Infrastructure Programs. We would like to acknowledge Kathryn Gudsnuk for programmatic support. This work was supported by the following grants: RF1MH114126-01 from the National Institute of Mental Health to BPL, JTT, and ESL; UG3MH120095-01, -02, -03 from the National Institute of Mental Health to BPL, JTT, ESL, and FKK, UF1MH128339-01 from the National Institute of Mental Health to BT, TB, TLD, BPL, and JTT, RF1MH121274-01 from the National Institute for Mental Health to BT and U19MH114830 to HZ. We also would like to acknowledge the estate of Paul G. Allen for his vision, encouragement, and support.

Figures and Figure Legends

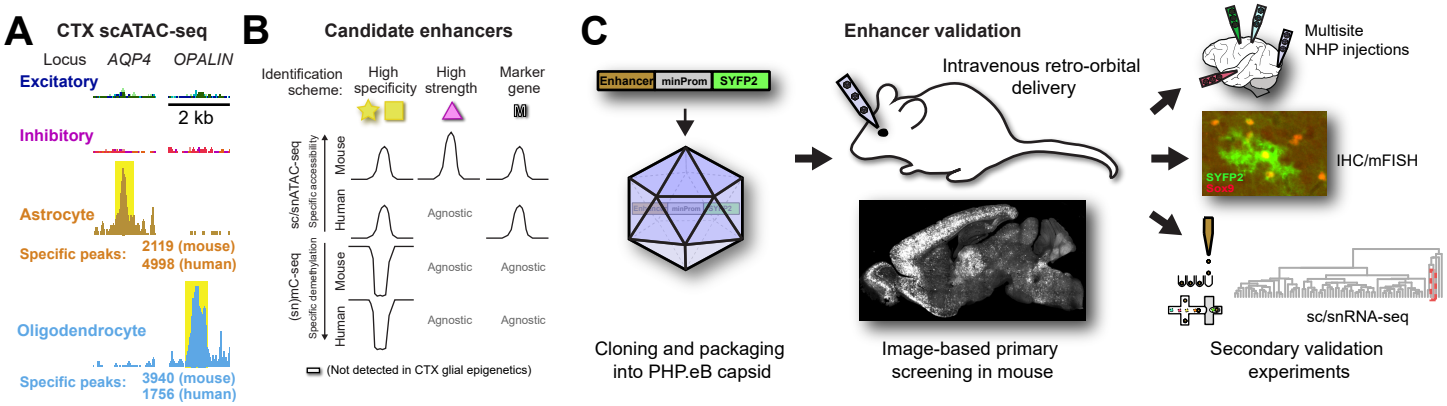
A
CTX scATAC-seq
Locus
AQP4
OPALIN
Excitatory
2 kb
Inhibitory
Astrocyte
Specific peaks:
2119 (mouse)
4998 (human)
Oligodendrocyte
Specific peaks:
3940 (mouse)
1756 (human)
B
Candidate enhancers
Identification scheme:
High specificity
High strength
Marker gene
sc/snATAC-seq
Specific accessibility
Mouse
Human
Agnostic
(sn)mC-seq
Specific demethylation
Mouse
Human
Agnostic
Agnostic
Agnostic
Agnostic
(Not detected in CTX glial epigenetics)
C
Enhancer validation
Enhancer
minProm
SYFP2
Intravenous retro-orbital delivery
Multisite NHP injections
IHC/mFISH
SYFP2
Dcx3
sc/snRNA-seq
Cloning and packaging into PHP.eB capsid
Image-based primary screening in mouse
Secondary validation experiments

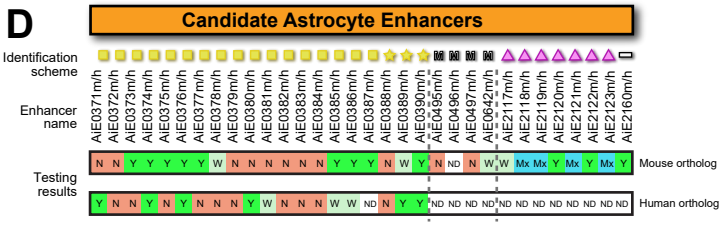
D
Candidate Astrocyte Enhancers
Identification scheme
Enhancer name
AiE0371m/h
AiE0372m/h
AiE0373m/h
AiE0374m/h
AiE0375m/h
AiE0376m/h
AiE0377m/h
AiE0378m/h
AiE0379m/h
AiE0380m/h
AiE0381m/h
AiE0382m/h
AiE0383m/h
AiE0384m/h
AiE0385m/h
AiE0386m/h
AiE0387m/h
AiE0388m/h
AiE0389m/h
AiE0390m/h
AiE0495m/h
AiE0496m/h
AiE0497m/h
AiE0642m/h
AiE2117m/h
AiE2118m/h
AiE2119m/h
AiE2120m/h
AiE2121m/h
AiE2122m/h
AiE2123m/h
AiE2160m/h
Testing results
N N Y Y Y Y Y W N N N N N N Y Y Y N W Y N ND N W W Mx Mx Y Mx Y Mx Y
Mouse ortholog
Y N N Y N Y N N N Y W N N N W W ND N Y Y ND ND ND ND ND ND ND ND ND ND ND ND ND
Human ortholog
Overall Specific Astrocyte success rate = 25 / 50 = 50%

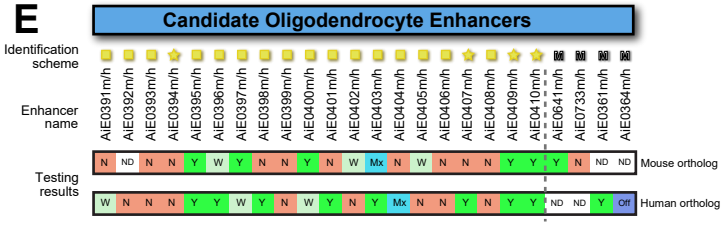
E
Candidate Oligodendrocyte Enhancers
Identification scheme
Enhancer name
AiE0391m/h
AiE0392m/h
AiE0393m/h
AiE0394m/h
AiE0395m/h
AiE0396m/h
AiE0397m/h
AiE0398m/h
AiE0399m/h
AiE0400m/h
AiE0401m/h
AiE0402m/h
AiE0403m/h
AiE0404m/h
AiE0405m/h
AiE0406m/h
AiE0407m/h
AiE0408m/h
AiE0409m/h
AiE0410m/h
AiE0641m/h
AiE0733m/h
AiE0361m/h
AiE0364m/h
Testing results
N ND N N Y W Y N N Y N W Mx N W N N N Y Y Y N ND ND
Mouse ortholog
W N N N Y Y W Y N W Y N Y Mx N N Y N Y Y ND ND Y Off
Human ortholog
Overall Specific Oligodendrocyte success rate = 21 / 43 = 49%

825 **Figure 1: Astrocyte and oligodendrocyte enhancer discovery from single cell epigenetics.**
826
827 (**A**) Example astrocyte- and oligodendrocyte-specific peaks near the loci of astrocyte-specific gene
828 *AQP4* and oligodendrocyte-specific gene *OPALIN*, identified in human MTG snATAC-seq data[33].

829 (**B**) Differing approaches to identify candidate enhancers. Specific accessibility peaks are depicted as
830 peaks, and specifically demethylated regions are depicted as troughs. Schemes not utilizing a particular
831 data modality are shown as "Agnostic". Marker gene selection criteria can use accessibility from either
832 mouse or human. Icons represent identification schemes; gold star candidate enhancers undergo more
833 stringent criteria than those with gold squares (see Methods for details).

834 (**C**) Workflow for enhancer cloning, packaging, screening, and validation. Enhancers are cloned into a
835 pAAV plasmid upstream of a minimal human beta-globin promoter and SYFP2 reporter, and plasmids
836 are packaged into PHP.eB AAVs. Enhancer-AAVs are injected intravenously into retro-orbital sinus,
837 and expression is assessed by imaging. Promising enhancer-AAVs then go on to secondary validation
838 experiments consisting of cross-species validation, molecular characterization by IHC and/or
839 multiplexed FISH, and flow cytometry for single cell RNA-seq.

840 (**D-E**) Candidate identification schemes and summarized screening results for astrocyte-specific (**D**)
841 and oligodendrocyte-specific enhancers (**E**). Overall 50% (25/50) of candidate astrocyte enhancers,
842 and 49% (21/43) of candidate oligodendrocyte enhancers, show the intended specificity after
843 intravenous delivery of PHP.eB AAVs. Testing result bar: Y = yes, enhancer-AAV gives strong or
844 moderate on-target expression pattern; N = no, enhancer-AAV fails to express; W = weak on-target
845 expression pattern; Mx = mixed expression pattern consisting of on-target cells plus unwanted neuronal
846 populations; Off = off-target expression pattern; ND = no data. Note both enhancers giving
847 strong/moderate ("Y") and weak ("W") specific expression are grouped here for overall success rate
848 analysis.

849

850

851

852

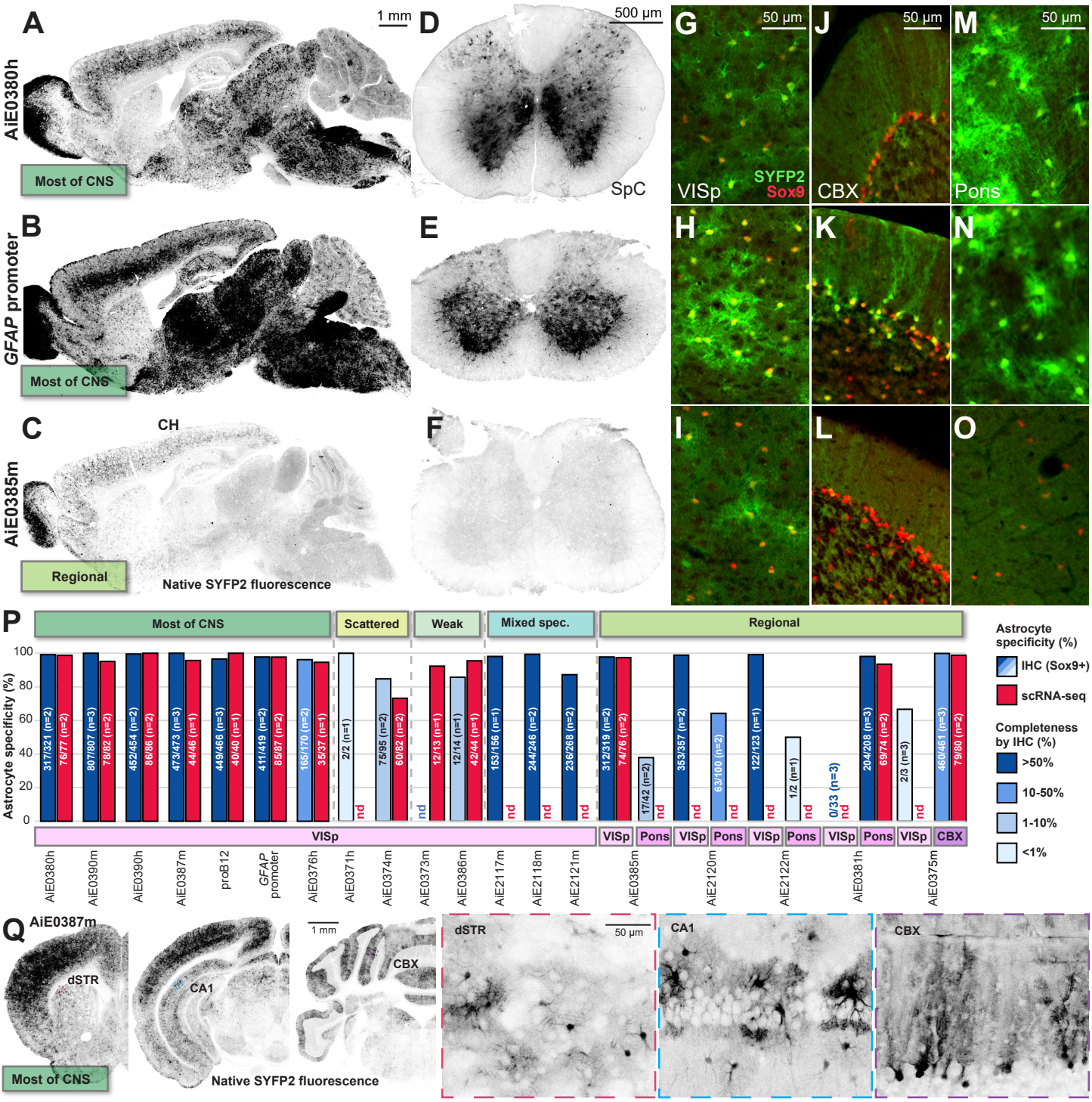
A
1 mm
AiE0380h
Most of CNS
D
500 µm
SpC
G
50 µm
VISp
SYFP2
Sox9
J
50 µm
CBX
M
50 µm
Pons
B
GFAP promoter
Most of CNS
E
H
K
N
C
CH
AiE0385m
Regional
Native SYFP2 fluorescence
F
I
L
O
P
Most of CNS
Scattered
Weak
Mixed spec.
Regional
Astrocyte specificity (%)
Astrocyte specificity (%)
IHC (Sox9+)
scRNA-seq
Completeness by IHC (%)
>50%
10-50%
1-10%
<1%
317/321 (n=2)
76/77 (n=2)
807/807 (n=3)
78/82 (n=2)
452/454 (n=2)
86/86 (n=2)
473/473 (n=3)
44/46 (n=1)
449/466 (n=3)
40/40 (n=1)
411/419 (n=2)
85/87 (n=2)
165/170 (n=2)
35/37 (n=1)
2/2 (n=1)
nd
75/95 (n=2)
60/82 (n=2)
nd
12/13 (n=1)
12/14 (n=1)
42/44 (n=1)
153/156 (n=1)
nd
244/246 (n=2)
nd
236/268 (n=2)
nd
312/319 (n=2)
74/76 (n=2)
17/42 (n=2)
nd
353/357 (n=2)
nd
63/100 (n=2)
nd
122/123 (n=1)
nd
1/2 (n=1)
nd
0/33 (n=3)
nd
204/208 (n=3)
69/74 (n=2)
2/3 (n=3)
nd
460/461 (n=3)
79/80 (n=2)
VISp
VISp
Pons
VISp
Pons
VISp
Pons
VISp
Pons
VISp
CBX
AiE0380h
AiE0390m
AiE0390h
AiE0387m
proB12
GFAP promoter
AiE0376h
AiE0371h
AiE0374m
AiE0373m
AiE0386m
AiE2117m
AiE2118m
AiE2121m
AiE0385m
AiE2120m
AiE2122m
AiE0381h
AiE0375m
Q
AiE0387m
dSTR
Most of CNS
CA1
1 mm
CBX
Native SYFP2 fluorescence
dSTR
50 µm
CA1
CBX

853 **Figure 2: A collection of astrocyte-specific enhancer-AAV vectors with varying regional**
854 **specificities and expression densities.**
855
856 (**A-B**) Astrocyte-specific enhancer-AAVs marking many astrocytes throughout most of the CNS.
857 AiE0380h (**A**, n = 8 animals tested) and *GFAP* promoter (**B**, n = 3) mark many astrocytes throughout
858 gray matter in FB, MB, HB, and CBX.

859 (**C**) AiE0385m shows a regional pattern labeling astrocytes in cerebrum (CH) but not in MB, HB, or
860 CBX (n = 6).

861 (**D-F**) Astrocyte-specific enhancer-AAVs labeling astrocytes in lumbar SpC. AiE0380h (**D**) and *GFAP*
862 promoter (**E**) label many astrocytes in SpC gray matter, but AiE0385m (**F**) does not label SpC
863 astrocytes.

864 (**G-O**) Positive confirmation of molecular astrocyte identity across brain regions. SYFP2+ astrocytes are
865 colabeled with anti-Sox9 immunoreactivity in VISp, CBX, and Pons. Images in G-O represent n = 2
866 animals each assessed by IHC.

867 (**P**) Quantification of specificity for astrocytes by astrocyte enhancer-AAVs. Specificity and
868 completeness for astrocyte labeling by enhancer-AAVs was quantified by costaining with anti-Sox9
869 antibody in VISp, Pons, and CBX. Specificity is defined as the number of SYFP2+Sox9+ / total SYFP2+
870 cells x 100%. Completeness is defined as the number of SYFP2+Sox9+ / total Sox9+ cells x 100%.
871 Brains from one to three mice per condition were analyzed, with range 131-827 cells counted (median
872 311) per brain region analyzed. AiE0375m-labeling was only quantified in the Purkinje cell layer of
873 CBX, not in the granule or molecular layers. Specificity was also quantified by scRNA-seq, defined as
874 the percentage of sorted SYFP2+ cells mapping as astrocytes within the VISp molecular taxonomy[89].
875 Overall, specificity is high for many astrocyte-specific vectors, with "Scattered" and "Weak" vectors
876 showing low completeness, and "Regional" vectors showing more completeness in certain regions. One
877 to three animals were analyzed per vector per modality, as indicated. The same IHC specificity data for
878 *GFAP* promoter-SYFP2 are repeated in **Figure 6B.**

879 (**Q**) Distinct astrocyte morphologies throughout the brain with AiE0387m enhancer-AAV targeting "Most
880 of CNS". Images were acquired on a serial two-phtoton tomography blockface imaging platform (STPT,
881 TissueCyte, n = 4 tested).

882 Abbreviations: CH cerebrum, dSTR dorsal striatum, CA1 cornu ammonis 1, CBX cerebellar cortex, SpC
883 spinal cord, VISp primary visual cortex.

884
885

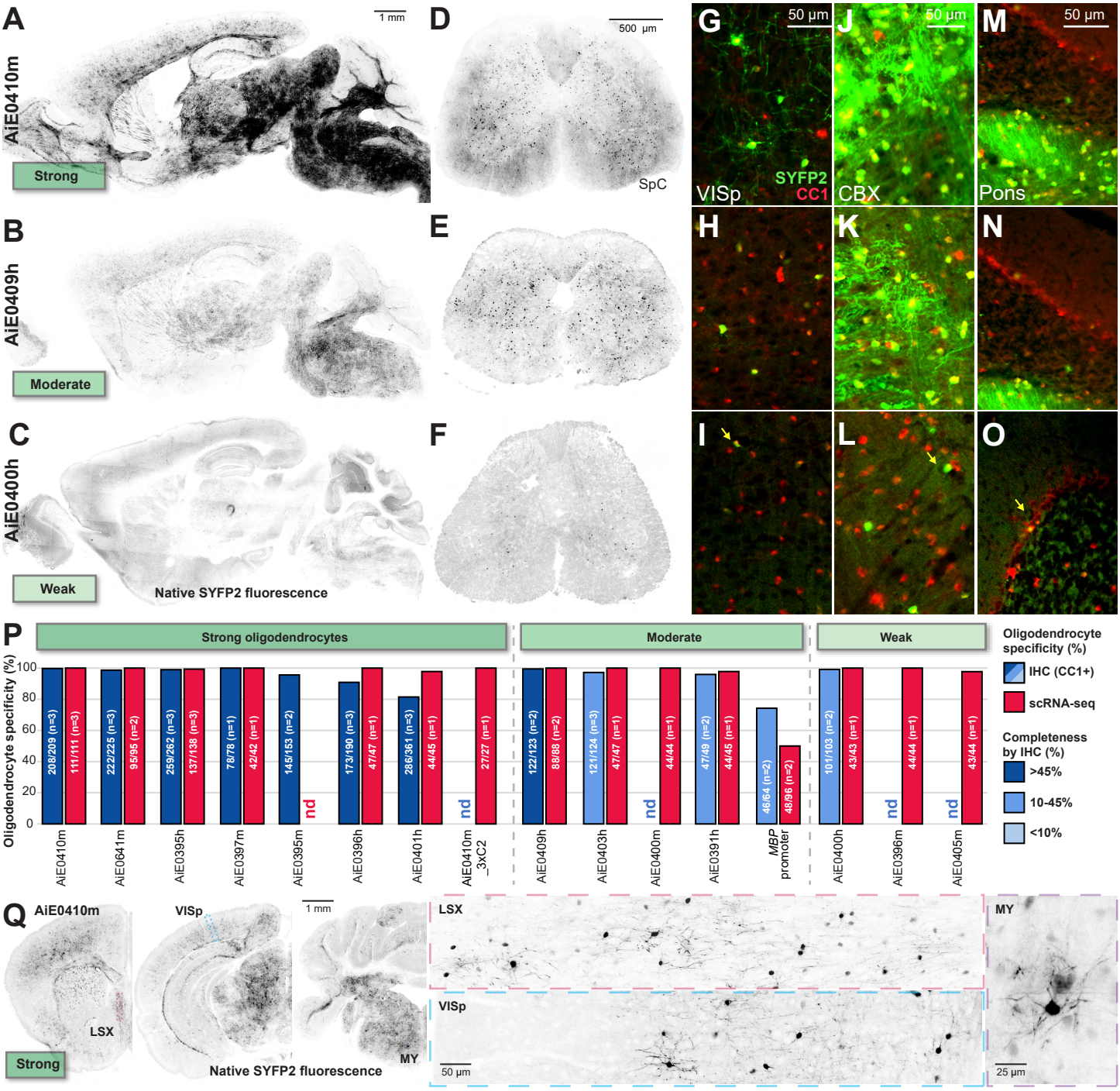
A
AiE0410m
Strong
1 mm
B
AiE0409h
Moderate
C
AiE0400h
Weak
Native SYFP2 fluorescence
D
500 µm
SpC
E
F
G
50 µm
SYFP2
CC1
VISp
J
CBX
M
Pons
H
K
N
I
L
O
P
Strong oligodendrocytes
Moderate
Weak
Oligodendrocyte specificity (%)
100
80
60
40
20
0
208/209 (n=3)
111/111 (n=3)
222/225 (n=3)
95/95 (n=2)
259/262 (n=3)
137/138 (n=3)
78/78 (n=1)
42/42 (n=1)
145/153 (n=2)
nd
173/190 (n=3)
47/47 (n=1)
286/361 (n=3)
44/45 (n=1)
nd
27/27 (n=1)
122/123 (n=2)
88/88 (n=2)
121/124 (n=3)
47/47 (n=1)
nd
44/44 (n=1)
47/49 (n=2)
44/45 (n=1)
46/64 (n=2)
48/96 (n=2)
101/103 (n=2)
43/43 (n=1)
nd
44/44 (n=1)
nd
43/44 (n=1)
AiE0410m
AiE0641m
AiE0395h
AiE0397m
AiE0395m
AiE0396h
AiE0401h
AiE0410m_3xC2
AiE0409h
AiE0403h
AiE0400m
AiE0391h
MBP promoter
AiE0400h
AiE0396m
AiE0405m
Oligodendrocyte specificity (%)
IHC (CC1+)
scRNA-seq
Completeness by IHC (%)
>45%
10-45%
<10%
Q
AiE0410m
LSX
Strong
VISp
1 mm
MY
Native SYFP2 fluorescence
LSX
VISp
50 µm
MY
25 µm

886 **Figure 3: A collection of oligodendrocyte-specific enhancer-AAV vectors with varying levels of**
887 **expression.**
888
889 (**A-C**) Oligodendrocyte enhancer-AAVs marking many oligodendrocytes throughout most of the CNS.
890 AiE0410m (**A**, n = 7 animals tested), AiE0409h (**B**, n = 5), and AiE0400h (**C**, n = 4) label many
891 oligodendrocytes throughout FB, MB, HB, and CBX, but at differing expression levels.

892 (**D-F**) Oligodendrocyte enhancer-AAVs marking oligodendrocytes in lumbar SpC. AiE0410m (**D**),
893 AiE0409h (**E**), and AiE0400h (**F**) mark oligodendrocytes in gray and white matter of SpC, but at
894 different intensities.

895 (**G-O**) Positive confirmation of molecular oligodendrocyte identity across brain regions. SYFP2+
896 oligodendrocytes are colabeled with CC1 immunoreactivity in VISp, CBX, and Pons. Two to three
897 animals per enhancer-AAV were analyzed.

898 (**P**) Quantification of specificity for oligodendrocytes by oligodendrocyte enhancer-AAVs. Specificity and
899 completeness for oligodendrocyte labeling by enhancer-AAVs was quantified by costaining with CC1
900 antibody in VISp. Specificity is defined as the number of SYFP2+CC1+ / total SYFP2+ cells x 100%.
901 Completeness is defined as the number of SYFP2+CC1+ / total CC1+ cells x 100%. Brains from one to
902 three mice per condition were analyzed, with range 101-332 cells counted (median 147) per brain
903 region analyzed. Specificity was also quantified by scRNA-seq, defined as the percentage of sorted
904 SYFP2+ cells mapping as oligodendrocytes within the VISp molecular taxonomy[89]. One to three
905 animals were analyzed per vector per modality, as indicated. Overall, specificity is high for many
906 oligodendrocyte-specific vectors, with “Weak” vectors showing low completeness.

907 (Q) Myelinating oligodendrocyte morphologies throughout the brain with AiE0410m. Sections were
908 visualized with STPT (n = 2 tested).

909 Abbreviations: SpC spinal cord, VISp primary visual cortex, CBX cerebellar cortex, LSX lateral septal
910 complex, MY medulla.

911
912

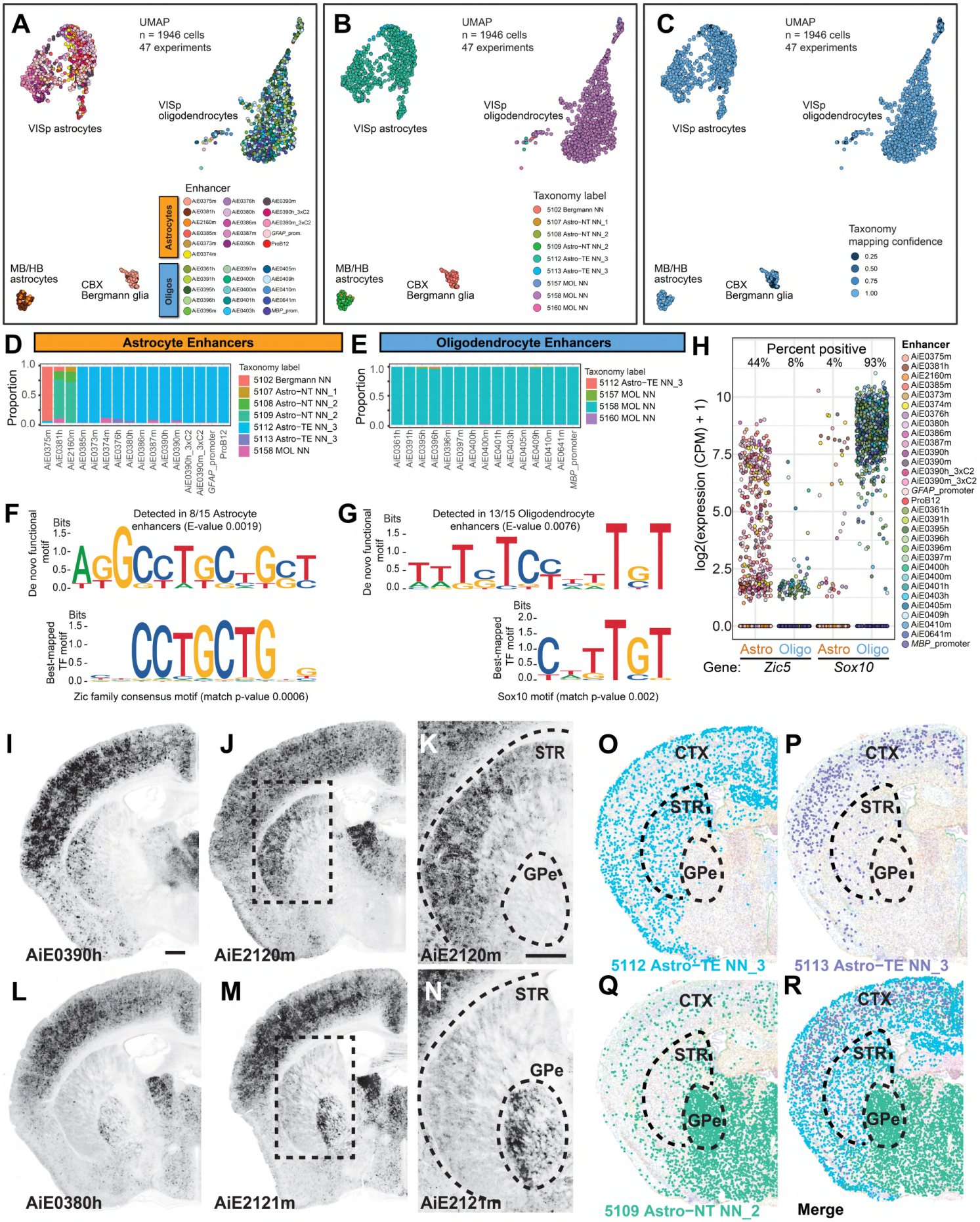
A
UMAP
n = 1946 cells
47 experiments
VISp astrocytes
VISp oligodendrocytes
MB/HB astrocytes
CBX Bergmann glia
Enhancer
Astrocytes
Oligos
B
Taxonomy label
5102 Bergmann NN
5107 Astro−NT NN_1
5108 Astro−NT NN_2
5109 Astro−NT NN_2
5112 Astro−TE NN_3
5113 Astro−TE NN_3
5157 MOL NN
5158 MOL NN
5160 MOL NN
C
Taxonomy mapping confidence
0.25
0.50
0.75
1.00
D
Astrocyte Enhancers
Proportion
E
Oligodendrocyte Enhancers
H
Percent positive
44% 8% 4% 93%
log2(expression (CPM) + 1)
Astro Oligo Astro Oligo
Gene: Zic5 Sox10
F
Detected in 8/15 Astrocyte enhancers (E-value 0.0019)
De novo functional motif
Best-mapped TF motif
Zic family consensus motif (match p-value 0.0006)
G
Detected in 13/15 Oligodendrocyte enhancers (E-value 0.0076)
Sox10 motif (match p-value 0.002)
I
AiE0390h
J
AiE2120m
K
STR
GPe
AiE2120m
O
CTX
STR
GPe
5112 Astro−TE NN_3
P
5113 Astro−TE NN_3
L
AiE0380h
M
AiE2121m
N
AiE2121m
Q
5109 Astro−NT NN_2
R
Merge

913 **Figure 4: Transcriptomic identities of prospectively targeted astrocytes and oligodendrocytes.**
914
915 (**A-C**) Groups of transcriptomically profiled single cells, as visualized by UMAP. Single cells labeled by
916 various astrocyte- and oligodendrocyte-specific enhancer-AAVs (n = 1946 quality-filtered cells) were
917 profiled from 47 brains in 47 independent experiments by SMARTerV4[89], one to three animals per
918 enhancer. Libraries were aligned to mm10 and transformed into UMAP space for visualization, with
919 coloring by enhancer (**A**), mapped taxonomic cell type cluster (**B**), and taxonomic mapping confidence
920 (**C**). Overall CTX astrocytes group away from CTX oligodendrocytes as expected, and MB/HB
921 astrocytes and Bergmann glia astrocytes group away from CTX astrocytes, consistent with recent
922 results[18]. Note that AiE0381h- and AiE2160m-labeled astrocytes were dissected from MB/HB region,
923 and AiE0375m-labeled Bergmann glia were dissected from CBX region, but the remainder of the cells
924 were dissected from VISp.

925 (**D-E**) Quantifications of taxonomic cell type cluster mapping by enhancer vector. Prospectively labeled
926 astrocytes from all enhancer-AAV vectors dissected from VISp predominantly map to cluster "5112
927 Astro-TE NN_3", whereas those from MB/HB dissections (AiE0381h and AiE2160m) predominantly
928 map to cluster "5109 Astro-NT NN_2", and AiE0375m-labeled astrocytes from CBX dissections
929 predominantly map to cluster "5102 Bergmann NN". In contrast, all prospectively labeled
930 oligodendrocytes predominantly map to cluster "5158 MOL NN". Cluster identities are from a recent
931 whole mouse brain taxonomy study[18].

932 (**F-H**) De novo motif detection in astrocyte- and oligodendrocyte-specific enhancer sequences using
933 MEME-CHIP[61] identifies one strong consensus motif in each set of sequences (top). These de novo
934 motifs were mapped against databases of known TF motifs using TomTom (bottom), which identified
935 the top hits as the Zic family consensus motifs for astrocytes, and Sox family motif for oligodendrocytes
936 (Sox10 shown). These TFs (Zic5 and Sox10) show highly specific expression differences between
937 astrocytes and oligodendrocytes from prospective scRNA-seq profiling (**H**). *** non-parametric
938 Wilcoxon rank-sum test W = 577624 (*Zic5*) or W = 9838 (*Sox10*), $p < 1e-16$ each.

939 (**I-N**) Intrinsic SYFP2 expression from the indicated enhancer-AAVs after retro-orbital administration.
940 Images were generated by STPT. Boxes in I and L correspond to K and N, respectively. Scale in I and
941 K is 500 µm.

942 (**O-R**) MERFISH data showing the distribution of three astrocyte cell types revealed by single cell gene
943 expression from the whole mouse brain[18].

944 Abbreviations: CTX cerebral cortex, STR striatum, GPe globus pallidus, external segment.

945

946

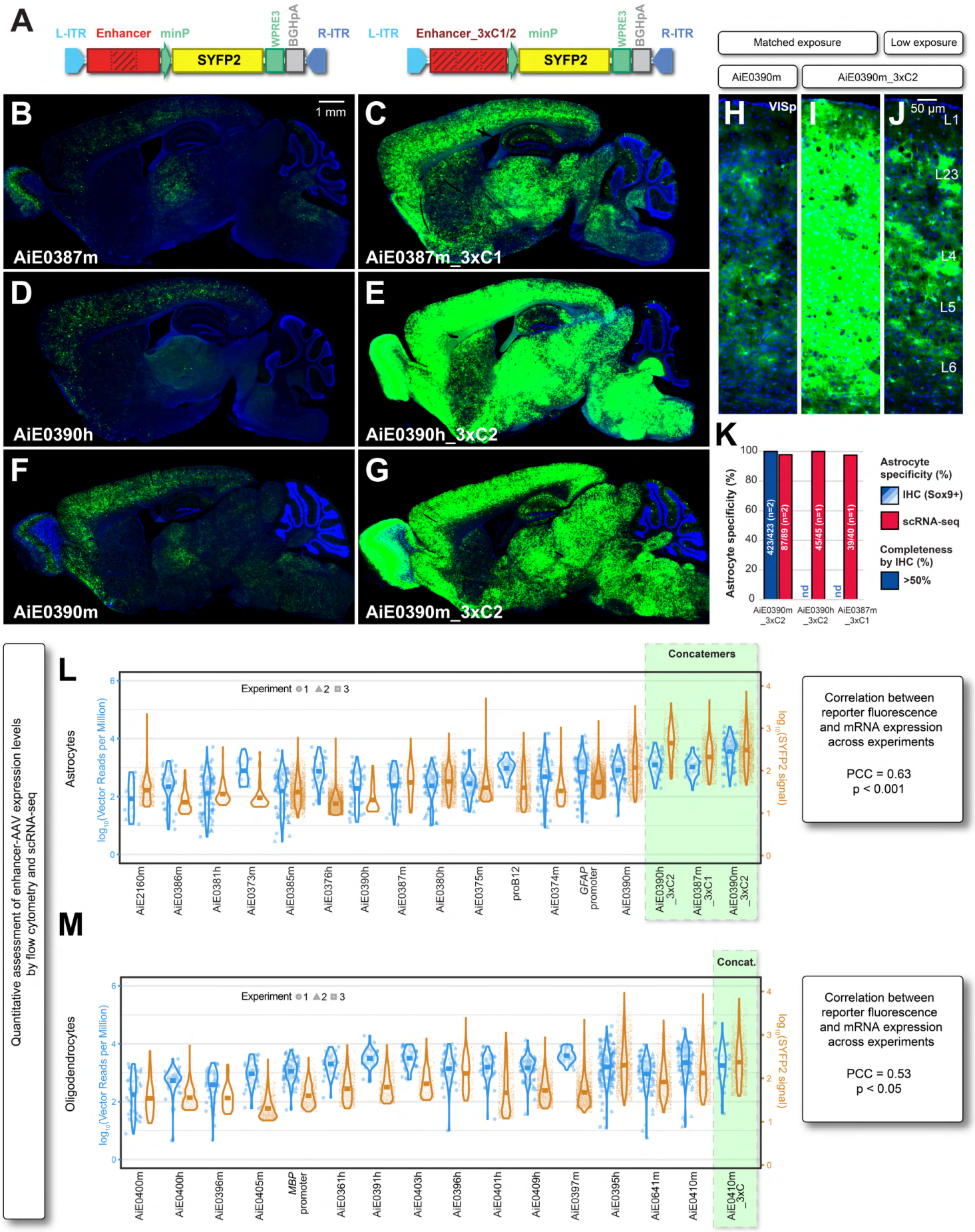
A
L-ITR
Enhancer
minP
SYFP2
WPRE3
BGHpA
R-ITR
L-ITR
Enhancer_3xC1/2
minP
SYFP2
WPRE3
BGHpA
R-ITR
B
1 mm
AiE0387m
C
AiE0387m_3xC1
D
AiE0390h
E
AiE0390h_3xC2
F
AiE0390m
G
AiE0390m_3xC2
Matched exposure
Low exposure
AiE0390m
AiE0390m_3xC2
H
VISp
I
J
50 µm
L1
L23
L4
L5
L6
K
Astrocyte specificity (%)
423/423 (n=2)
87/89 (n=2)
nd
45/45 (n=1)
nd
39/40 (n=1)
AiE0390m _3xC2
AiE0390h _3xC2
AiE0387m _3xC1
Astrocyte specificity (%)
IHC (Sox9+)
scRNA-seq
Completeness by IHC (%)
>50%
Quantitative assessment of enhancer-AAV expression levels by flow cytometry and scRNA-seq
L
Astrocytes
Concatemers
Experiment 1 2 3
log10(Vector Reads per Million)
log10(SYFP2 signal)
AiE2160m
AiE0386m
AiE0381h
AiE0373m
AiE0385m
AiE0376h
AiE0390h
AiE0387m
AiE0380h
AiE0375m
proB12
AiE0374m
GFAP promoter
AiE0390m
AiE0390h _3xC2
AiE0387m _3xC1
AiE0390m _3xC2
Correlation between reporter fluorescence and mRNA expression across experiments
PCC = 0.63
p < 0.001
M
Oligodendrocytes
Concat.
Experiment 1 2 3
log10(Vector Reads per Million)
log10(SYFP2 signal)
AiE0400m
AiE0400h
AiE0396m
AiE0405m
MBP promoter
AiE0361h
AiE0391h
AiE0403h
AiE0396h
AiE0401h
AiE0409h
AiE0397m
AiE0395h
AiE0641m
AiE0410m
AiE0410m _3xC
Correlation between reporter fluorescence and mRNA expression across experiments
PCC = 0.53
p < 0.05

947 **Figure 5: Optimizing astrocyte and oligodendrocyte enhancer strength.**
948
949 (**A**) Native Enhancer and for Enhancer_3xC2 vector designs. The central approximate third of the
950 enhancer (the "Core2" element) is marked by dark hatches, and this element is triply concatemerized in
951 the Enhancer_3xC2 vector. Alternatively, the first or third segment ("Core1" or "Core3") may be
952 concatemerized (determined empirically).

953 (**B-J**) Dramatic increase in expression levels while maintaining specificity using Enhancer_3xC1/2
954 vector designs. Brains from mice injected with the Enhancer or Enhancer_3xC1/2 vectors were
955 processed and imaged in parallel in these experiments. (**H-J**) Zoom in view of AiE0390m- and
956 AiE0390m_3xC2-injected mouse VISp shows high specificity for morphological astrocytes throughout
957 cortical layers in both cases. Data represent one to two animals per vector with parallel tissue
958 processing and imaging.

959 (**K**) Quantification of specificity for astrocytes by concatemer astrocyte enhancer-AAVs within VISp by
960 IHC and scRNA-seq as described in **Figure 2P**. The same IHC data for AiE0390m_3xC2 are repeated
961 in **Figure 6B**.

962 (**L-M**) Direct correlated quantification of enhancer strength by flow cytometry and scRNA-seq, for both
963 astrocyte- (**L**) and oligodendrocyte-specific (**M**) enhancer-AAVs. The left (blue) y-axis represents the
964 log-transformed vector transgene reads per million in individual sorted scRNA-seq-profiled cells. The
965 right (brown) y-axis represents the log-transformed SYFP2 signal intensity of positively gated vector-
966 expressing cells observed on the flow cytometer, quantified as the fold signal of positive cells
967 normalized to non-expressing cell autofluorescence (taken as background). Points represent individual
968 cells observed by scRNA-seq and by flow cytometry, visualized also as violins, and with the horizontal
969 bar representing mean expression levels across all cells expressing that enhancer-AAV, across one to
970 three replicate experiments per vector. Across all experiments, we observe significant correlation
971 between mean expression intensity at the RNA level by scRNA-seq, and mean SYFP2 reporter
972 expression by signal intensity (astrocytes: $n = 26$ experiments, Pearson correlation coefficient [PCC]
973 0.63, $t = 3.97$, $df = 24$, $p = 0.00057$; oligodendrocyte $n = 22$ experiments, PCC 0.53, $t = 2.82$, $df = 20$, p
974 $= 0.011$; correlation t-tests). Furthermore, 3xC astrocyte enhancers are among the strongest enhancers
975 we have characterized, typically several fold stronger than their native counterparts. One to three
976 animals were analyzed per enhancer-AAV vector (the same dataset described in **Figure 4A**).

977 Abbreviations: VISp primary visual cortex.

978

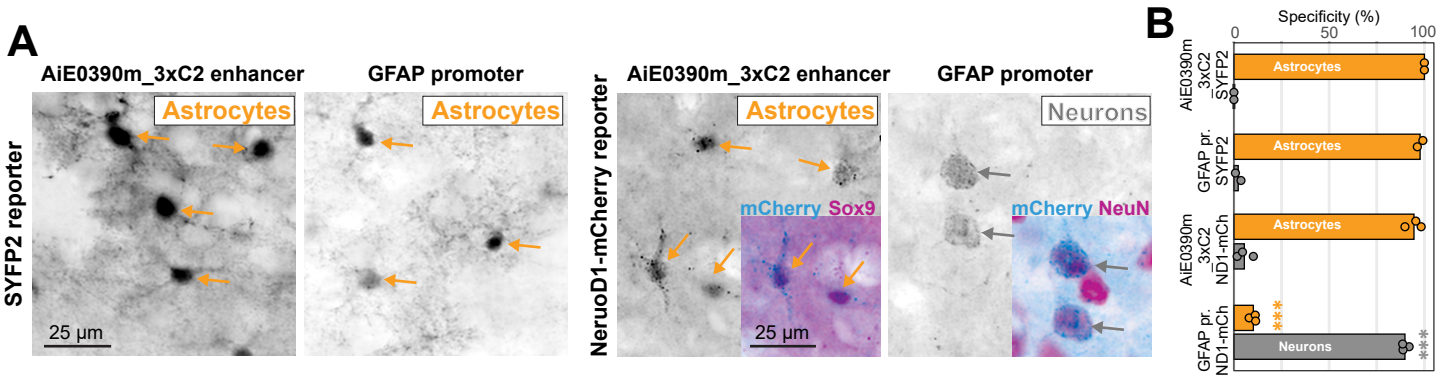
A
AiE0390m_3xC2 enhancer
GFAP promoter
SYFP2 reporter
Astrocytes
Astrocytes
25 µm
NeruoD1-mCherry reporter
AiE0390m_3xC2 enhancer
GFAP promoter
Astrocytes
Neurons
mCherry Sox9
mCherry NeuN
25 µm
B
Specificity (%)
0
50
100
AiE0390m 3xC2 SYFP2
GFAP pr. SYFP2
AiE0390m 3xC2 ND1-mCh
GFAP pr. ND1-mCh
Astrocytes
Astrocytes
Astrocytes
Neurons
***
***

979 **Figure 6: Robust specificities of astrocyte enhancer-AAVs with a difficult transgene cargo.**

980 (**A-B**) Specific delivery of a difficult transgene cargo with an optimized astrocyte-specific transgene.
981 Mice received the indicated enhancer-AAVs driving either SYFP2 or NeuroD1-mCherry by intravenous
982 PHP.eB AAVs (5e11 gc per animal), and expression analyzed in brain by IHC with NeuN neuronal
983 marker or Sox9 astrocyte marker. Specificity for neurons and astrocytes was quantified as
984 (Reporter+[NeuN or Sox9]+ cells) / (All Reporter+ cells) in primary visual cortex (VISp, Layer 5 cells
985 shown, n=2-3 animals per condition). The same IHC specificity data for *GFAP* promoter-SYFP2 and
986 AiE0390m_3xC2-SYFP2 are repeated in **Figures 2P** and **5K**, respectively. Two to three animals were
987 analyzed per condition (each dot represents one animal). *** ANOVA with Tukey's post hoc adjustment
988 for multiple comparisons, $F = 647$, $p < 1e-7$, for *GFAP* promoter-driven NeuroD1-mCherry compared to
989 every other condition.

990

991

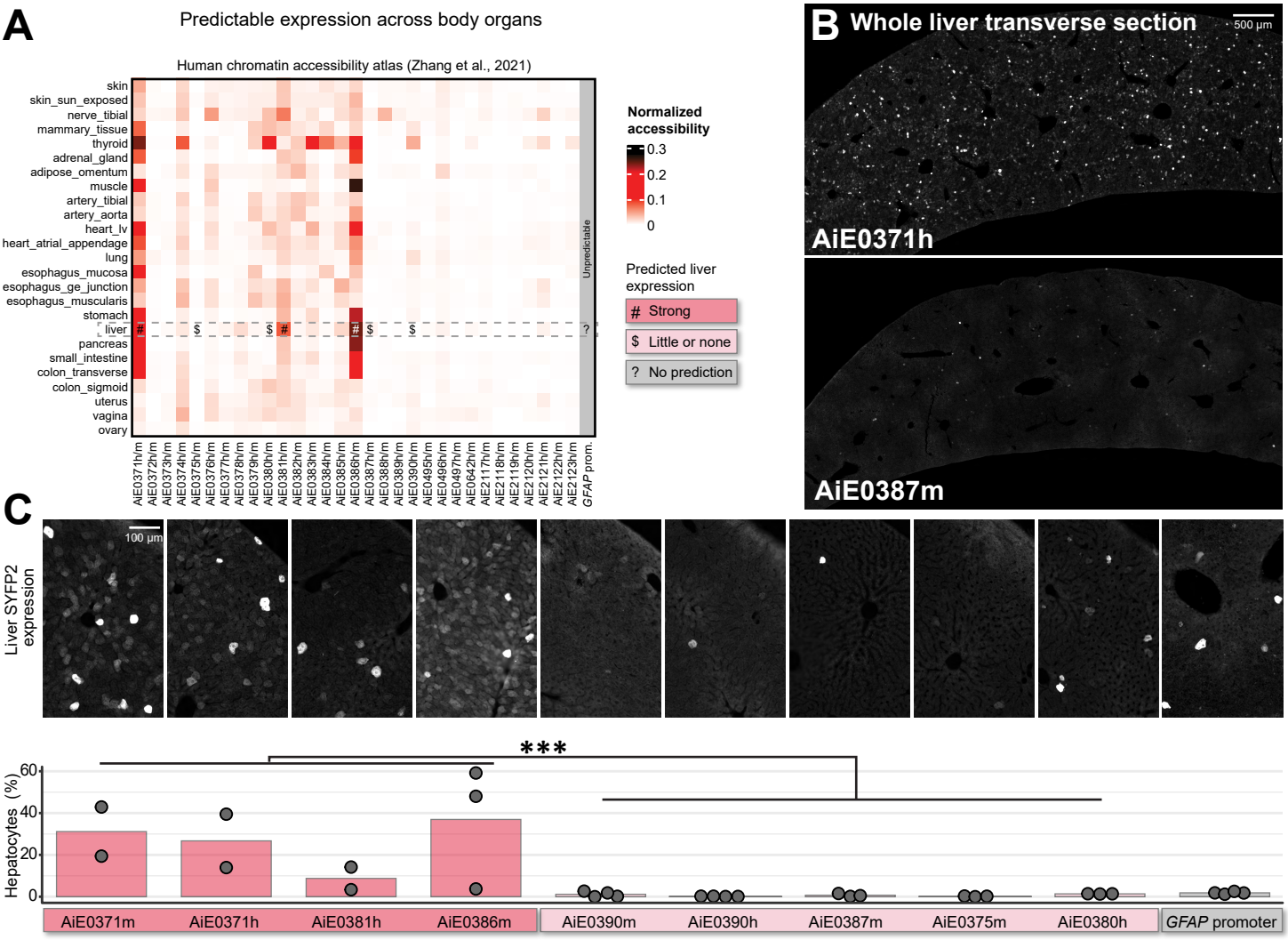
A
Predictable expression across body organs
Human chromatin accessibility atlas (Zhang et al., 2021)
skin
skin_sun_exposed
nerve_tibial
mammary_tissue
thyroid
adrenal_gland
adipose_omentum
muscle
artery_tibial
artery_aorta
heart_lv
heart_atrial_appendage
lung
esophagus_mucosa
esophagus_ge_junction
esophagus_muscularis
stomach
liver
pancreas
small_intestine
colon_transverse
colon_sigmoid
uterus
vagina
ovary
Unpredictable
AiE0371h/m
AiE0372h/m
AiE0373h/m
AiE0374h/m
AiE0375h/m
AiE0376h/m
AiE0377h/m
AiE0378h/m
AiE0379h/m
AiE0380h/m
AiE0381h/m
AiE0382h/m
AiE0383h/m
AiE0384h/m
AiE0385h/m
AiE0386h/m
AiE0387h/m
AiE0388h/m
AiE0389h/m
AiE0390h/m
AiE0495h/m
AiE0496h/m
AiE0497h/m
AiE0642h/m
AiE2117h/m
AiE2118h/m
AiE2119h/m
AiE2120h/m
AiE2121h/m
AiE2122h/m
AiE2123h/m
GFAP prom.
Normalized accessibility
0.3
0.2
0.1
0
Predicted liver expression
Strong
$ Little or none
? No prediction
B
Whole liver transverse section
500 µm
AiE0371h
AiE0387m
C
Liver SYFP2 expression
100 µm
***
Hepatocytes (%)
60
40
20
0
AiE0371m
AiE0371h
AiE0381h
AiE0386m
AiE0390m
AiE0390h
AiE0387m
AiE0375m
AiE0380h
GFAP promoter

992 **Figure 7: Predictability of astrocyte enhancer-AAV expression patterns across body organs.**
993
994 (**A**) Accessibility profiles of astrocyte-specific enhancers in the human whole-body accessibility atlas[70].
995 Single-cell profiles were grouped within each tissue into pseudo-bulk aggregates, then normalized
996 according to the signal (reads in peaks) within the dataset. Accessibility profiles are likely to predict
997 enhancer activities within each tissue. Focusing on liver, some astrocyte-specific enhancers are
998 predicted to have "Strong" expression, and some are predicted to have very "Little or none" expression.
999 In contrast, accessibility atlases do not predict expression of *GFAP* promoter across tissues.

1000 (**B**) Whole livers from mice injected intravenously with AiE0371h- and AiE0387m-enhancer-AAV
1001 vectors, stained with anti-GFP antibody. AiE0371h has high liver accessibility, is predicted to have high
1002 liver expression, and shows many strong SYFP2-expressing hepatocytes throughout the liver as
1003 predicted. In contrast, AiE0387m has little liver accessibility and so is predicted to have little liver
1004 expression, and in fact shows few positive SYFP2-expressing hepatocytes as predicted.

1005 (**C**) Agreement between liver expression predictions and liver expression measurements across several
1006 astrocyte-specific enhancer-AAV vectors. AiE0371m, AiE0371h, AiE0381h, and AiE0386m all show
1007 many SYFP2-expressing hepatocytes as predicted. AiE0390m, AiE0390h, AiE0375m, AiE0387m, and
1008 AiE0380h all show few weak SYFP2-expressing hepatocytes as predicted. *GFAP* promoter shows few
1009 but strongly expressing hepatocytes, which was not predictable from the accessibility atlases. Liver
1010 images in **B** and **C** represent two to four mice analyzed for each vector (each dot represents one
1011 mouse). *** non-parametric Wilcoxon rank sum test, $W = 153$, $p < 1e\text{-}4$ for the comparison of Strong
1012 versus "Little or none"-predicted enhancers.

1013

1014

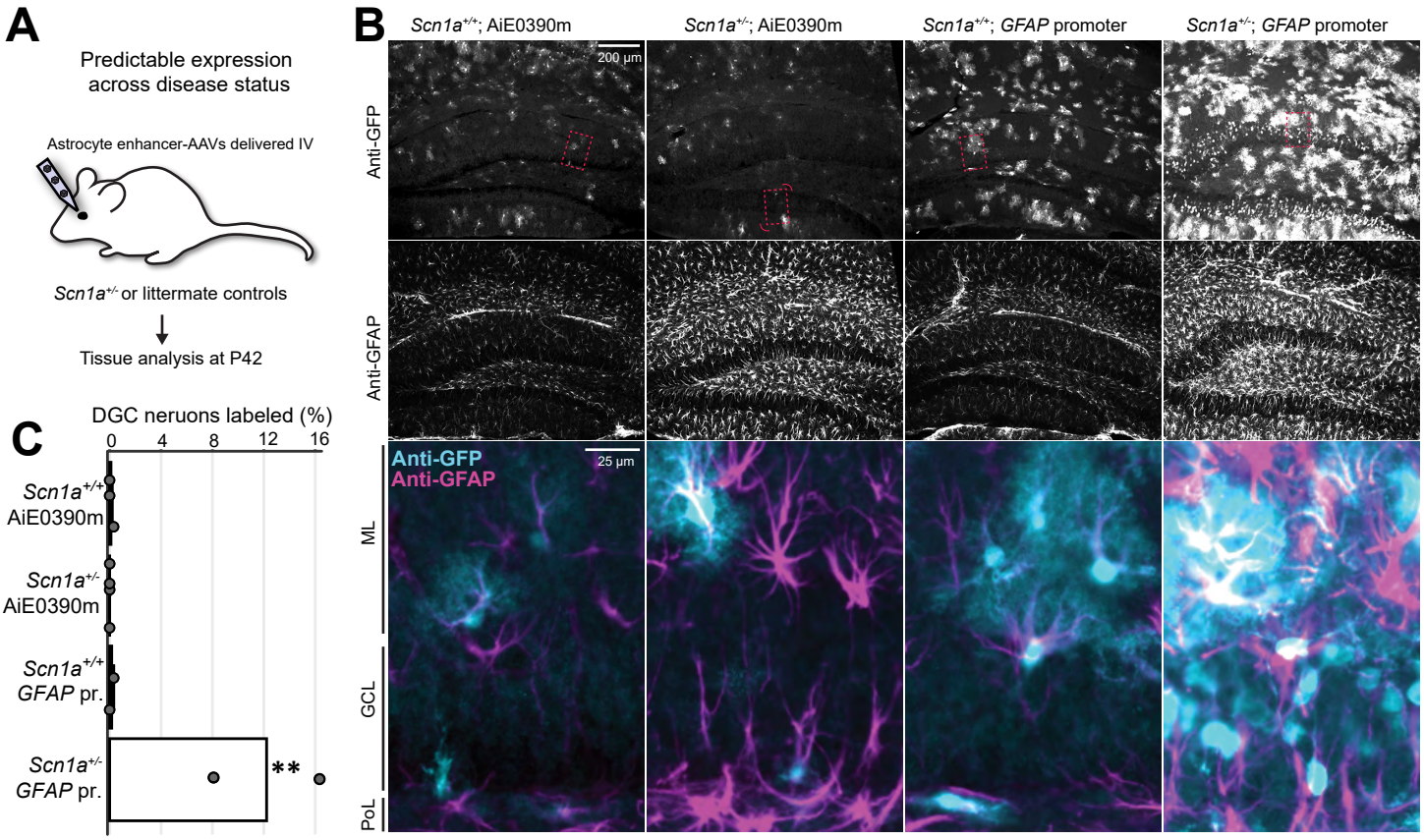
A
Predictable expression across disease status
Astrocyte enhancer-AAVs delivered IV
Scn1a+/- or littermate controls
Tissue analysis at P42
B
Scn1a+/+; AiE0390m
Scn1a+/-; AiE0390m
Scn1a+/+; GFAP promoter
Scn1a+/-; GFAP promoter
200 µm
Anti-GFP
Anti-GFAP
Anti-GFP
Anti-GFAP
25 µm
ML
GCL
PoL
C
DGC neruons labeled (%)
0
4
8
12
16
Scn1a+/+ AiE0390m
Scn1a+/- AiE0390m
Scn1a+/+ GFAP pr.
Scn1a+/- GFAP pr.
**

1015 **Figure 8: Predictability of astrocyte enhancer-AAV expression patterns across disease states.**

1016 (**A-C**) Testing fidelity of enhancer-AAV expression across disease states. We used Dravet syndrome
1017 model *Scn1a*$^{+/-}$ mice to induce epilepsy-associated hippocampal gliosis, injected enhancer-AAVs prior
1018 to the critical period, and analyzed tissue for expression patterns after the critical period (**A**). We
1019 assessed hippocampal gliosis with anti-GFAP antibody and enhancer-AAV expression with anti-GFP
1020 antibody (**B**). AiE0390m maintained specific expression and similar levels in hippocampal astrocytes
1021 regardless of epileptic gliosis. In contrast, *GFAP* promoter expression strongly increased in gliotic
1022 astrocytes, and also was observed in dentate gyrus granule cells. Red dashed rectangles indicate the
1023 position of the expanded zoomed view, and the curved red arrows indicate a rotated view for one zoom.
1024 (**C**) Quantification of DGC labeling reveals a much greater number of DGC neurons labeled with GFAP
1025 promoter in Dravet syndrome model mice. Two to four animals were analyzed per condition (each dot
1026 represents one mouse). ** ANOVA with Tukey's post hoc adjustments, $F = 16$, $p < 0.01$ for the *GFAP*
1027 promoter in *Scn1a*$^{+/-}$ mice compared to each other condition.

1028 Abbreviations: ML molecular layer, GCL granule cell layer, PoL polymorphic layer.

1029
1030

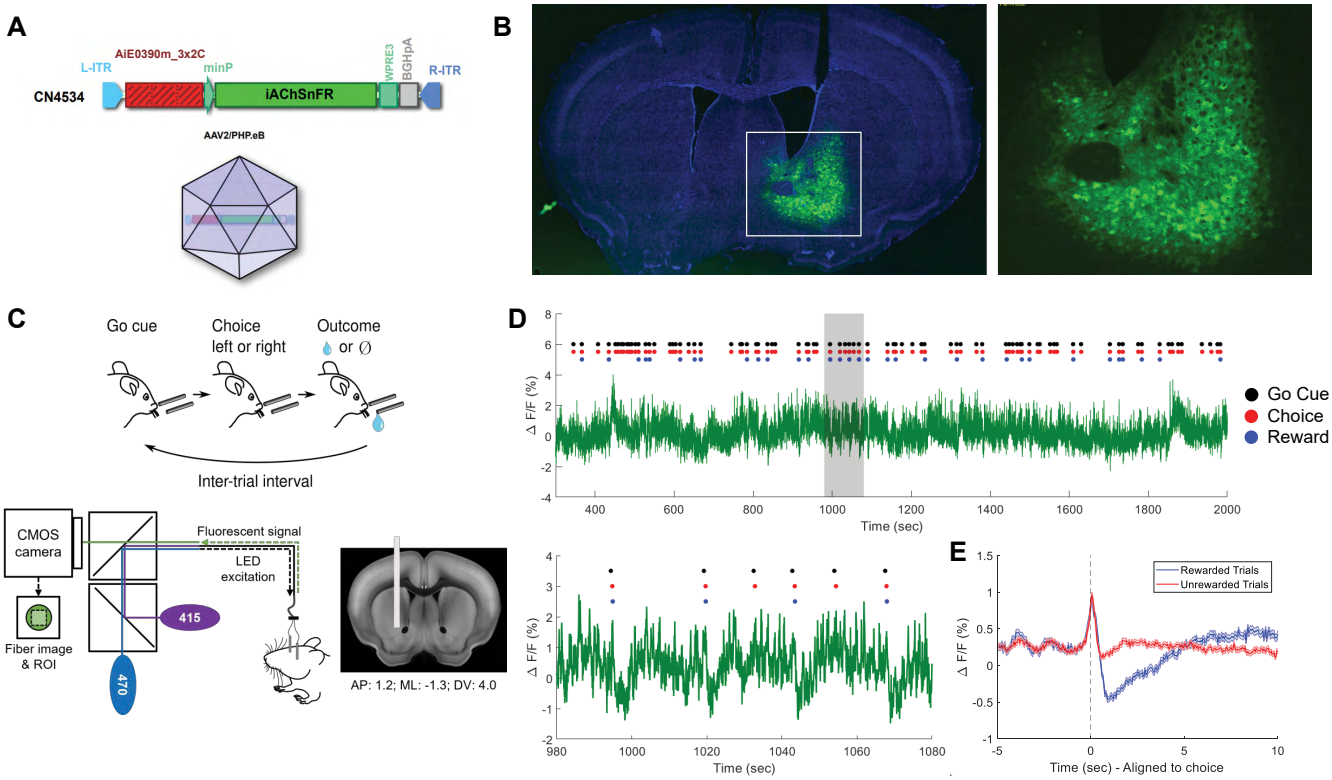
A
AiE0390m_3x2C
L-ITR
minP
WPRE3
BGHpA
R-ITR
CN4534
iAChSnFR
AAV2/PHP.eB
B
C
Go cue
Choice
left or right
Outcome
or ∅
Inter-trial interval
CMOS
camera
Fluorescent signal
LED
excitation
415
470
Fiber image
& ROI
AP: 1.2; ML: -1.3; DV: 4.0
D
Δ F/F (%)
Time (sec)
Go Cue
Choice
Reward
E
Rewarded Trials
Unrewarded Trials
Time (sec) - Aligned to choice

1031 **Figure 9: Astrocyte specific sensing of cholinergic signals in the nucleus accumbens during**
1032 **behavior.**
1033
1034 (**A**) AiE0390m_3xC2 driving expression of iAChSnFR. Enhancer vector is cloned into a pAAV plasmid
1035 and packaged into PHP.eB AAVs.

1036 (**B**) Coronal section showing stereotaxic injection of enhancer virus expressing iAChSnFR in the
1037 nucleus accumbens (injection coordinates: AP: 1.2, ML: 1.3, DV: 4.1).

1038 (**C**) Behavior and imaging experiment setup. Top: dynamic foraging behavior task schematic. Bottom:
1039 Fiber photometry instrumentation schematic and fiber location in a coronal section.

1040 (**D**) Fiber photometry signals of acetylcholine fluctuations during task performance. Top: ~30 min
1041 segment of a 2-hour session of dynamic foraging. Black dots represent the auditory cue, red dots
1042 represent time of first lick, blue dots represent water reward delivery. Bottom: 100 second (980-1080
1043 seconds) zoom in on above session with 6 individual trials (4 rewarded and 2 unrewarded trials). Data
1044 from one mouse shown, representative of three mice assayed.

1045 (**E**) Trial-averaged signals of rewarded and unrewarded trials aligned to time of first lick (mean±sem).

1046
1047

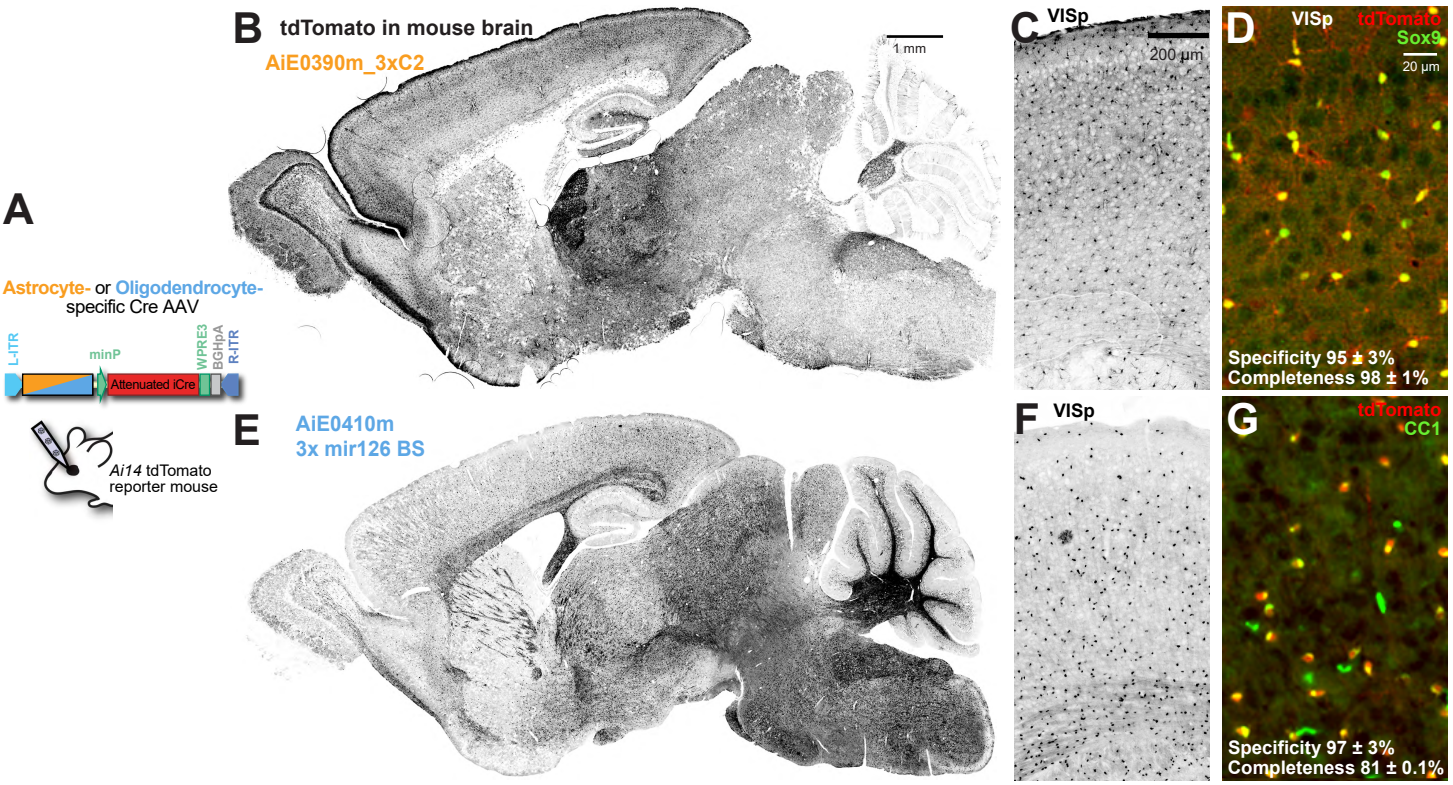
A
Astrocyte- or Oligodendrocyte-specific Cre AAV
L-ITR
minP
Attenuated iCre
WPRE3
BGHpA
R-ITR
Ai14 tdTomato reporter mouse
B tdTomato in mouse brain
AiE0390m_3xC2
1 mm
C VISp
200 µm
D VISp tdTomato Sox9
20 µm
Specificity 95 ± 3%
Completeness 98 ± 1%
E AiE0410m
3x mir126 BS
F VISp
G tdTomato CC1
Specificity 97 ± 3%
Completeness 81 ± 0.1%

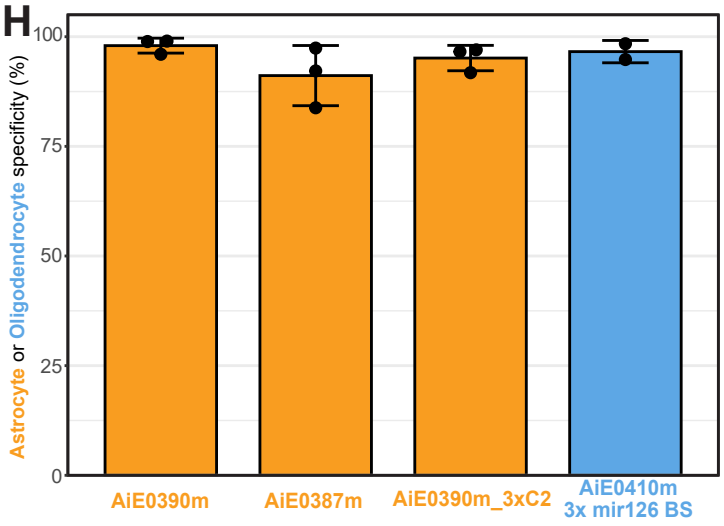
H
Astrocyte or Oligodendrocyte specificity (%)
100
75
50
25
0
AiE0390m
AiE0387m
AiE0390m_3xC2
AiE0410m 3x mir126 BS

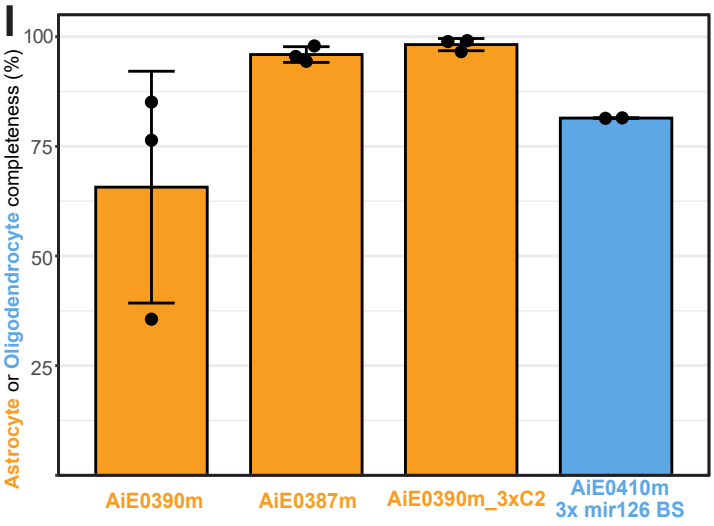
I
Astrocyte or Oligodendrocyte completeness (%)
100
75
50
25
AiE0390m
AiE0387m
AiE0390m_3xC2
AiE0410m 3x mir126 BS

1048 **Figure 10: Astrocyte- and oligodendrocyte-specific Cre AAVs.**
1049
1050 (**A**) Design and testing of astrocyte- and oligodendrocyte-specific attenuated Cre-expressing enhancer-
1051 AAVs.

1052 (**B-D**) Specific Cre recombination in astrocytes driven by AiE0390m_3xC2. Ai14 reporter recombination
1053 is observed in astrocytes throughout the mouse brain (**B**). Recombination within VISp is highly specific
1054 (**C**), as evidenced by highly specific and complete recombination in Sox9+ astrocytes (**D**).

1055 (**E-G**) Specific Cre recombination in astrocytes driven by AiE0410m. This vector also includes three
1056 3'UTR mir126 binding sites to eliminate unwanted expression in mir126-expressing endothelial cells[75].
1057 Ai14 reporter recombination is observed in oligodendrocytes throughout the mouse brain (**E**).
1058 Recombination within VISp is highly specific (**F**), as evidenced by highly specific and complete
1059 recombination in CC1+ oligodendrocytes (**G**).

1060 (**H-I**) Quantification of recombination specificity (**H**) and completeness (**I**). Specificity is defined as
1061 (tdTomato+Sox9 or CC1+ cells) / (all tdTomato+ cells) x 100%. Completeness is defined as
1062 (tdTomato+Sox9 or CC1+ cells) / (all Sox9 or CC1+ cells) x 100%. Two to three animals were analyzed
1063 for each condition (each dot represents one mouse).

1064

1065

1066
1067

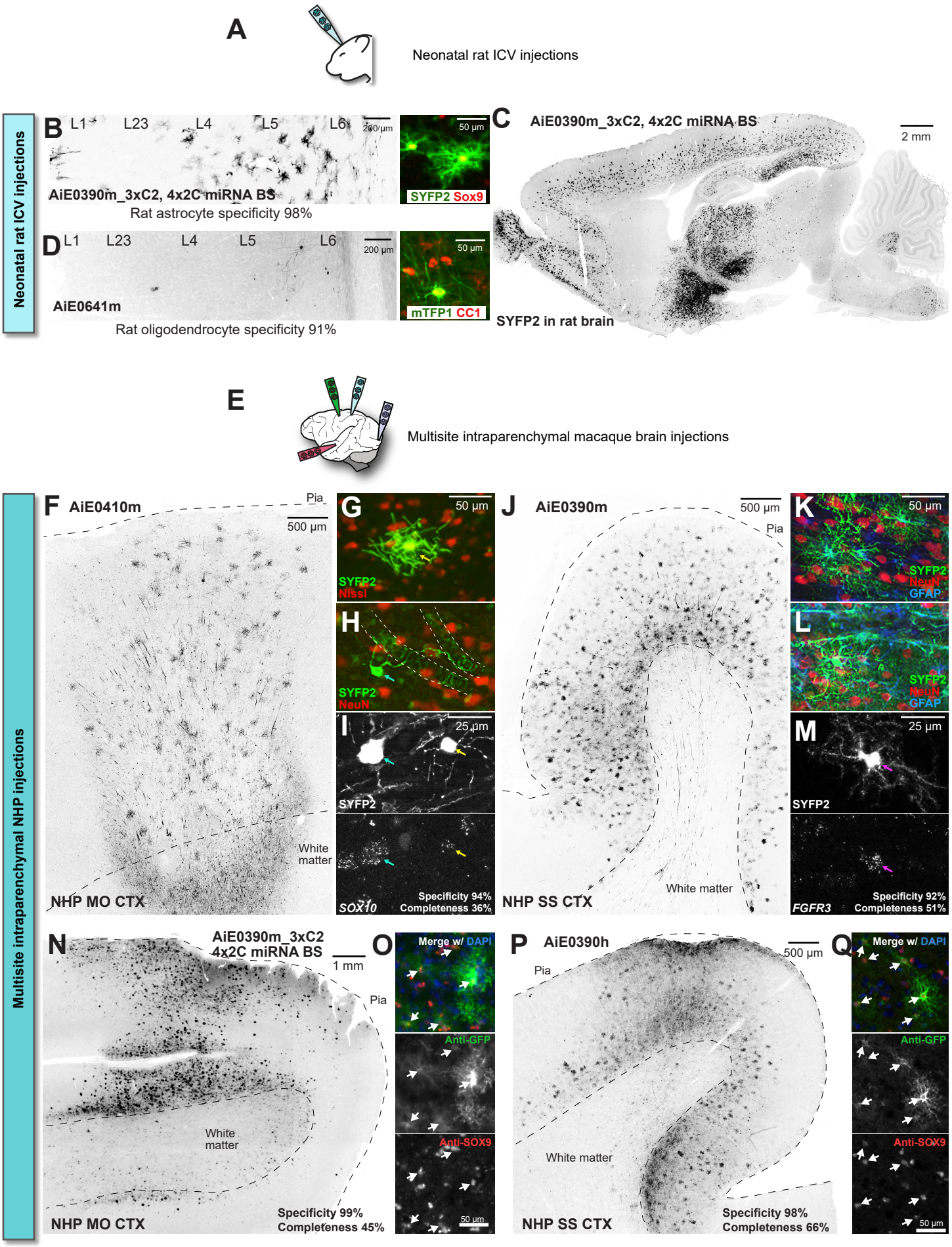
A
Neonatal rat ICV injections
Neonatal rat ICV injections
B
L1
L23
L4
L5
L6
200 µm
AiE0390m_3xC2, 4x2C miRNA BS
Rat astrocyte specificity 98%
50 µm
SYFP2 Sox9
D
L1
L23
L4
L5
L6
200 µm
AiE0641m
Rat oligodendrocyte specificity 91%
50 µm
mTFP1 CC1
C
AiE0390m_3xC2, 4x2C miRNA BS
2 mm
SYFP2 in rat brain
E
Multisite intraparenchymal macaque brain injections
Multisite intraparenchymal NHP injections
F
AiE0410m
Pia
500 µm
White matter
NHP MO CTX
G
50 µm
SYFP2
Nissl
H
SYFP2
NeuN
I
25 µm
SYFP2
SOX10
Specificity 94%
Completeness 36%
J
AiE0390m
500 µm
Pia
White matter
NHP SS CTX
K
50 µm
SYFP2
NeuN
GFAP
L
SYFP2
NeuN
GFAP
M
25 µm
SYFP2
FGFR3
Specificity 92%
Completeness 51%
N
AiE0390m_3xC2
4x2C miRNA BS
1 mm
Pia
White matter
NHP MO CTX
Specificity 99%
Completeness 45%
O
Merge w/ DAPI
Anti-GFP
Anti-SOX9
50 µm
P
AiE0390h
500 µm
Pia
White matter
NHP SS CTX
Specificity 98%
Completeness 66%
Q
Merge w/ DAPI
Anti-GFP
Anti-SOX9
50 µm

1068 **Figure 11: Genetic targeting of astrocytes and oligodendrocytes across species.**
1069
1070 (**A**) Testing enhancer-AAV vectors by neonatal rat ICV injections.

1071 (**B-C**) Validation of astrocyte-specific enhancer-AAV vectors in rat by IHC with Sox9 antibody.
1072 AiE0390m_3xC2 vector also incorporates 4X2C 3'UTR miRNA binding sites to prevent any off-target
1073 labeling in excitatory neurons[76]. Each image represents one animal tested.

1074 (**D**) Validation of oligodendrocyte-specific enhancer-AAV vector in rat. AiE0641m shows specific
1075 expression in CC1+ VISp oligodendrocytes. Each image represents one animal tested.

1076 (**E**) Multiple stereotactic intraparenchymal injections into macaque brain.

1077 (**F-I**) Prospective labeling of macaque oligodendrocytes in vivo. AiE0410m enhancer-AAV vector gives
1078 widespread labeling of oligodendrocytes throughout the depth of motor cortex (**F**). Most labeled
1079 macaque oligodendrocytes exhibit multipolar ramified morphology indicative of local axon myelination
1080 (**G**). Some labeled oligodendrocytes exhibit morphologies suggesting wrapping around wider tubular
1081 structures highlighted with dashed white lines (**H**). SYFP2-expressing cells of both morphological types
1082 express the oligodendrocyte/OPC marker *SOX10* with high specificity (**I**). One animal tested.

1083 (**J-Q**) Prospective labeling of macaque astrocytes in vivo. AiE0390m enhancer-AAV vector gives
1084 widespread labeling of astrocytes throughout the depth of somatosensory cortex (**J**). A few large Layer
1085 5 pyramidal neurons are also labeled. Labeled astrocytes show the expected bushy morphology and
1086 GFAP immunoreactivity of astrocytes in parenchyma (**K**) and sometimes reside near walls of large-
1087 diameter tubular structures (**L**). SYFP2-expressing astrocytes express the astrocyte marker *FGFR3*
1088 with high specificity (**M**). In another animal, an injection of AiE0390m_3xC2 vector with 4X2C 3'UTR
1089 miRNA binding sites gives high specificity (99%, **N**) for SOX9+ astrocytes in MO (**O**), without any large
1090 Layer 5 pyramidal neurons labeled. In another animal, AiE0390h vector gives high specificity (98%) of
1091 labeling for SOX9+ astrocytes (**P-Q**). Each vector represents one animal tested.

1092 Abbreviations: VISp primary visual cortex, MO motor cortex, SS somatosensory cortex.

1093

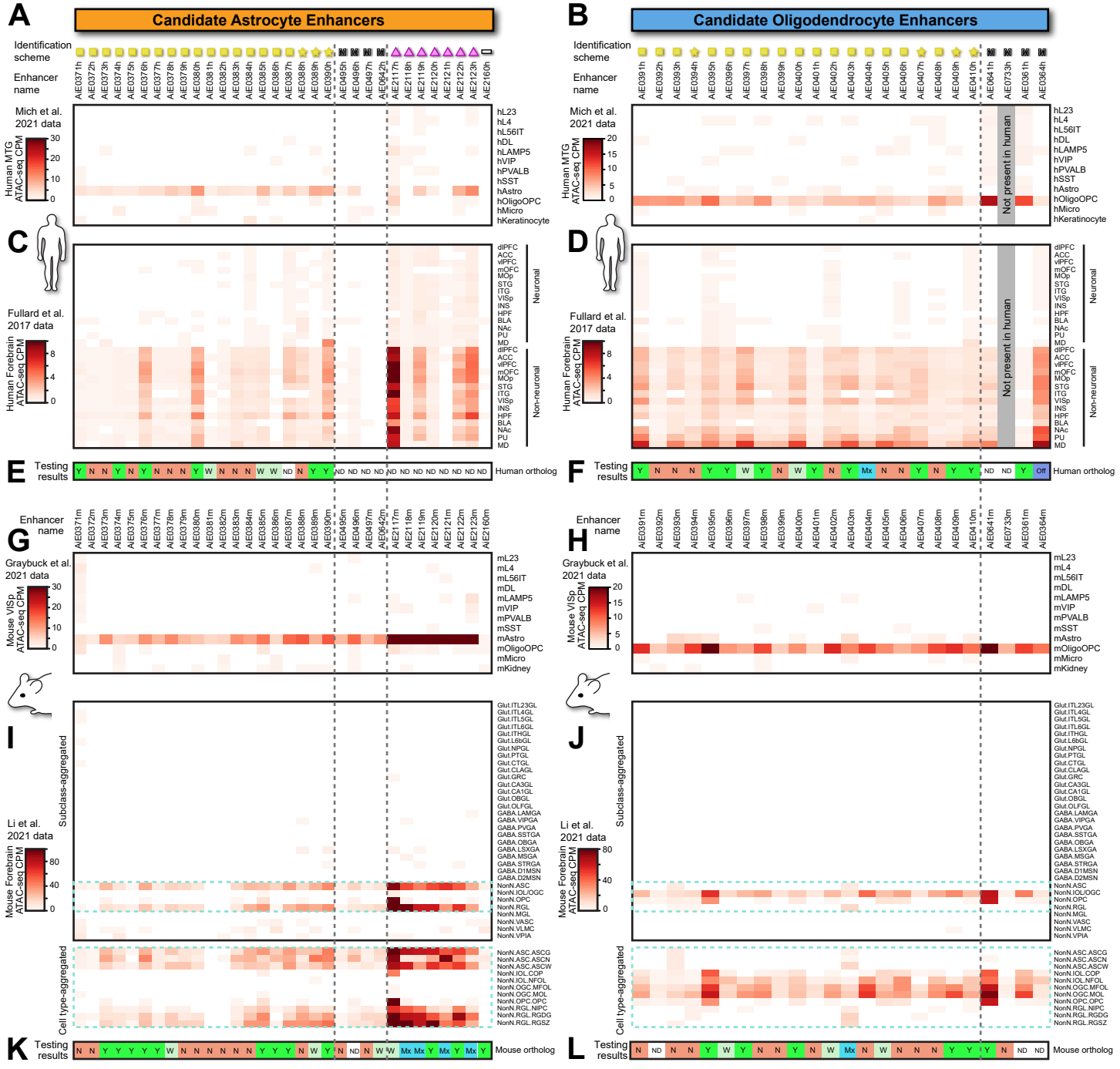
A
Candidate Astrocyte Enhancers
B
Candidate Oligodendrocyte Enhancers
Identification scheme
Enhancer name
Mich et al. 2021 data
Human MTG ATAC-seq CPM
hL23
hL4
hL56IT
hDL
hLAMP5
hVIP
hPVALB
hSST
hAstro
hOligoOPC
hMicro
hKeratinocyte
Not present in human
C
D
Fullard et al. 2017 data
Human Forebrain ATAC-seq CPM
dlPFC
ACC
vlPFC
mOFC
MOp
STG
ITG
VISp
INS
HPF
BLA
NAc
PU
MD
Neuronal
Non-neuronal
E
F
Testing results
Human ortholog
G
H
Graybuck et al. 2021 data
Mouse VISp ATAC-seq CPM
mL23
mL4
mL56IT
mDL
mLAMP5
mVIP
mPVALB
mSST
mAstro
mOligoOPC
mMicro
mKidney
I
J
Li et al. 2021 data
Mouse Forebrain ATAC-seq CPM
Subclass-aggregated
Cell type-aggregated
K
L
Mouse ortholog

1094 **Figure 1—figure supplement 1: Epigenetic characterization of candidate enhancers in additional**
1095 **chromatin accessibility datasets.**
1096
1097 (**A-D**) Accessibility profiles of all tested candidate human astrocyte-specific (**A**, **C**) and human
1098 oligodendrocyte-specific (**B**, **D**) enhancers. Human enhancer regions are characterized in the datasets
1099 of Mich et al.[33] (**A-B**), who performed snATAC-seq on neurosurgical MTG samples, and of Fullard et
1100 al.[94] (**C-D**), who performed bulk ATAC-seq on neuronal (sorted $NeuN^+$) and non-neuronal (sorted $NeuN^-$
1101) nuclei from dissections spanning multiple regions of human postmortem forebrain. Overall, many
1102 candidate astrocyte- and oligodendrocyte-specific enhancers show accessibility specific to non-
1103 neuronal cells across much of the human forebrain. For each genomic region we show their peak
1104 nomination scheme matching to **Figure 1B**, enhancer name.

1105 (**E-F**) Screening results from testing human candidate enhancers (repeated from **Figure 1D-E**, provided
1106 again for visualization). Testing result bar: Y = yes, enhancer-AAV gives strong or moderate on-target
1107 expression pattern; N = no, enhancer-AAV fails to express; W = weak on-target expression pattern; Mx
1108 = mixed specificities consisting of on-target cells plus unwanted neuronal populations; Off = off-target
1109 expression pattern, ND = no data.

1110 (**G-J**) Accessibility profiles for all tested candidate mouse astrocyte-specific (**G**, **I**) and oligodendrocyte-
1111 specific enhancers (**H**, **J**). Mouse enhancer regions are characterized in the VISp scATAC-seq dataset
1112 of Graybuck et al.[34] (**G-H**) and in the full mouse cerebrum dataset of Li et al.[56] (**I-J**).

1113 (**K-L**) Screening results from testing mouse candidate enhancers (repeated from **Figure 1D-E**, provided
1114 again for visualization).

1115
1116

1117

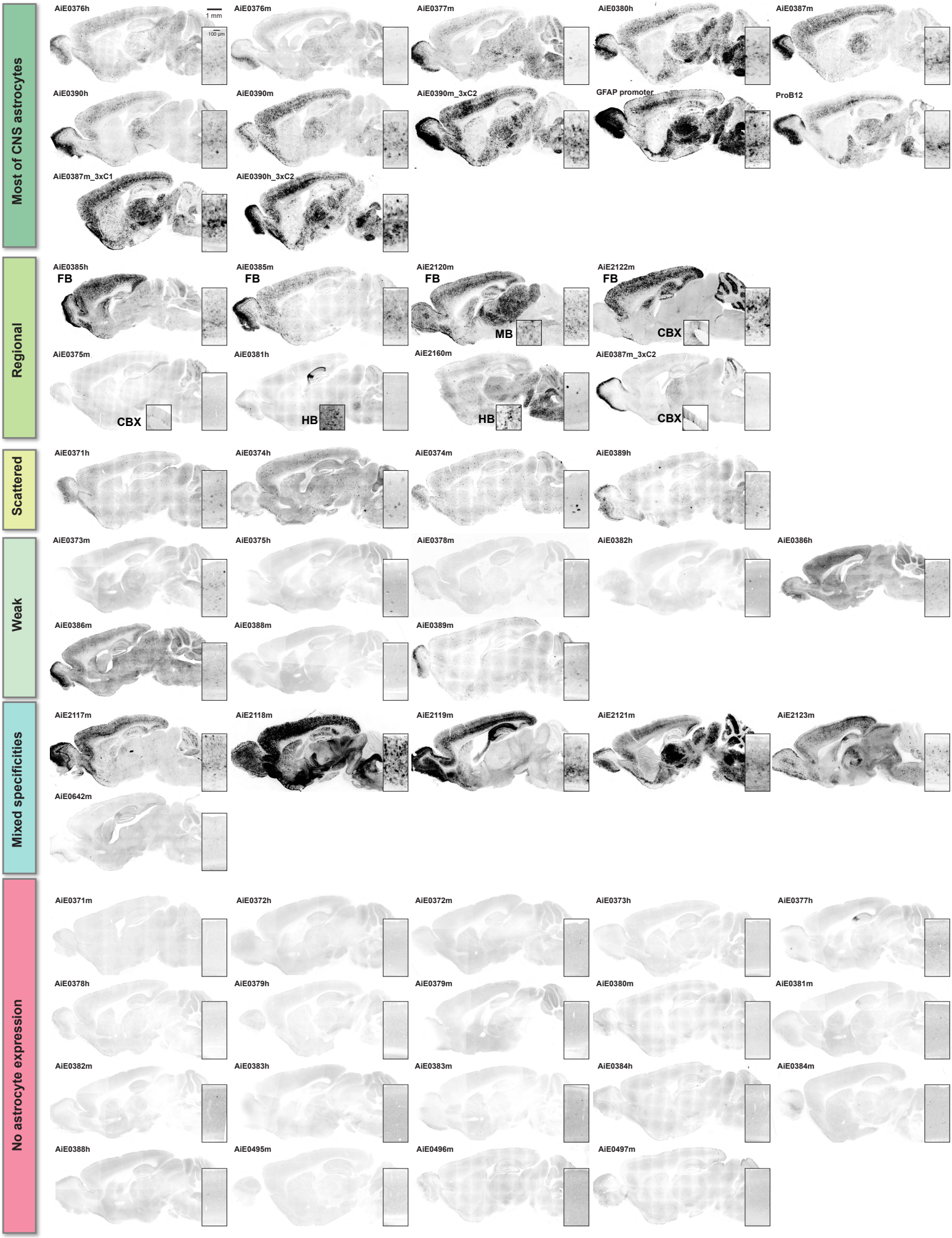
Most of CNS astrocytes
AiE0376h
1 mm
100 µm
AiE0376m
AiE0377m
AiE0380h
AiE0387m
AiE0390h
AiE0390m
AiE0390m_3xC2
GFAP promoter
ProB12
AiE0387m_3xC1
AiE0390h_3xC2
Regional
AiE0385h
FB
AiE0385m
FB
AiE2120m
FB
MB
AiE2122m
FB
CBX
AiE0375m
CBX
AiE0381h
HB
AiE2160m
HB
AiE0387m_3xC2
CBX
Scattered
AiE0371h
AiE0374h
AiE0374m
AiE0389h
Weak
AiE0373m
AiE0375h
AiE0378m
AiE0382h
AiE0386h
AiE0386m
AiE0388m
AiE0389m
Mixed specificities
AiE2117m
AiE2118m
AiE2119m
AiE2121m
AiE2123m
AiE0642m
No astrocyte expression
AiE0371m
AiE0372h
AiE0372m
AiE0373h
AiE0377h
AiE0378h
AiE0379h
AiE0379m
AiE0380m
AiE0381m
AiE0382m
AiE0383h
AiE0383m
AiE0384h
AiE0384m
AiE0388h
AiE0495m
AiE0496m
AiE0497m

1118 **Figure 2—figure supplement 1: Full screening results of all candidate enhancer-AAVs targeting**
1119 **astrocytes.**

1120 We injected mice with the indicated enhancer-AAV vectors between P42 and P56, then after 3-4 weeks
1121 we harvested brains, sliced them on a sliding microtome with freezing stage at 30 μm thickness, co-
1122 stained the sections with DAPI, then mounted them with Vectashield Vybrance. Insets show a full
1123 cortical column from VISp (primary visual cortex), and in some cases also the labeling in MB (midbrain)
1124 or HB (hindbrain) or CBX (cerebellar cortex) is also shown. Astrocyte-specific enhancer-AAV vectors
1125 are broadly grouped by expression pattern into the following categories: “Most of CNS astrocytes”,
1126 “Regional” meaning present at medium-to-high levels in one or more broad brain regions but not all,
1127 “Scattered” meaning a few astrocytes are strongly labeled throughout the brain, “Weak” meaning many
1128 astrocytes throughout the brain are labeled at low level, “Mixed specificities” meaning one or more off-
1129 target neuron populations are also labeled in addition to astrocytes, and “No astrocyte expression”
1130 meaning failure to detect any clear astrocytes in these whole-brain sagittal images. These
1131 epifluorescent screening images represent n = 1 to 27 animals tested per enhancer (median 2
1132 animals), and were sometimes taken on multiple different microscopes (see **Table S2** for full summary
1133 of screened animals).

1134
1135

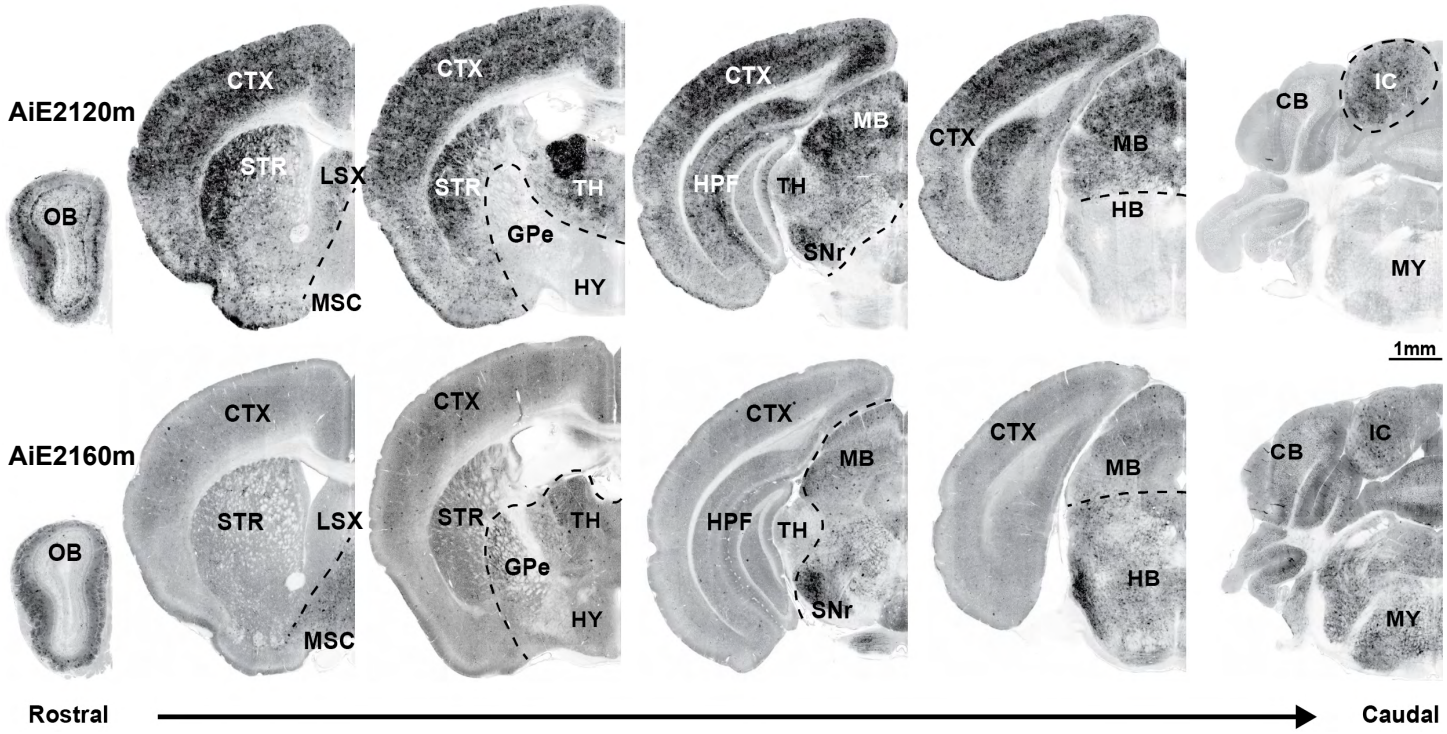
AiE2120m
AiE2160m
OB
CTX
STR
LSX
MSC
GPe
TH
HY
HPF
SNr
MB
HB
CB
IC
MY
1mm
Rostral
Caudal

1136 **Figure 2—figure supplement 2: Distinct astrocyte-specific expression domains of AiE2120m and**
1137 **AiE2160m.**
1138
1139 We injected mice with the indicated astrocyte-specific SYFP2-expressing enhancer-AAVs and
1140 performed whole-brain serial two-photon tomography using the TissueCyte platform[88]. These vectors
1141 display largely non-overlapping zones of astrocyte expression: AiE2120m is expressed in astrocytes
1142 within multiple forebrain structures including CTX, STR, OB, LSX, HPF, and TH, as well as MB,
1143 whereas AiE2160m is expressed in MB, CBX, and HB structures as well as complementary forebrain
1144 structures including HY, MSC, and GPe, and OB. In the OB AiE2120m is expressed in astrocytes within
1145 the granule cell layer, internal plexiform layer, and periglomerular cell layer, whereas AiE2160m is
1146 expressed in a complementary pattern of astrocytes within the external plexiform layer. Each image
1147 series shows one animal representative of two to three animals tested.
1148
1149 Abbreviations: CTX cerebral cortex, STR striatum, OB olfactory bulb, LSX lateral septal complex, HPF
1150 hippocampal formation, TH thalamus, MB midbrain, CBX cerebellar cortex, HB hindbrain, HY
1151 hypothalamus, MSC medial septal complex, GPe globus pallidus, external layer.
1152

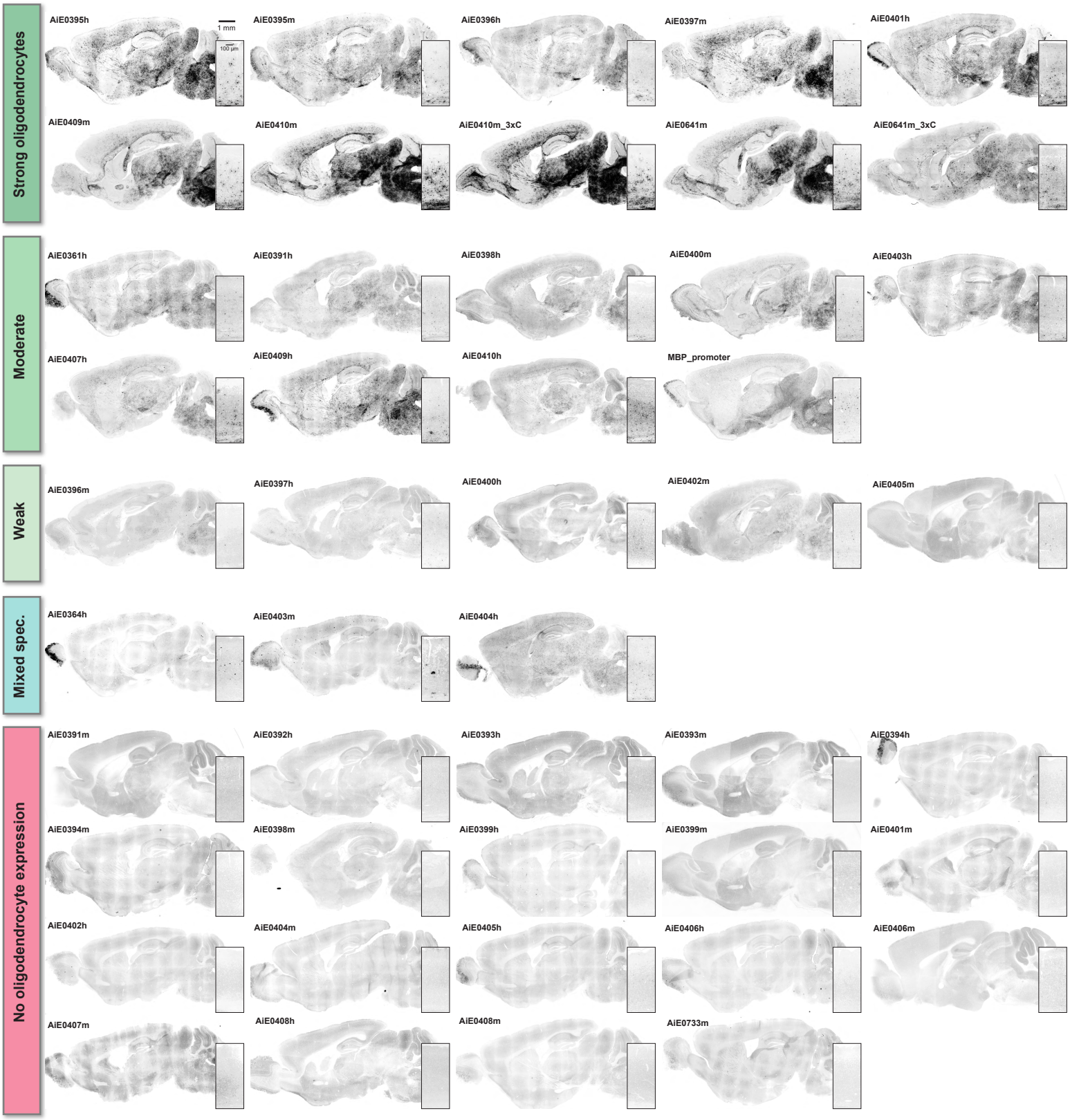
Strong oligodendrocytes
AiE0395h
1 mm
100 µm
AiE0395m
AiE0396h
AiE0397m
AiE0401h
AiE0409m
AiE0410m
AiE0410m_3xC
AiE0641m
AiE0641m_3xC
Moderate
AiE0361h
AiE0391h
AiE0398h
AiE0400m
AiE0403h
AiE0407h
AiE0409h
AiE0410h
MBP_promoter
Weak
AiE0396m
AiE0397h
AiE0400h
AiE0402m
AiE0405m
Mixed spec.
AiE0364h
AiE0403m
AiE0404h
No oligodendrocyte expression
AiE0391m
AiE0392h
AiE0393h
AiE0393m
AiE0394h
AiE0394m
AiE0398m
AiE0399h
AiE0399m
AiE0401m
AiE0402h
AiE0404m
AiE0405h
AiE0406h
AiE0406m
AiE0407m
AiE0408h
AiE0408m
AiE0733m

1153 **Figure 3—figure supplement 1: Full screening results of all candidate enhancer-AAVs targeting**
1154 **oligodendrocytes.**

1155 We injected mice with the indicated enhancer-AAV vectors between P42 and P56, then after 3-4 weeks
1156 we harvested brains, sliced them on a sliding microtome with freezing stage at 30 μm thickness, co-
1157 stained the sections with DAPI, and mounted them with Vectashield Vybrance. Oligodendrocyte-
1158 specific enhancer-AAV vectors are broadly grouped by expression pattern into the following categories:
1159 “Strong oligodendrocytes”, “Weak” meaning many oligodendrocytes throughout the brain are labeled at
1160 low level, “Mixed specificities” meaning several off-target neuron or astrocyte populations are also
1161 present in addition to oligodendrocytes, and “No oligodendrocyte expression” meaning failure to detect
1162 any clear oligodendrocytes in these whole-brain sagittal images. These epifluorescent screening
1163 images represent n = 1 to 20 animals tested per enhancer (median 2 animals), and were sometimes
1164 taken on multiple different microscopes (see **Table S2** for full summary of screened animals).
1165

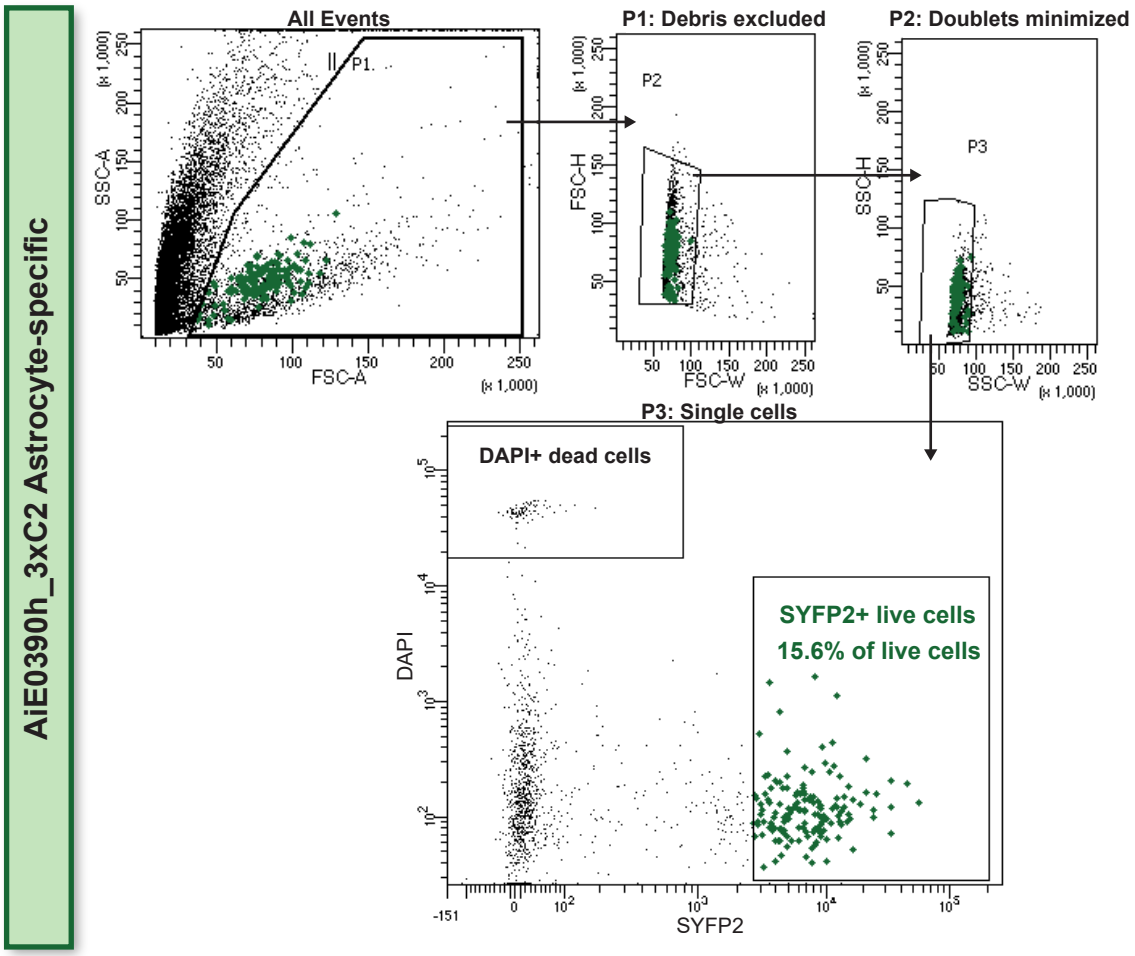
AiE0390h_3xC2 Astrocyte-specific
All Events
P1: Debris excluded
P2: Doublets minimized
P1
P2
P3
SSC-A
FSC-A
FSC-H
FSC-W
SSC-H
SSC-W
(x 1,000)
P3: Single cells
DAPI+ dead cells
SYFP2+ live cells
15.6% of live cells
DAPI
SYFP2

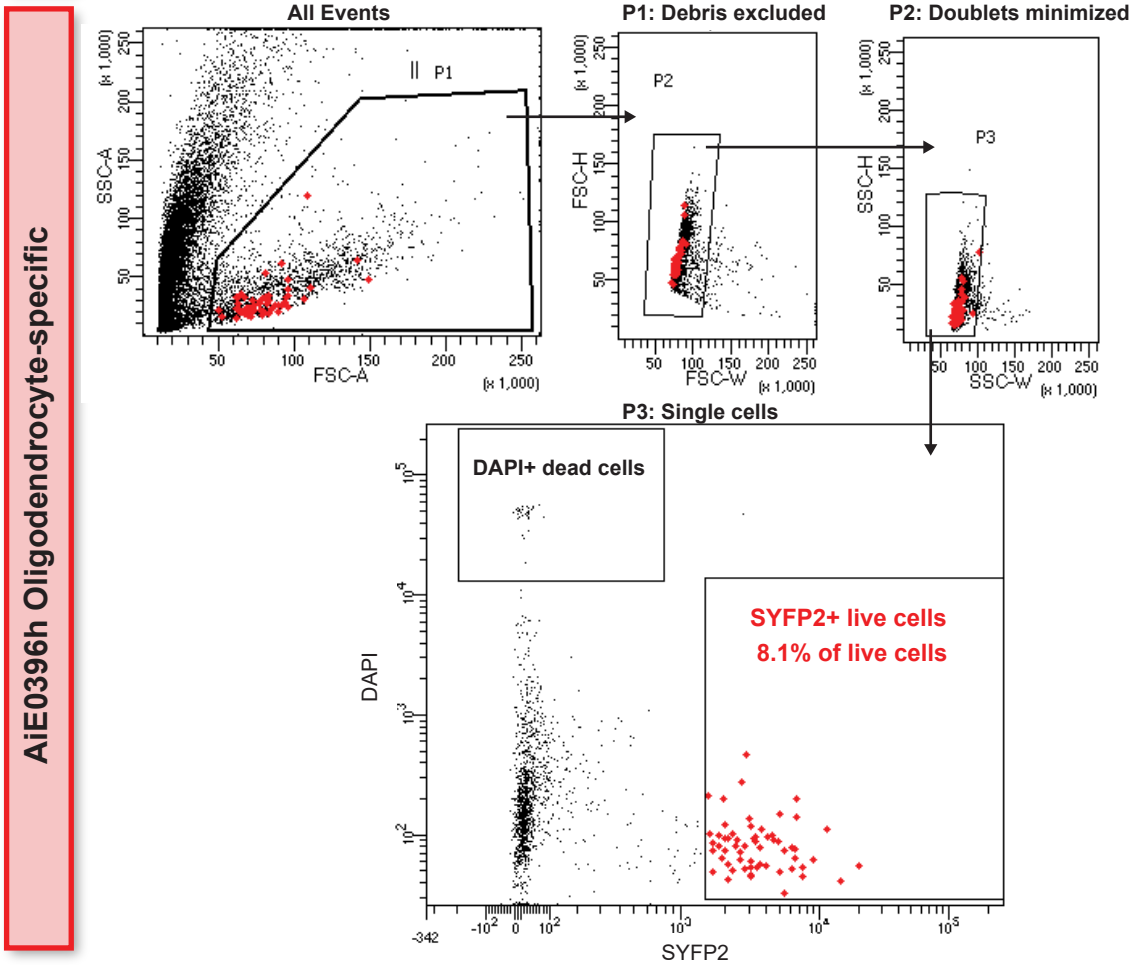
AiE0396h Oligodendrocyte-specific
All Events
P1: Debris excluded
P2: Doublets minimized
P1
P2
P3
SSC-A
FSC-A
FSC-H
FSC-W
SSC-H
SSC-W
(x 1,000)
P3: Single cells
DAPI+ dead cells
SYFP2+ live cells
8.1% of live cells
DAPI
SYFP2

1166 **Figure 5—figure supplement 1: Sorting enhancer-AAV-labeled astrocytes and oligodendrocytes.**
1167
1168 Example gating strategies for sorting AiE0390h_3xC2-labeled astrocytes and AiE0396h-labeled
1169 oligodendrocytes from mouse VISp. Each flow gating strategy represents one animal tested for that
1170 vector (n = 26 total animals for astrocytes and n = 21 for oligodendrocytes).

1171

1172

AiE0390m in NHP somatosensory cortex

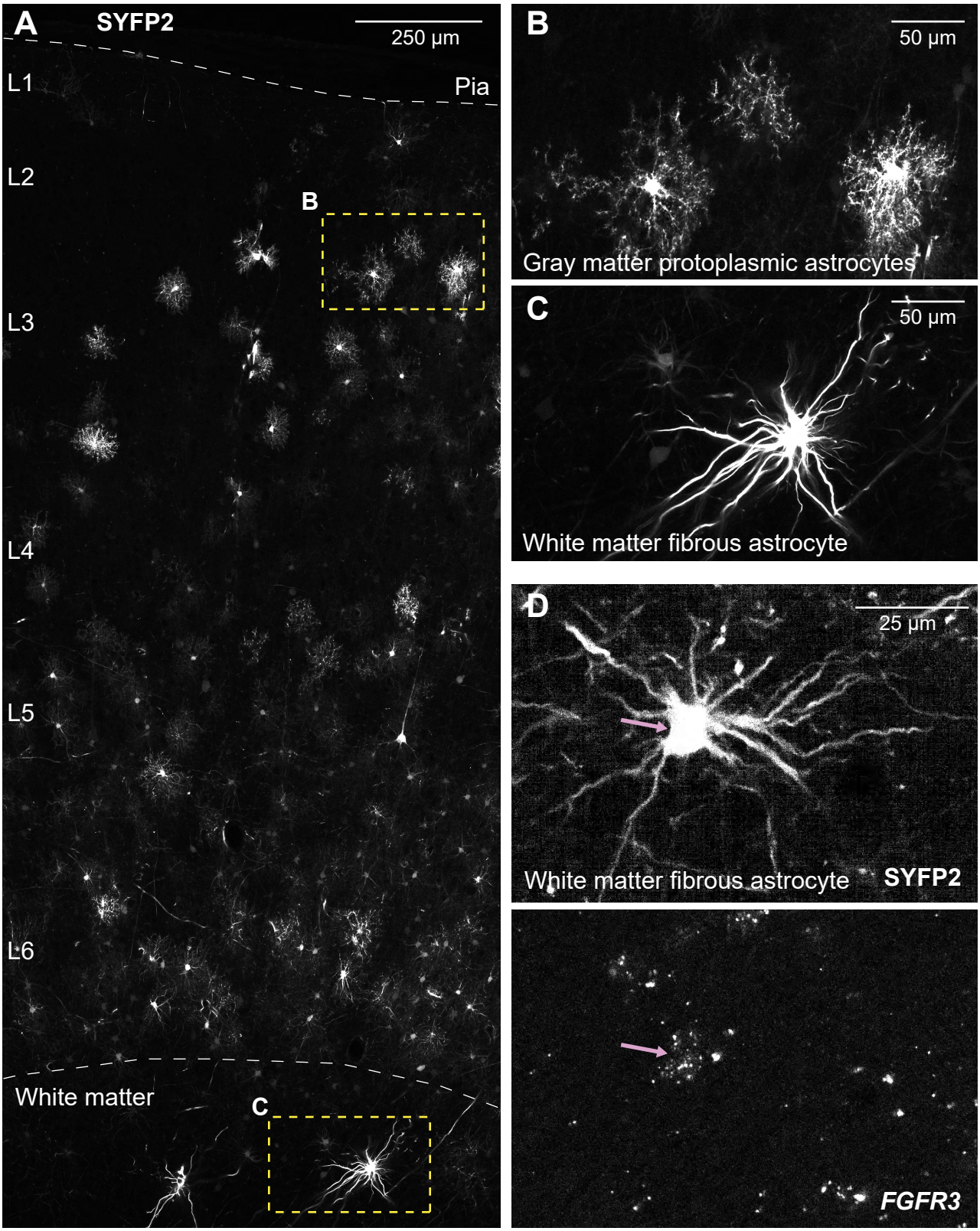

1173 **Figure 11—figure supplement 1: Diverse morphologies of macaque astrocytes labeled by**
1174 **enhancer-AAVs.**
1175
1176 (**A-C**) Labeling of both gray matter protoplasmic astrocytes and white matter fibrous astrocytes by
1177 AiE0390m enhancer-AAV. We show full cortical column of a somatosensory cortex injection site in A,
1178 with expanded insets to show protoplasmic astrocytes in gray matter (**B**) and fibrous astrocytes in white
1179 matter (**C**). Images represent one animal tested.

1180 (**D**) Confirmation of astrocyte identity by mFISH. Fibrous astrocytes in white matter express the
1181 astrocyte marker *FGFR3*, similar to gray matter protoplasmic astrocytes (**Figure 8M**).

1182

1183 **Table S1.**

Enhancer name	Identification scheme	Genome	Chr	Start	Stop	Enhancer_group	PhyloP	Length	Specificity	Strength (CPM)	Screen result	Expression pattern	Included in GLM model
eHGT_361h	Marker_gene	hg38	chrX	103780509	103781455	Human_Oligo	1.823	855	0.635	11.72	Yes	Oligodendrocytes_moderate	No
eHGT_361m	Marker_gene	mm10	chrX	136826512	136827460	Mouse_Oligo	1.488	807	0.879	12.03	No_data	No_data	No
eHGT_364h	Marker_gene	hg38	chr21	33051808	33052323	Human_Oligo	2.5	458	0.614	2.29	Mixed_spe	Mixed_specificity_oligodendrocy	No
eHGT_364m	Marker_gene	mm10	chr16	91246204	91246699	Mouse_Oligo	1.99	444	0.945	9.54	No_data	No_data	No
eHGT_371h	High_specificity	hg38	chr3	13485182	13485473	Human_Astro	0.967	269	0.454	3.81	Yes	Scattered_astrocytes	Yes
eHGT_371m	High_specificity	mm10	chr6	91160424	91160736	Mouse_Astro	0.87	241	0.216	4.28	No	No_astrocyte_expression	Yes
eHGT_372h	High_specificity	hg38	chr7	121914818	121915080	Human_Astro	0.33	216	0.668	2.6	No	No_astrocyte_expression	Yes
eHGT_372m	High_specificity	mm10	chr6	22910076	22910291	Mouse_Astro	0.194	187	0.742	2.85	No	No_astrocyte_expression	Yes
eHGT_373h	High_specificity	hg38	chr5	97134713	97135080	Human_Astro	0.537	329	0.72	3.81	No	No_astrocyte_expression	Yes
eHGT_373m	High_specificity	mm10	chr17	17409626	17409965	Mouse_Astro	0.531	319	0.909	11.78	Yes	Most_astrocytes_weak	Yes
eHGT_374h	High_specificity	hg38	chr15	64845370	64845672	Human_Astro	1.618	266	0.424	2.86	Yes	Scattered_astrocytes	Yes
eHGT_374m	High_specificity	mm10	chr9	65576810	65577101	Mouse_Astro	1.091	259	0.542	5.35	Yes	Scattered_astrocytes	Yes
eHGT_375h	High_specificity	hg38	chr13	99961720	99962046	Human_Astro	4.977	268	0.659	2.51	No	No_astrocyte_expression	Yes
eHGT_375m	High_specificity	mm10	chr14	122455334	122455655	Mouse_Astro	3.82	268	0.867	5.71	Yes	Bergmann_glia_astrocytes	Yes
eHGT_376h	High_specificity	hg38	chr3	188076136	188076690	Human_Astro	1.341	457	0.646	4.24	Yes	Most_astrocytes_strong	Yes
eHGT_376m	High_specificity	mm10	chr16	24326000	24326508	Mouse_Astro	1.083	435	0.865	11.78	Yes	Most_astrocytes_strong	Yes
eHGT_377h	High_specificity	hg38	chr10	80406003	80406485	Human_Astro	0.687	453	0.782	4.41	No	No_astrocyte_expression	Yes
eHGT_377m	High_specificity	mm10	chr14	41015471	41016233	Mouse_Astro	0.541	747	0.656	7.85	Yes	Most_astrocytes_strong	Yes
eHGT_378h	High_specificity	hg38	chr11	120182373	120182964	Human_Astro	2.312	559	0.681	6.32	No	No_astrocyte_expression	No
eHGT_378m	High_specificity	mm10	chr9	43268975	43269581	Mouse_Astro	1.699	559	0.911	12.49	Weak	Most_astrocytes_weak	No
eHGT_379h	High_specificity	hg38	chr3	64837170	64837760	Human_Astro	0.151	496	0.659	4.93	No	No_astrocyte_expression	Yes
eHGT_379m	High_specificity	mm10	chr6	93093752	93094309	Mouse_Astro	0.216	460	0.939	8.21	No	No_astrocyte_expression	Yes
eHGT_380h	High_specificity	hg38	chr6	44045566	44046145	Human_Astro	0.591	527	0.633	10.82	Yes	Most_astrocytes_strong	Yes
eHGT_380m	High_specificity	mm10	chr17	45765782	45766284	Mouse_Astro	0.536	479	0.727	7.14	No	No_astrocyte_expression	Yes
eHGT_381h	High_specificity	hg38	chr7	131400918	131401149	Human_Astro	2.166	173	0.4	1.9	Weak	Mid/hindbrain_astrocytes	No
eHGT_381m	High_specificity	mm10	chr6	31434638	31434879	Mouse_Astro	1.8	172	0.927	5.35	No	No_astrocyte_expression	No
eHGT_382h	High_specificity	hg38	chr10	113047655	113048169	Human_Astro	0.544	435	0.685	3.98	No	No_astrocyte_expression	Yes
eHGT_382m	High_specificity	mm10	chr19	55825471	55825949	Mouse_Astro	0.439	424	0.694	5.71	No	No_astrocyte_expression	Yes
eHGT_383h	High_specificity	hg38	chr2	220959419	220959789	Human_Astro	1.026	312	0.858	3.38	No	No_astrocyte_expression	Yes
eHGT_383m	High_specificity	mm10	chr1	76942759	76943103	Mouse_Astro	0.81	315	0.902	11.42	No	No_astrocyte_expression	Yes
eHGT_384h	High_specificity	hg38	chr6	121897357	121897797	Human_Astro	1.695	351	0.342	2.77	No	No_astrocyte_expression	Yes
eHGT_384m	High_specificity	mm10	chr10	56893293	56893720	Mouse_Astro	1.576	366	0.846	9.64	No	No_astrocyte_expression	Yes
eHGT_385h	High_specificity	hg38	chr9	123741938	123742543	Human_Astro	6.233	563	0.655	7.88	Weak	Telencephalon_astrocytes	No
eHGT_385m	High_specificity	mm10	chr2	38111566	38112219	Mouse_Astro	4.798	572	0.714	14.27	Yes	Telencephalon_astrocytes	No
eHGT_386h	High_specificity	hg38	chr1	15736012	15736372	Human_Astro	0.595	287	0.417	2.51	Weak	Most_astrocytes_weak	No
eHGT_386m	High_specificity	mm10	chr4	141623748	141624075	Mouse_Astro	1.042	231	0.527	5	Yes	Most_astrocytes_weak	No
eHGT_387h	High_specificity	hg38	chr1	219881964	219882484	Human_Astro	0.601	467	0.729	6.06	No_data	No_data	No
eHGT_387m	High_specificity	mm10	chr1	185493675	185494167	Mouse_Astro	0.633	425	0.959	15.35	Yes	Most_astrocytes_strong	No
eHGT_388h	High_specificity	hg38	chr12	20657459	20657845	Human_Astro	2.912	369	0.754	3.98	No	No_astrocyte_expression	Yes
eHGT_388m	High_specificity	mm10	chr6	141495577	141496010	Mouse_Astro	2.283	362	0.879	16.77	No	No_astrocyte_expression	Yes
eHGT_389h	High_specificity	hg38	chr20	63252174	63252906	Human_Astro	0.003	694	0.648	9.52	Yes	Scattered_astrocytes	No
eHGT_389m	High_specificity	mm10	chr2	180952658	180953361	Mouse_Astro	0.351	667	0.695	8.56	Weak	Most_astrocytes_weak	No
eHGT_390h	High_specificity	hg38	chr7	42152720	42153410	Human_Astro	7.463	634	0.699	8.91	Yes	Most_astrocytes_strong	Yes
eHGT_390m	High_specificity	mm10	chr13	15543638	15544333	Mouse_Astro	5.544	639	0.869	16.42	Yes	Most_astrocytes_strong	Yes
eHGT_391h	High_specificity	hg38	chr11	729607	730042	Human_Oligo	-0.132	419	0.688	7.49	Weak	Oligodendrocytes_moderate	No
eHGT_391m	High_specificity	mm10	chr7	141365022	141365541	Mouse_Oligo	0.135	474	0.901	13.2	No	No_oligodendrocyte_expression	No
eHGT_392h	High_specificity	hg38	chr4	48787039	48787541	Human_Oligo	1.369	431	0.776	6.88	No	No_oligodendrocyte_expression	No
eHGT_392m	High_specificity	mm10	chr5	73264044	73264568	Mouse_Oligo	1.225	448	0.832	4.25	No_data	No_data	No
eHGT_393h	High_specificity	hg38	chr18	66603993	66604511	Human_Oligo	2.036	451	0.755	7.23	No	No_oligodendrocyte_expression	Yes
eHGT_393m	High_specificity	mm10	chr1	110977271	110977865	Mouse_Oligo	1.391	548	0.593	6.16	No	No_oligodendrocyte_expression	Yes
eHGT_394h	High_specificity	hg38	chr3	171776470	171776980	Human_Oligo	0.518	444	0.782	5.2	No	No_oligodendrocyte_expression	Yes
eHGT_394m	High_specificity	mm10	chr3	27977667	27978413	Mouse_Oligo	0.254	661	0.738	12.62	No	No_oligodendrocyte_expression	Yes
eHGT_395h	High_specificity	hg38	chr9	128374105	128374728	Human_Oligo	2.782	595	0.742	9.96	Yes	Oligodendrocytes_strong	Yes
eHGT_395m	High_specificity	mm10	chr2	29830874	29831537	Mouse_Oligo	2.002	632	0.881	24.5	Yes	Oligodendrocytes_strong	Yes
eHGT_396h	High_specificity	hg38	chr11	117295457	117295798	Human_Oligo	1.384	302	0.561	3.88	Yes	Oligodendrocytes_strong	No

1184

eHGT_396m	High_specificity	mm10	chr9	45854220	45854539	Mouse_Oligo	1.185	288	0.824	7.33	Weak	Oligodendrocytes_weak	No
eHGT_397h	High_specificity	hg38	chr15	44188767	44189188	Human_Oligo	1.986	396	0.591	4.67	Weak	Oligodendrocytes_weak	No
eHGT_397m	High_specificity	mm10	chr2	121799010	121799455	Mouse_Oligo	1.661	385	0.759	6.16	Yes	Oligodendrocytes_strong	No
eHGT_398h	High_specificity	hg38	chr16	57270420	57270919	Human_Oligo	1.042	475	0.793	7.49	Yes	Oligodendrocytes_moderate	Yes
eHGT_398m	High_specificity	mm10	chr8	94684265	94684766	Mouse_Oligo	1.199	446	0.806	11.74	No	No_oligodendrocyte_expression	Yes
eHGT_399h	High_specificity	hg38	chr2	36902653	36902934	Human_Oligo	4.206	253	0.628	2.73	No	No_oligodendrocyte_expression	Yes
eHGT_399m	High_specificity	mm10	chr17	78684296	78684576	Mouse_Oligo	3.818	249	0.885	4.11	No	No_oligodendrocyte_expression	Yes
eHGT_400h	High_specificity	hg38	chr4	114636222	114636638	Human_Oligo	2.948	372	0.605	3.88	Weak	Oligodendrocytes_weak	No
eHGT_400m	High_specificity	mm10	chr3	125898885	125899302	Mouse_Oligo	2.414	373	0.819	7.63	Yes	Oligodendrocytes_moderate	No
eHGT_401h	High_specificity	hg38	chr1	44592226	44592529	Human_Oligo	1.081	256	0.55	3.17	Yes	Oligodendrocytes_strong	Yes
eHGT_401m	High_specificity	mm10	chr4	117326998	117327312	Mouse_Oligo	1.024	271	0.778	3.96	No	No_oligodendrocyte_expression	Yes
eHGT_402h	High_specificity	hg38	chr17	75697915	75698299	Human_Oligo	0.976	320	0.626	4.67	No	No_oligodendrocyte_expression	No
eHGT_402m	High_specificity	mm10	chr11	115956504	115956883	Mouse_Oligo	0.956	326	0.919	13.94	Weak	Oligodendrocytes_weak	No
eHGT_403h	High_specificity	hg38	chr11	67410338	67410731	Human_Oligo	0.524	382	0.588	4.5	Yes	Oligodendrocytes_moderate	No
eHGT_403m	High_specificity	mm10	chr19	4183762	4184154	Mouse_Oligo	1.019	346	0.586	8.51	Mixed_spe	Mixed_specificity_oligodendroc	No
eHGT_404h	High_specificity	hg38	chr2	163943542	163943945	Human_Oligo	1.738	370	0.721	5.2	Mixed_spe	Mixed_specificity_oligodendrocy	No
eHGT_404m	High_specificity	mm10	chr2	64325556	64326248	Mouse_Oligo	1.562	599	0.933	12.18	No	No_oligodendrocyte_expression	No
eHGT_405h	High_specificity	hg38	chr3	185175495	185175886	Human_Oligo	0.607	362	0.49	4.05	No	No_oligodendrocyte_expression	No
eHGT_405m	High_specificity	mm10	chr16	21724337	21724697	Mouse_Oligo	0.444	335	0.91	8.36	Weak	Oligodendrocytes_weak	No
eHGT_406h	High_specificity	hg38	chr2	88735239	88735593	Human_Oligo	-0.058	304	0.518	3.26	No	No_oligodendrocyte_expression	Yes
eHGT_406m	High_specificity	mm10	chr6	70774375	70774694	Mouse_Oligo	0.091	256	0.696	5.87	No	No_oligodendrocyte_expression	Yes
eHGT_407h	High_specificity	hg38	chr6	46098744	46099007	Human_Oligo	0.581	253	0.614	2.47	Yes	Oligodendrocytes_moderate	Yes
eHGT_407m	High_specificity	mm10	chr17	44121834	44122162	Mouse_Oligo	0.545	271	0.847	7.48	No	No_oligodendrocyte_expression	Yes
eHGT_408h	High_specificity	hg38	chr8	60867028	60867631	Human_Oligo	3.002	574	0.53	6.61	No	No_oligodendrocyte_expression	Yes
eHGT_408m	High_specificity	mm10	chr4	8867749	8868420	Mouse_Oligo	2.361	596	0.769	11.88	No	No_oligodendrocyte_expression	Yes
eHGT_409h	High_specificity	hg38	chr14	67539037	67539541	Human_Oligo	2.042	452	0.564	4.5	Yes	Oligodendrocytes_moderate	Yes
eHGT_409m	High_specificity	mm10	chr12	79035271	79035759	Mouse_Oligo	1.603	437	0.908	13.5	Yes	Oligodendrocytes_strong	Yes
eHGT_410h	High_specificity	hg38	chr9	81717541	81717791	Human_Oligo	2.177	202	0.579	1.41	Yes	Oligodendrocytes_moderate	Yes
eHGT_410m	High_specificity	mm10	chr4	72233773	72234067	Mouse_Oligo	1.838	203	0.817	9.68	Yes	Oligodendrocytes_strong	Yes
eHGT_495h	Marker_gene	hg38	chr19	33217923	33218346	Human_Astro	1.481	364	0.302	0.95	No_data	No_data	No
eHGT_495m	Marker_gene	mm10	chr7	35192340	35192802	Mouse_Astro	0.977	396	0.818	7.85	No	No_astrocyte_expression	No
eHGT_496h	Marker_gene	hg38	chr19	33225554	33226354	Human_Astro	1.18	749	0.516	4.76	No_data	No_data	No
eHGT_496m	Marker_gene	mm10	chr7	35185913	35186648	Mouse_Astro	0.955	686	0.734	15.35	No_data	No_data	No
eHGT_497h	Marker_gene	hg38	chr3	55237236	55237718	Human_Astro	1.648	437	0.037	0.09	No_data	No_data	No
eHGT_497m	Marker_gene	mm10	chr14	28781601	28782057	Mouse_Astro	1.444	410	0.966	7.49	No	No_astrocyte_expression	No
eHGT_641h	Marker_gene	hg38	chr21	33116993	33117641	Human_Oligo	4.073	557	0.755	16.66	No_data	No_data	No
eHGT_641m	Marker_gene	mm10	chr16	91305334	91305956	Mouse_Oligo	3.233	529	0.92	23.32	Yes	Oligodendrocytes_strong	No
eHGT_642h	Marker_gene	hg38	chr17	44539855	44540164	Human_Astro	2.026	230	0.463	0.26	No_data	No_data	No
eHGT_642m	Marker_gene	mm10	chr11	102579463	102579768	Mouse_Astro	1.655	228	0.86	11.06	Mixed_spe	Non-specific_astrocytes	No
eHGT_733m	Marker_gene	mm10	chr2	29273794	29274249	Mouse_Oligo	0.127	366	0.876	5.72	No	No_oligodendrocyte_expression	No
MGT_E117h	High_strength	hg38	chr7	23230417	23231661	Human_Astro	1.333	1213	0.197	4.15	No_data	No_data	No
MGT_E117m	High_strength	mm10	chr6	49020855	49022070	Mouse_Astro	1.202	1174	0.852	49.25	Mixed_spe	Non-specific_astrocytes	No
MGT_E118h	High_strength	hg38	chr13	25910516	25911691	Human_Astro	3.328	1146	0.062	0.26	No_data	No_data	No
MGT_E118m	High_strength	mm10	chr14	59736768	59737951	Mouse_Astro	2.384	1143	0.889	47.11	Mixed_spe	Mixed_specificity_astrocytes	No
MGT_E119h	High_strength	hg38	chr18	59386813	59388237	Human_Astro	4.406	1421	0.532	6.58	No_data	No_data	No
MGT_E119m	High_strength	mm10	chr18	66022617	66024006	Mouse_Astro	3.435	1386	0.926	38.9	Mixed_spe	Mixed_specificity_astrocytes	No
MGT_E120h	High_strength	hg38	chr2	134072857	134074292	Human_Astro	0.875	1436	0.333	2.16	No_data	No_data	No
MGT_E120m	High_strength	mm10	chr1	127159651	127161393	Mouse_Astro	0.697	1661	0.896	37.83	Yes	Forebrain_midbrain_astrocytes	No
MGT_E121h	High_strength	hg38	chr17	68641683	68642415	Human_Astro	0.531	733	0.139	0.17	No_data	No_data	No
MGT_E121m	High_strength	mm10	chr11	109753663	109754656	Mouse_Astro	0.322	994	0.911	38.9	Mixed_spe	Mixed_specificity_astrocytes	No
MGT_E122h	High_strength	hg38	chr4	175988170	175989315	Human_Astro	1.134	1121	0.675	8.65	No_data	No_data	No
MGT_E122m	High_strength	mm10	chr8	54791804	54792949	Mouse_Astro	1.078	1117	0.922	37.47	Yes	Forebrain_cerebellum_astrocyte	No
MGT_E123h	High_strength	hg38	chr14	80206581	80208078	Human_Astro	2.747	1497	0.701	12.12	No_data	No_data	No
MGT_E123m	High_strength	mm10	chr12	90733627	90735117	Mouse_Astro	2.427	1490	0.808	36.76	Mixed_spe	Mixed_specificity_astrocytes	No
MGT_E160h	None	hg38	chr2	48184996	48185538	Human_Astro	0.314	538	0	0	No_data	No_data	No
MGT_E160m	None	mm10	chr17	88297369	88297914	Mouse_Astro	0.347	516	0.282	1.07	Yes	Mid/hindbrain_astrocytes	No

1186 **Table S1: Genomic coordinates, sequence characterization, and mouse screening results of all**
1187 **tested astrocyte and oligodendrocyte enhancers.**

1188 Calculations of parameters are as described in Methods section.

1189

Table S2.

Mouse ID	Genotype	Enhancer ID	Vector ID	Vector Full Name	Data Modality	Targeted Cell Population	Fluor	Delivery Method	Publication
642124	C57BL/6J	AiE0361h	AiP12979	pAAV-AiE0361h-minBG-SYFP2-WPRE3-BGHpA	scRNA-seq	Oligo	SYFP2	RO	Mich et al., 2025 bioRxiv
567931	C57BL/6J	AiE0361h	AiP12979	pAAV-AiE0361h-minBG-SYFP2-WPRE3-BGHpA	EPI	Oligo	SYFP2	RO	Mich et al., 2025 bioRxiv
637260	C57BL/6J	AiE0361h	AiP12979	pAAV-AiE0361h-minBG-SYFP2-WPRE3-BGHpA	STPT	Oligo	SYFP2	RO	Ben-Simon, et al. 2025 Cell
621157	C57BL/6J	AiE0361h	AiP12979	pAAV-AiE0361h-minBG-SYFP2-WPRE3-BGHpA	EPI	Oligo	SYFP2	RO	Ben-Simon, et al. 2025 Cell
567932	C57BL/6J	AiE0364h	AiP12980	pAAV-AiE0364h-minBG-SYFP2-WPRE3-BGHpA	EPI	Oligo	SYFP2	RO	Mich et al., 2025 bioRxiv
621158	C57BL/6J	AiE0364h	AiP12980	pAAV-AiE0364h-minBG-SYFP2-WPRE3-BGHpA	EPI	Oligo	SYFP2	RO	Ben-Simon, et al. 2025 Cell
636670	C57BL/6J	AiE0371h	AiP12141	pAAV-AiE0371h-minBG-SYFP2-WPRE3-BGHpA	EPI, IHC	Astro	SYFP2	RO	Mich et al., 2025 bioRxiv
725447	C57BL/6J	AiE0371h	AiP12141	pAAV-AiE0371h-minBG-SYFP2-WPRE3-BGHpA	EPI, IHC	Astro	SYFP2	RO	Mich et al., 2025 bioRxiv
743804	C57BL/6J	AiE0371h	AiP12141	pAAV-AiE0371h-minBG-SYFP2-WPRE3-BGHpA	EPI, IHC	Astro	SYFP2	RO	Mich et al., 2025 bioRxiv
567934	C57BL/6J	AiE0371h	AiP12141	pAAV-AiE0371h-minBG-SYFP2-WPRE3-BGHpA	EPI	Astro	SYFP2	RO	Mich et al., 2025 bioRxiv
615690	C57BL/6J	AiE0371h	AiP12141	pAAV-AiE0371h-minBG-SYFP2-WPRE3-BGHpA	STPT	Astro	SYFP2	RO	Ben-Simon, et al. 2025 Cell
623007	C57BL/6J	AiE0371h	AiP12141	pAAV-AiE0371h-minBG-SYFP2-WPRE3-BGHpA	EPI	Astro	SYFP2	RO	Ben-Simon, et al. 2025 Cell
671755	CD-1_IGS	AiE0371h	AiP12141	pAAV-AiE0371h-minBG-SYFP2-WPRE3-BGHpA	STPT	Astro	SYFP2	ICV	Ben-Simon, et al. 2025 Cell
499663	C57BL/6J	AiE0371m	AiP12082	pAAV-AiE0371m-minBG-SYFP2-WPRE3-BGHpA	EPI	Astro	SYFP2	RO	Mich et al., 2025 bioRxiv
636669	C57BL/6J	AiE0371m	AiP12082	pAAV-AiE0371m-minBG-SYFP2-WPRE3-BGHpA	EPI, IHC	Astro	SYFP2	RO	Mich et al., 2025 bioRxiv
725446	C57BL/6J	AiE0371m	AiP12082	pAAV-AiE0371m-minBG-SYFP2-WPRE3-BGHpA	EPI, IHC	Astro	SYFP2	RO	Mich et al., 2025 bioRxiv
743802	C57BL/6J	AiE0371m	AiP12082	pAAV-AiE0371m-minBG-SYFP2-WPRE3-BGHpA	EPI, IHC	Astro	SYFP2	RO	Mich et al., 2025 bioRxiv
513373	C57BL/6J	AiE0372h	AiP12142	pAAV-AiE0372h-minBG-SYFP2-WPRE3-BGHpA	EPI	Astro	SYFP2	RO	Mich et al., 2025 bioRxiv
499664	C57BL/6J	AiE0372m	AiP12083	pAAV-AiE0372m-minBG-SYFP2-WPRE3-BGHpA	EPI	Astro	SYFP2	RO	Mich et al., 2025 bioRxiv
722734	C57BL/6J	AiE0372m	AiP12083	pAAV-AiE0372m-minBG-SYFP2-WPRE3-BGHpA	EPI	Astro	SYFP2	RO	Ben-Simon, et al. 2025 Cell
616877	C57BL/6J	AiE0372m	AiP12083	pAAV-AiE0372m-minBG-SYFP2-WPRE3-BGHpA	STPT	Astro	SYFP2	RO	Ben-Simon, et al. 2025 Cell
551395	C57BL/6J	AiE0373h	AiP12504	pAAV-AiE0373h-minBG-SYFP2-WPRE3-BGHpA	EPI	Astro	SYFP2	RO	Mich et al., 2025 bioRxiv
499665	C57BL/6J	AiE0373m	AiP12084	pAAV-AiE0373m-minBG-SYFP2-WPRE3-BGHpA	EPI	Astro	SYFP2	RO	Mich et al., 2025 bioRxiv
616737	C57BL/6J	AiE0373m	AiP12084	pAAV-AiE0373m-minBG-SYFP2-WPRE3-BGHpA	scRNA-seq	Astro	SYFP2	RO	Mich et al., 2025 bioRxiv
623015	C57BL/6J	AiE0373m	AiP12084	pAAV-AiE0373m-minBG-SYFP2-WPRE3-BGHpA	EPI	Astro	SYFP2	RO	Ben-Simon, et al. 2025 Cell
679835	C57BL/6J	AiE0373m	AiP12084	pAAV-AiE0373m-minBG-SYFP2-WPRE3-BGHpA	EPI	Astro	SYFP2	RO	Ben-Simon, et al. 2025 Cell
550273	C57BL/6J	AiE0374h	AiP12493	pAAV-AiE0374h-minBG-SYFP2-WPRE3-BGHpA	EPI	Astro	SYFP2	RO	Mich et al., 2025 bioRxiv
550277	C57BL/6J	AiE0374h	AiP12493	pAAV-AiE0374h-minBG-SYFP2-WPRE3-BGHpA	EPI	Astro	SYFP2	RO	Mich et al., 2025 bioRxiv
623008	C57BL/6J	AiE0374h	AiP12493	pAAV-AiE0374h-minBG-SYFP2-WPRE3-BGHpA	EPI	Astro	SYFP2	RO	Ben-Simon, et al. 2025 Cell
647376	C57BL/6J	AiE0374h	AiP12493	pAAV-AiE0374h-minBG-SYFP2-WPRE3-BGHpA	STPT	Astro	SYFP2	RO	Ben-Simon, et al. 2025 Cell
615013	C57BL/6J	AiE0374m	AiP12098	pAAV-AiE0374m-minBG-SYFP2-WPRE3-BGHpA	EPI, IHC	Astro	SYFP2	RO	Mich et al., 2025 bioRxiv
625965	C57BL/6J	AiE0374m	AiP12098	pAAV-AiE0374m-minBG-SYFP2-WPRE3-BGHpA	EPI, IHC	Astro	SYFP2	RO	Mich et al., 2025 bioRxiv
636674	C57BL/6J	AiE0374m	AiP12098	pAAV-AiE0374m-minBG-SYFP2-WPRE3-BGHpA	EPI, IHC	Astro	SYFP2	RO	Mich et al., 2025 bioRxiv
614201	C57BL/6J	AiE0374m	AiP12098	pAAV-AiE0374m-minBG-SYFP2-WPRE3-BGHpA	scRNA-seq	Astro	SYFP2	RO	Mich et al., 2025 bioRxiv
630481	C57BL/6J	AiE0374m	AiP12098	pAAV-AiE0374m-minBG-SYFP2-WPRE3-BGHpA	scRNA-seq	Astro	SYFP2	RO	Mich et al., 2025 bioRxiv
567935	C57BL/6J	AiE0374m	AiP12098	pAAV-AiE0374m-minBG-SYFP2-WPRE3-BGHpA	EPI	Astro	SYFP2	RO	Mich et al., 2025 bioRxiv
623016	C57BL/6J	AiE0374m	AiP12098	pAAV-AiE0374m-minBG-SYFP2-WPRE3-BGHpA	EPI	Astro	SYFP2	RO	Ben-Simon, et al. 2025 Cell
615691	C57BL/6J	AiE0374m	AiP12098	pAAV-AiE0374m-minBG-SYFP2-WPRE3-BGHpA	STPT	Astro	SYFP2	RO	Ben-Simon, et al. 2025 Cell
671754	CD-1_IGS	AiE0374m	AiP12098	pAAV-AiE0374m-minBG-SYFP2-WPRE3-BGHpA	STPT	Astro	SYFP2	ICV	Ben-Simon, et al. 2025 Cell
637359	Scn1a-R613X	AiE0374m	AiP14081	pAAV-AiE0374m-minBG-SYFP2-P2A-3XFLAG-10aa-H2B*	EPI, IHC	Astro	SYFP2	RO	Mich et al., 2025 bioRxiv
637362	Scn1a-R613X	AiE0374m	AiP14081	pAAV-AiE0374m-minBG-SYFP2-P2A-3XFLAG-10aa-H2B*	EPI, IHC	Astro	SYFP2	RO	Mich et al., 2025 bioRxiv
637358	Scn1a +/+	AiE0374m	AiP14081	pAAV-AiE0374m-minBG-SYFP2-P2A-3XFLAG-10aa-H2B*	EPI, IHC	Astro	SYFP2	RO	Mich et al., 2025 bioRxiv
637356	Scn1a +/+	AiE0374m	AiP14081	pAAV-AiE0374m-minBG-SYFP2-P2A-3XFLAG-10aa-H2B*	EPI, IHC	Astro	SYFP2	RO	Mich et al., 2025 bioRxiv
513374	C57BL/6J	AiE0375h	AiP12143	pAAV-AiE0375h-minBG-SYFP2-WPRE3-BGHpA	EPI	Astro	SYFP2	RO	Mich et al., 2025 bioRxiv
499666	C57BL/6J	AiE0375m	AiP12085	pAAV-AiE0375m-minBG-SYFP2-WPRE3-BGHpA	EPI	Astro	SYFP2	RO	Mich et al., 2025 bioRxiv
615009	C57BL/6J	AiE0375m	AiP12085	pAAV-AiE0375m-minBG-SYFP2-WPRE3-BGHpA	EPI, IHC	Astro	SYFP2	RO	Mich et al., 2025 bioRxiv
621237	C57BL/6J	AiE0375m	AiP13073	pAAV-AiE0375m-minBG-H2B-nsSYFP2-WPRE3-BGHpA	EPI	Astro	SYFP2	RO	Mich et al., 2025 bioRxiv
625958	C57BL/6J	AiE0375m	AiP12085	pAAV-AiE0375m-minBG-SYFP2-WPRE3-BGHpA	EPI, IHC	Astro	SYFP2	RO	Mich et al., 2025 bioRxiv
627902	C57BL/6J	AiE0375m	AiP13073	pAAV-AiE0375m-minBG-H2B-nsSYFP2-WPRE3-BGHpA	EPI	Astro	SYFP2	RO	Mich et al., 2025 bioRxiv
637136	C57BL/6J	AiE0375m	AiP12085	pAAV-AiE0375m-minBG-SYFP2-WPRE3-BGHpA	EPI, IHC	Astro	SYFP2	RO	Mich et al., 2025 bioRxiv
745309	C57BL/6J	AiE0375m	AiP12085	pAAV-AiE0375m-minBG-SYFP2-WPRE3-BGHpA	EPI, IHC	Astro	SYFP2	RO	Mich et al., 2025 bioRxiv
745315	C57BL/6J	AiE0375m	AiP12085	pAAV-AiE0375m-minBG-SYFP2-WPRE3-BGHpA	EPI, IHC	Astro	SYFP2	RO	Mich et al., 2025 bioRxiv
614198	C57BL/6J	AiE0375m	AiP12085	pAAV-AiE0375m-minBG-SYFP2-WPRE3-BGHpA	scRNA-seq	Astro	SYFP2	RO	Mich et al., 2025 bioRxiv
651221	C57BL/6J	AiE0375m	AiP12085	pAAV-AiE0375m-minBG-SYFP2-WPRE3-BGHpA	scRNA-seq	Astro	SYFP2	RO	Mich et al., 2025 bioRxiv
616878	C57BL/6J	AiE0375m	AiP12085	pAAV-AiE0375m-minBG-SYFP2-WPRE3-BGHpA	STPT	Astro	SYFP2	RO	Ben-Simon, et al. 2025 Cell
623017	C57BL/6J	AiE0375m	AiP12085	pAAV-AiE0375m-minBG-SYFP2-WPRE3-BGHpA	EPI	Astro	SYFP2	RO	Ben-Simon, et al. 2025 Cell
671752	CD-1_IGS	AiE0375m	AiP12085	pAAV-AiE0375m-minBG-SYFP2-WPRE3-BGHpA	STPT	Astro	SYFP2	ICV	Ben-Simon, et al. 2025 Cell
615010	C57BL/6J	AiE0376h	AiP12144	pAAV-AiE0376h-minBG-SYFP2-WPRE3-BGHpA	EPI, IHC	Astro	SYFP2	RO	Mich et al., 2025 bioRxiv
621239	C57BL/6J	AiE0376h	AiP13074	pAAV-AiE0376h-minBG-H2B-nsSYFP2-WPRE3-BGHpA	EPI	Astro	SYFP2	RO	Mich et al., 2025 bioRxiv
625960	C57BL/6J	AiE0376h	AiP12144	pAAV-AiE0376h-minBG-SYFP2-WPRE3-BGHpA	EPI, IHC	Astro	SYFP2	RO	Mich et al., 2025 bioRxiv
627903	C57BL/6J	AiE0376h	AiP13074	pAAV-AiE0376h-minBG-H2B-nsSYFP2-WPRE3-BGHpA	EPI	Astro	SYFP2	RO	Mich et al., 2025 bioRxiv
614199	C57BL/6J	AiE0376h	AiP12144	pAAV-AiE0376h-minBG-SYFP2-WPRE3-BGHpA	scRNA-seq	Astro	SYFP2	RO	Mich et al., 2025 bioRxiv
514392	C57BL/6J	AiE0376h	AiP12144	pAAV-AiE0376h-minBG-SYFP2-WPRE3-BGHpA	EPI	Astro	SYFP2	RO	Mich et al., 2025 bioRxiv
623009	C57BL/6J	AiE0376h	AiP12144	pAAV-AiE0376h-minBG-SYFP2-WPRE3-BGHpA	EPI	Astro	SYFP2	RO	Ben-Simon, et al. 2025 Cell
671756	CD-1_IGS	AiE0376h	AiP12144	pAAV-AiE0376h-minBG-SYFP2-WPRE3-BGHpA	STPT	Astro	SYFP2	ICV	Ben-Simon, et al. 2025 Cell
567936	C57BL/6J	AiE0376m	AiP12120	pAAV-AiE0376m-minBG-SYFP2-WPRE3-BGHpA	EPI	Astro	SYFP2	RO	Mich et al., 2025 bioRxiv
615688	C57BL/6J	AiE0376m	AiP12120	pAAV-AiE0376m-minBG-SYFP2-WPRE3-BGHpA	STPT	Astro	SYFP2	RO	Ben-Simon, et al. 2025 Cell
623018	C57BL/6J	AiE0376m	AiP12120	pAAV-AiE0376m-minBG-SYFP2-WPRE3-BGHpA	EPI	Astro	SYFP2	RO	Ben-Simon, et al. 2025 Cell
514393	C57BL/6J	AiE0377h	AiP12145	pAAV-AiE0377h-minBG-SYFP2-WPRE3-BGHpA	EPI	Astro	SYFP2	RO	Mich et al., 2025 bioRxiv
576009	C57BL/6J	AiE0377m	AiP13060	pAAV-AiE0377m-minBG-SYFP2-WPRE3-BGHpA	EPI	Astro	SYFP2	RO	Mich et al., 2025 bioRxiv
623019	C57BL/6J	AiE0377m	AiP13060	pAAV-AiE0377m-minBG-SYFP2-WPRE3-BGHpA	EPI	Astro	SYFP2	RO	Ben-Simon, et al. 2025 Cell
615686	C57BL/6J	AiE0377m	AiP13060	pAAV-AiE0377m-minBG-SYFP2-WPRE3-BGHpA	STPT	Astro	SYFP2	RO	Ben-Simon, et al. 2025 Cell
554425	C57BL/6J	AiE0378h	AiP12676	pAAV-AiE0378h-minBG-SYFP2-WPRE3-BGHpA	EPI	Astro	SYFP2	RO	Mich et al., 2025 bioRxiv
560757	C57BL/6J	AiE0378m	AiP12827	pAAV-AiE0378m-minBG-SYFP2-WPRE3-BGHpA	EPI	Astro	SYFP2	RO	Mich et al., 2025 bioRxiv
740048	C57BL/6J	AiE0378m	AiP12827	pAAV-AiE0378m-minBG-SYFP2-WPRE3-BGHpA	EPI	Astro	SYFP2	RO	Ben-Simon, et al. 2025 Cell
740048	C57BL/6J	AiE0378m	AiP12827	pAAV-AiE0378m-minBG-SYFP2-WPRE3-BGHpA	EPI	Astro	SYFP2	RO	Ben-Simon, et al. 2025 Cell
740048	C57BL/6J	AiE0378m	AiP12827	pAAV-AiE0378m-minBG-SYFP2-WPRE3-BGHpA	EPI	Astro	SYFP2	RO	Ben-Simon, et al. 2025 Cell
740048	C57BL/6J	AiE0378m	AiP12827	pAAV-AiE0378m-minBG-SYFP2-WPRE3-BGHpA	EPI	Astro	SYFP2	RO	Ben-Simon, et al. 2025 Cell
550274	C57BL/6J	AiE0379h	AiP12494	pAAV-AiE0379h-minBG-SYFP2-WPRE3-BGHpA	EPI	Astro	SYFP2	RO	Mich et al., 2025 bioRxiv
550278	C57BL/6J	AiE0379h	AiP12494	pAAV-AiE0379h-minBG-SYFP2-WPRE3-BGHpA	EPI	Astro	SYFP2	RO	Mich et al., 2025 bioRxiv
499667	C57BL/6J	AiE0379m	AiP12086	pAAV-AiE0379m-minBG-SYFP2-WPRE3-BGHpA	EPI	Astro	SYFP2	RO	Mich et al., 2025 bioRxiv
615012	C57BL/6J	AiE0380h	AiP13098	pAAV-AiE0380h-minBG-SYFP2-WPRE3-BGHpA	EPI, IHC	Astro	SYFP2	RO	Mich et al., 2025 bioRxiv
625962	C57BL/6J	AiE0380h	AiP13098	pAAV-AiE0380h-minBG-SYFP2-WPRE3-BGHpA	EPI, IHC	Astro	SYFP2	RO	Mich et al., 2025 bioRxiv
644030	C57BL/6J	AiE0380h	AiP14080	pAAV-AiE0380h-minBG-SYFP2-P2A-3XFLAG-10aa-H2B*	EPI, IHC	Astro	SYFP2	RO	Mich et al., 2025 bioRxiv
743809	C57BL/6J	AiE0380h	AiP13098	pAAV-AiE0380h-minBG-SYFP2-WPRE3-BGHpA	EPI, IHC	Astro	SYFP2	RO	Mich et al., 2025 bioRxiv
745313	C57BL/6J	AiE0380h	AiP13098	pAAV-AiE0380h-minBG-SYFP2-WPRE3-BGHpA	EPI, IHC	Astro	SYFP2	RO	Mich et al., 2025 bioRxiv
614200	C57BL/6J	AiE0380h	AiP13098	pAAV-AiE0380h-minBG-SYFP2-WPRE3-BGHpA	scRNA-seq	Astro	SYFP2	RO	Mich et al., 2025 bioRxiv
651225	C57BL/6J	AiE0380h	AiP13098	pAAV-AiE0380h-minBG-SYFP2-WPRE3-BGHpA	scRNA-seq	Astro	SYFP2	RO	Mich et al., 2025 bioRxiv
572497	C57BL/6J	AiE0380h	AiP13098	pAAV-AiE0380h-minBG-SYFP2-WPRE3-BGHpA	EPI	Astro	SYFP2	RO	Mich et al., 2025 bioRxiv

623010	C57BL/6J	AiE0380h	AiP13098	pAAV-AiE0380h-minBG-SYFP2-WPRE3-BGHpA	EPI	Astro	SYFP2	RO	Ben-Simon, et al. 2025 Cell
616741	C57BL/6J	AiE0380h	AiP13098	pAAV-AiE0380h-minBG-SYFP2-WPRE3-BGHpA	STPT	Astro	SYFP2	RO	Ben-Simon, et al. 2025 Cell
634487	C57BL/6J	AiE0380h	AiP13098	pAAV-AiE0380h-minBG-SYFP2-WPRE3-BGHpA	STPT	Astro	SYFP2	RO	Ben-Simon, et al. 2025 Cell
671753	CD-1_IGS	AiE0380h	AiP13098	pAAV-AiE0380h-minBG-SYFP2-WPRE3-BGHpA	STPT	Astro	SYFP2	ICV	Ben-Simon, et al. 2025 Cell
567937	C57BL/6J	AiE0380m	AiP12121	pAAV-AiE0380m-minBG-SYFP2-WPRE3-BGHpA	EPI	Astro	SYFP2	RO	Mich et al., 2025 bioRxiv
615014	C57BL/6J	AiE0381h	AiP12146	pAAV-AiE0381h-minBG-SYFP2-WPRE3-BGHpA	EPI, IHC	Astro	SYFP2	RO	Mich et al., 2025 bioRxiv
636671	C57BL/6J	AiE0381h	AiP12146	pAAV-AiE0381h-minBG-SYFP2-WPRE3-BGHpA	EPI, IHC	Astro	SYFP2	RO	Mich et al., 2025 bioRxiv
725448	C57BL/6J	AiE0381h	AiP12146	pAAV-AiE0381h-minBG-SYFP2-WPRE3-BGHpA	EPI, IHC	Astro	SYFP2	RO	Mich et al., 2025 bioRxiv
743805	C57BL/6J	AiE0381h	AiP12146	pAAV-AiE0381h-minBG-SYFP2-WPRE3-BGHpA	EPI, IHC	Astro	SYFP2	RO	Mich et al., 2025 bioRxiv
615516	C57BL/6J	AiE0381h	AiP12146	pAAV-AiE0381h-minBG-SYFP2-WPRE3-BGHpA	scRNA-seq	Astro	SYFP2	RO	Mich et al., 2025 bioRxiv
651222	C57BL/6J	AiE0381h	AiP12146	pAAV-AiE0381h-minBG-SYFP2-WPRE3-BGHpA	scRNA-seq	Astro	SYFP2	RO	Mich et al., 2025 bioRxiv
567938	C57BL/6J	AiE0381h	AiP12146	pAAV-AiE0381h-minBG-SYFP2-WPRE3-BGHpA	EPI, IHC	Astro	SYFP2	RO	Mich et al., 2025 bioRxiv
615689	C57BL/6J	AiE0381h	AiP12146	pAAV-AiE0381h-minBG-SYFP2-WPRE3-BGHpA	STPT	Astro	SYFP2	RO	Ben-Simon, et al. 2025 Cell
632617	C57BL/6J	AiE0381h	AiP12146	pAAV-AiE0381h-minBG-SYFP2-WPRE3-BGHpA	STPT	Astro	SYFP2	RO	Ben-Simon, et al. 2025 Cell
641421	C57BL/6J	AiE0381h	AiP12146	pAAV-AiE0381h-minBG-SYFP2-WPRE3-BGHpA	EPI	Astro	SYFP2	RO	Ben-Simon, et al. 2025 Cell
501914	C57BL/6J	AiE0381m	AiP12100	pAAV-AiE0381m-minBG-SYFP2-WPRE3-BGHpA	EPI	Astro	SYFP2	RO	Mich et al., 2025 bioRxiv
514394	C57BL/6J	AiE0382h	AiP12147	pAAV-AiE0382h-minBG-SYFP2-WPRE3-BGHpA	EPI	Astro	SYFP2	RO	Mich et al., 2025 bioRxiv
501915	C57BL/6J	AiE0382m	AiP12101	pAAV-AiE0382m-minBG-SYFP2-WPRE3-BGHpA	EPI	Astro	SYFP2	RO	Mich et al., 2025 bioRxiv
514395	C57BL/6J	AiE0383h	AiP12148	pAAV-AiE0383h-minBG-SYFP2-WPRE3-BGHpA	EPI	Astro	SYFP2	RO	Mich et al., 2025 bioRxiv
501912	C57BL/6J	AiE0383m	AiP12097	pAAV-AiE0383m-minBG-SYFP2-WPRE3-BGHpA	EPI	Astro	SYFP2	RO	Mich et al., 2025 bioRxiv
567939	C57BL/6J	AiE0384h	AiP12149	pAAV-AiE0384h-minBG-SYFP2-WPRE3-BGHpA	EPI	Astro	SYFP2	RO	Mich et al., 2025 bioRxiv
500565	C57BL/6J	AiE0384m	AiP12087	pAAV-AiE0384m-minBG-SYFP2-WPRE3-BGHpA	EPI	Astro	SYFP2	RO	Mich et al., 2025 bioRxiv
550275	C57BL/6J	AiE0385h	AiP12495	pAAV-AiE0385h-minBG-SYFP2-WPRE3-BGHpA	EPI	Astro	SYFP2	RO	Mich et al., 2025 bioRxiv
623011	C57BL/6J	AiE0385h	AiP12495	pAAV-AiE0385h-minBG-SYFP2-WPRE3-BGHpA	EPI	Astro	SYFP2	RO	Ben-Simon, et al. 2025 Cell
647375	C57BL/6J	AiE0385h	AiP12495	pAAV-AiE0385h-minBG-SYFP2-WPRE3-BGHpA	STPT	Astro	SYFP2	RO	Ben-Simon, et al. 2025 Cell
615015	C57BL/6J	AiE0385m	AiP12122	pAAV-AiE0385m-minBG-SYFP2-WPRE3-BGHpA	EPI, IHC	Astro	SYFP2	RO	Mich et al., 2025 bioRxiv
635183	C57BL/6J	AiE0385m	AiP14074	pAAV-AiE0385m-minBG-SYFP2-P2A-3XFLAG-10aa-H2B*	EPI	Astro	SYFP2	RO	Mich et al., 2025 bioRxiv
637137	C57BL/6J	AiE0385m	AiP12122	pAAV-AiE0385m-minBG-SYFP2-WPRE3-BGHpA	EPI, IHC	Astro	SYFP2	RO	Mich et al., 2025 bioRxiv
615515	C57BL/6J	AiE0385m	AiP12122	pAAV-AiE0385m-minBG-SYFP2-WPRE3-BGHpA	scRNA-seq	Astro	SYFP2	RO	Mich et al., 2025 bioRxiv
651224	C57BL/6J	AiE0385m	AiP12122	pAAV-AiE0385m-minBG-SYFP2-WPRE3-BGHpA	scRNA-seq	Astro	SYFP2	RO	Mich et al., 2025 bioRxiv
567940	C57BL/6J	AiE0385m	AiP12122	pAAV-AiE0385m-minBG-SYFP2-WPRE3-BGHpA	EPI	Astro	SYFP2	RO	Mich et al., 2025 bioRxiv
623021	C57BL/6J	AiE0385m	AiP12122	pAAV-AiE0385m-minBG-SYFP2-WPRE3-BGHpA	EPI	Astro	SYFP2	RO	Ben-Simon, et al. 2025 Cell
615687	C57BL/6J	AiE0385m	AiP12122	pAAV-AiE0385m-minBG-SYFP2-WPRE3-BGHpA	STPT	Astro	SYFP2	RO	Ben-Simon, et al. 2025 Cell
551390	C57BL/6J	AiE0386h	AiP12496	pAAV-AiE0386h-minBG-SYFP2-WPRE3-BGHpA	EPI	Astro	SYFP2	RO	Mich et al., 2025 bioRxiv
623012	C57BL/6J	AiE0386h	AiP12496	pAAV-AiE0386h-minBG-SYFP2-WPRE3-BGHpA	EPI	Astro	SYFP2	RO	Ben-Simon, et al. 2025 Cell
636672	C57BL/6J	AiE0386m	AiP12088	pAAV-AiE0386m-minBG-SYFP2-WPRE3-BGHpA	EPI, IHC	Astro	SYFP2	RO	Mich et al., 2025 bioRxiv
725449	C57BL/6J	AiE0386m	AiP12088	pAAV-AiE0386m-minBG-SYFP2-WPRE3-BGHpA	EPI, IHC	Astro	SYFP2	RO	Mich et al., 2025 bioRxiv
743803	C57BL/6J	AiE0386m	AiP12088	pAAV-AiE0386m-minBG-SYFP2-WPRE3-BGHpA	EPI, IHC	Astro	SYFP2	RO	Mich et al., 2025 bioRxiv
616738	C57BL/6J	AiE0386m	AiP12088	pAAV-AiE0386m-minBG-SYFP2-WPRE3-BGHpA	scRNA-seq	Astro	SYFP2	RO	Mich et al., 2025 bioRxiv
500566	C57BL/6J	AiE0386m	AiP12088	pAAV-AiE0386m-minBG-SYFP2-WPRE3-BGHpA	EPI	Astro	SYFP2	RO	Mich et al., 2025 bioRxiv
623022	C57BL/6J	AiE0386m	AiP12088	pAAV-AiE0386m-minBG-SYFP2-WPRE3-BGHpA	EPI	Astro	SYFP2	RO	Ben-Simon, et al. 2025 Cell
679856	C57BL/6J	AiE0387h	AiP12150	pAAV-AiE0387h-minBG-SYFP2-WPRE3-BGHpA	STPT	Astro	SYFP2	RO	Ben-Simon, et al. 2025 Cell
660181	C57BL/6J	AiE0387h	AiP12150	pAAV-AiE0387h-minBG-SYFP2-WPRE3-BGHpA	EPI	Astro	SYFP2	RO	Ben-Simon, et al. 2025 Cell
749615	Ai14(RCL-tdT	AiE0387m	AiP13999	pAAV-AiE0387m-minBG-iCre(R297T)-BGHpA	EPI, IHC	Astro	iCre(R297	RO	Ben-Simon, et al. 2025 Cell
751717	Ai14(RCL-tdT	AiE0387m	AiP13999	pAAV-AiE0387m-minBG-iCre(R297T)-BGHpA	IHC	Astro	iCre(R297	RO	Mich et al., 2025 bioRxiv
751911	Ai14(RCL-tdT	AiE0387m	AiP13999	pAAV-AiE0387m-minBG-iCre(R297T)-BGHpA	IHC	Astro	iCre(R297	RO	Mich et al., 2025 bioRxiv
542087	C57BL/6J	AiE0387m	AiP12102	pAAV-AiE0387m-minBG-SYFP2-WPRE3-BGHpA	EPI, IHC	Astro	SYFP2	RO	Mich et al., 2025 bioRxiv
608407	C57BL/6J	AiE0387m	AiP13635	pAAV-AiE0387m-minBG-SYFP2-P2A-3XFLAG-10aa-H2B-'	EPI	Astro	SYFP2	RO	Mich et al., 2025 bioRxiv
621234	C57BL/6J	AiE0387m	AiP13635	pAAV-AiE0387m-minBG-SYFP2-P2A-3XFLAG-10aa-H2B-'	EPI	Astro	SYFP2	RO	Mich et al., 2025 bioRxiv
625959	C57BL/6J	AiE0387m	AiP12102	pAAV-AiE0387m-minBG-SYFP2-WPRE3-BGHpA	EPI, IHC	Astro	SYFP2	RO	Mich et al., 2025 bioRxiv
636673	C57BL/6J	AiE0387m	AiP12102	pAAV-AiE0387m-minBG-SYFP2-WPRE3-BGHpA	EPI, IHC	Astro	SYFP2	RO	Mich et al., 2025 bioRxiv
648493	C57BL/6J	AiE0387m	AiP12102	pAAV-AiE0387m-minBG-SYFP2-WPRE3-BGHpA	EPI, IHC	Astro	SYFP2	RO	Mich et al., 2025 bioRxiv
648494	C57BL/6J	AiE0387m	AiP14309	pAAV-TeIN-LITR-AiE0387m-minBG-SYFP2-P2A-3XFLAG-:	EPI, IHC	Astro	SYFP2	RO	Mich et al., 2025 bioRxiv
648495	C57BL/6J	AiE0387m	AiP14309	pAAV-TeIN-LITR-AiE0387m-minBG-SYFP2-P2A-3XFLAG-:	EPI, IHC	Astro	SYFP2	RO	Mich et al., 2025 bioRxiv
743807	C57BL/6J	AiE0387m	AiP12102	pAAV-AiE0387m-minBG-SYFP2-WPRE3-BGHpA	EPI, IHC	Astro	SYFP2	RO	Mich et al., 2025 bioRxiv
745311	C57BL/6J	AiE0387m	AiP12102	pAAV-AiE0387m-minBG-SYFP2-WPRE3-BGHpA	EPI, IHC	Astro	SYFP2	RO	Mich et al., 2025 bioRxiv
593373	C57BL/6J	AiE0387m	AiP12102	pAAV-AiE0387m-minBG-SYFP2-WPRE3-BGHpA	scRNA-seq	Astro	SYFP2	RO	Mich et al., 2025 bioRxiv
502935	C57BL/6J	AiE0387m	AiP12102	pAAV-AiE0387m-minBG-SYFP2-WPRE3-BGHpA	EPI	Astro	SYFP2	RO	Mich et al., 2025 bioRxiv
630972	C57BL/6J	AiE0387m	AiP12102	pAAV-AiE0387m-minBG-SYFP2-WPRE3-BGHpA	EPI	Astro	SYFP2	RO	Ben-Simon, et al. 2025 Cell
629424	C57BL/6J	AiE0387m	AiP12102	pAAV-AiE0387m-minBG-SYFP2-WPRE3-BGHpA	STPT	Astro	SYFP2	RO	Ben-Simon, et al. 2025 Cell
634482	C57BL/6J	AiE0387m	AiP12102	pAAV-AiE0387m-minBG-SYFP2-WPRE3-BGHpA	STPT	Astro	SYFP2	RO	Ben-Simon, et al. 2025 Cell
639178	C57BL/6J	AiE0387m	AiP12102	pAAV-AiE0387m-minBG-SYFP2-WPRE3-BGHpA	EPI	Astro	SYFP2	RO	Ben-Simon, et al. 2025 Cell
629424	C57BL/6J	AiE0387m	AiP12102	pAAV-AiE0387m-minBG-SYFP2-WPRE3-BGHpA	STPT	Astro	SYFP2	RO	Ben-Simon, et al. 2025 Cell
634482	C57BL/6J	AiE0387m	AiP12102	pAAV-AiE0387m-minBG-SYFP2-WPRE3-BGHpA	STPT	Astro	SYFP2	RO	Ben-Simon, et al. 2025 Cell
610229	C57BL/6J	AiE0387m	AiP13635	pAAV-AiE0387m-minBG-SYFP2-P2A-3XFLAG-10aa-H2B-'	EPI	Astro	SYFP2	RO	Ben-Simon, et al. 2025 Cell
610229	C57BL/6J	AiE0387m	AiP13635	pAAV-AiE0387m-minBG-SYFP2-P2A-3XFLAG-10aa-H2B-'	EPI	Astro	SYFP2	RO	Ben-Simon, et al. 2025 Cell
652697	C57BL/6J	AiE0387m	AiP13635	pAAV-AiE0387m-minBG-SYFP2-P2A-3XFLAG-10aa-H2B-'	STPT	Astro	SYFP2	ICV	Ben-Simon, et al. 2025 Cell
652697	C57BL/6J	AiE0387m	AiP13635	pAAV-AiE0387m-minBG-SYFP2-P2A-3XFLAG-10aa-H2B-'	STPT	Astro	SYFP2	ICV	Ben-Simon, et al. 2025 Cell
652697	C57BL/6J	AiE0387m	AiP13635	pAAV-AiE0387m-minBG-SYFP2-P2A-3XFLAG-10aa-H2B-'	STPT	Astro	SYFP2	ICV	Ben-Simon, et al. 2025 Cell
631110	C57BL/6J	AiE0387m	AiP13635	pAAV-AiE0387m-minBG-SYFP2-P2A-3XFLAG-10aa-H2B-'	EPI	Astro	SYFP2	ICV	Ben-Simon, et al. 2025 Cell
631110	C57BL/6J	AiE0387m	AiP13635	pAAV-AiE0387m-minBG-SYFP2-P2A-3XFLAG-10aa-H2B-'	EPI	Astro	SYFP2	ICV	Ben-Simon, et al. 2025 Cell
631110	C57BL/6J	AiE0387m	AiP13635	pAAV-AiE0387m-minBG-SYFP2-P2A-3XFLAG-10aa-H2B-'	EPI	Astro	SYFP2	ICV	Ben-Simon, et al. 2025 Cell
631110	C57BL/6J	AiE0387m	AiP13635	pAAV-AiE0387m-minBG-SYFP2-P2A-3XFLAG-10aa-H2B-'	EPI	Astro	SYFP2	ICV	Ben-Simon, et al. 2025 Cell
652697	C57BL/6J	AiE0387m	AiP13635	pAAV-AiE0387m-minBG-SYFP2-P2A-3XFLAG-10aa-H2B-'	STPT	Astro	SYFP2	ICV	Ben-Simon, et al. 2025 Cell
634491	C57BL/6J	AiE0387m_3xC	AiP13568	pAAV-AiE0387m_3xC1-minBG-SYFP2-WPRE3-BGHpA	STPT	Astro	SYFP2	RO	Ben-Simon, et al. 2025 Cell
630973	C57BL/6J	AiE0387m_3xC	AiP13568	pAAV-AiE0387m_3xC1-minBG-SYFP2-WPRE3-BGHpA	EPI	Astro	SYFP2	RO	Ben-Simon, et al. 2025 Cell
634492	C57BL/6J	AiE0387m_3xC	AiP13569	pAAV-AiE0387m_3xC2-minBG-SYFP2-WPRE3-BGHpA	STPT	Astro	SYFP2	RO	Ben-Simon, et al. 2025 Cell
514396	C57BL/6J	AiE0388h	AiP12151	pAAV-AiE0388h-minBG-SYFP2-WPRE3-BGHpA	EPI	Astro	SYFP2	RO	Mich et al., 2025 bioRxiv
502936	C57BL/6J	AiE0388m	AiP12103	pAAV-AiE0388m-minBG-SYFP2-WPRE3-BGHpA	EPI	Astro	SYFP2	RO	Mich et al., 2025 bioRxiv
567941	C57BL/6J	AiE0389h	AiP12152	pAAV-AiE0389h-minBG-SYFP2-WPRE3-BGHpA	EPI	Astro	SYFP2	RO	Mich et al., 2025 bioRxiv
623013	C57BL/6J	AiE0389h	AiP12152	pAAV-AiE0389h-minBG-SYFP2-WPRE3-BGHpA	EPI	Astro	SYFP2	RO	Ben-Simon, et al. 2025 Cell
576010	C57BL/6J	AiE0389m	AiP13061	pAAV-AiE0389m-minBG-SYFP2-WPRE3-BGHpA	EPI	Astro	SYFP2	RO	Mich et al., 2025 bioRxiv
623023	C57BL/6J	AiE0389m	AiP13061	pAAV-AiE0389m-minBG-SYFP2-WPRE3-BGHpA	EPI	Astro	SYFP2	RO	Ben-Simon, et al. 2025 Cell
717604	Ai14(RCL-tdT	AiE0390h	AiP13998	pAAV-AiE0390h-minBG-iCre(R297T)-BGHpA	EPI	Astro	iCre(R297	RO	Ben-Simon, et al. 2025 Cell
750307	Ai14(RCL-tdT	AiE0390h	AiP13998	pAAV-AiE0390h-minBG-iCre(R297T)-BGHpA	STPT, IHC	Astro	iCre(R297	RO	Ben-Simon, et al. 2025 Cell
640524	Ai14(RCL-tdT	AiE0390h	AiP13998	pAAV-AiE0390h-minBG-iCre(R297T)-BGHpA	IHC	Astro	iCre(R297	RO	Mich et al., 2025 bioRxiv
738664	Ai14(RCL-tdT	AiE0390h	AiP13998	pAAV-AiE0390h-minBG-iCre(R297T)-BGHpA	IHC	Astro	iCre(R297	RO	Mich et al., 2025 bioRxiv
615011	C57BL/6J	AiE0390h	AiP12153	pAAV-AiE0390h-minBG-SYFP2-WPRE3-BGHpA	EPI, IHC	Astro	SYFP2	RO	Mich et al., 2025 bioRxiv
621240	C57BL/6J	AiE0390h	AiP12822	pAAV-AiE0390h-minRho-SYFP2-10aa-H2Bmod-WPRE3-(	EPI	Astro	SYFP2	RO	Mich et al., 2025 bioRxiv
625961	C57BL/6J	AiE0390h	AiP12153	pAAV-AiE0390h-minBG-SYFP2-WPRE3-BGHpA	EPI, IHC	Astro	SYFP2	RO	Mich et al., 2025 bioRxiv

743808	C57BL/6J	AiE0390h	AiP12153	pAAV-AiE0390h-minBG-SYFP2-WPRE3-BGHpA	EPI, IHC	Astro	SYFP2	RO	Mich et al., 2025 bioRxiv
745312	C57BL/6J	AiE0390h	AiP12153	pAAV-AiE0390h-minBG-SYFP2-WPRE3-BGHpA	EPI, IHC	Astro	SYFP2	RO	Mich et al., 2025 bioRxiv
584420	C57BL/6J	AiE0390h	AiP12153	pAAV-AiE0390h-minBG-SYFP2-WPRE3-BGHpA	scRNA-seq	Astro	SYFP2	RO	Mich et al., 2025 bioRxiv
584420	C57BL/6J	AiE0390h	AiP12153	pAAV-AiE0390h-minBG-SYFP2-WPRE3-BGHpA	scRNA-seq	Astro	SYFP2	RO	Mich et al., 2025 bioRxiv
514397	C57BL/6J	AiE0390h	AiP12153	pAAV-AiE0390h-minBG-SYFP2-WPRE3-BGHpA	EPI	Astro	SYFP2	RO	Mich et al., 2025 bioRxiv
639176	C57BL/6J	AiE0390h	AiP12153	pAAV-AiE0390h-minBG-SYFP2-WPRE3-BGHpA	STPT	Astro	SYFP2	RO	Ben-Simon, et al. 2025 Cell
630974	C57BL/6J	AiE0390h	AiP12153	pAAV-AiE0390h-minBG-SYFP2-WPRE3-BGHpA	EPI	Astro	SYFP2	RO	Ben-Simon, et al. 2025 Cell
639176	C57BL/6J	AiE0390h	AiP12153	pAAV-AiE0390h-minBG-SYFP2-WPRE3-BGHpA	STPT	Astro	SYFP2	RO	Ben-Simon, et al. 2025 Cell
623014	C57BL/6J	AiE0390h	AiP12153	pAAV-AiE0390h-minBG-SYFP2-WPRE3-BGHpA	EPI	Astro	SYFP2	RO	Ben-Simon, et al. 2025 Cell
630974	C57BL/6J	AiE0390h	AiP12153	pAAV-AiE0390h-minBG-SYFP2-WPRE3-BGHpA	EPI	Astro	SYFP2	RO	Ben-Simon, et al. 2025 Cell
639176	C57BL/6J	AiE0390h	AiP12153	pAAV-AiE0390h-minBG-SYFP2-WPRE3-BGHpA	STPT	Astro	SYFP2	RO	Ben-Simon, et al. 2025 Cell
630974	C57BL/6J	AiE0390h	AiP12153	pAAV-AiE0390h-minBG-SYFP2-WPRE3-BGHpA	EPI	Astro	SYFP2	RO	Ben-Simon, et al. 2025 Cell
671751	CD-1_IGS	AiE0390h	AiP12153	pAAV-AiE0390h-minBG-SYFP2-WPRE3-BGHpA	STPT	Astro	SYFP2	ICV	Ben-Simon, et al. 2025 Cell
630975	C57BL/6J	AiE0390h_3xC	AiP13571	pAAV-AiE0390h_3xC1-minBG-SYFP2-WPRE3-BGHpA	EPI	Astro	SYFP2	RO	Ben-Simon, et al. 2025 Cell
651220	C57BL/6J	AiE0390h_3xC	AiP13572	pAAV-AiE0390h_3xC2-minBG-SYFP2-WPRE3-BGHpA	scRNA-seq	Astro	SYFP2	RO	Mich et al., 2025 bioRxiv
647378	C57BL/6J	AiE0390h_3xC	AiP13572	pAAV-AiE0390h_3xC2-minBG-SYFP2-WPRE3-BGHpA	STPT	Astro	SYFP2	RO	Ben-Simon, et al. 2025 Cell
630976	C57BL/6J	AiE0390h_3xC	AiP13572	pAAV-AiE0390h_3xC2-minBG-SYFP2-WPRE3-BGHpA	EPI	Astro	SYFP2	RO	Ben-Simon, et al. 2025 Cell
630977	C57BL/6J	AiE0390h_3xC	AiP13573	pAAV-AiE0390h_3xC3-minBG-SYFP2-WPRE3-BGHpA	EPI	Astro	SYFP2	RO	Ben-Simon, et al. 2025 Cell
630977	C57BL/6J	AiE0390h_3xC	AiP13573	pAAV-AiE0390h_3xC3-minBG-SYFP2-WPRE3-BGHpA	EPI	Astro	SYFP2	RO	Ben-Simon, et al. 2025 Cell
615008	C57BL/6J	AiE0390m	AiP12089	pAAV-AiE0390m-minBG-SYFP2-WPRE3-BGHpA	EPI, IHC	Astro	SYFP2	RO	Mich et al., 2025 bioRxiv
621236	C57BL/6J	AiE0390m	AiP12818	pAAV-AiE0390m-minRho-SYFP2-10aa-H2Bmod-WPRE3-	EPI	Astro	SYFP2	RO	Mich et al., 2025 bioRxiv
625964	C57BL/6J	AiE0390m	AiP12089	pAAV-AiE0390m-minBG-SYFP2-WPRE3-BGHpA	EPI, IHC	Astro	SYFP2	RO	Mich et al., 2025 bioRxiv
629468	C57BL/6J	AiE0390m	AiP12089	pAAV-AiE0390m-minBG-SYFP2-WPRE3-BGHpA	EPI, IHC	Astro	SYFP2	RO	Mich et al., 2025 bioRxiv
627901	C57BL/6J	AiE0390m	AiP12818	pAAV-AiE0390m-minRho-SYFP2-10aa-H2Bmod-WPRE3-	EPI	Astro	SYFP2	RO	Mich et al., 2025 bioRxiv
743806	C57BL/6J	AiE0390m	AiP12089	pAAV-AiE0390m-minBG-SYFP2-WPRE3-BGHpA	EPI, IHC	Astro	SYFP2	RO	Mich et al., 2025 bioRxiv
745310	C57BL/6J	AiE0390m	AiP12089	pAAV-AiE0390m-minBG-SYFP2-WPRE3-BGHpA	EPI, IHC	Astro	SYFP2	RO	Mich et al., 2025 bioRxiv
616740	C57BL/6J	AiE0390m	AiP12089	pAAV-AiE0390m-minBG-SYFP2-WPRE3-BGHpA	scRNA-seq	Astro	SYFP2	RO	Mich et al., 2025 bioRxiv
556485	C57BL/6J	AiE0390m	AiP12089	pAAV-AiE0390m-minBG-SYFP2-WPRE3-BGHpA	scRNA-seq	Astro	SYFP2	RO	Mich et al., 2025 bioRxiv
500567	C57BL/6J	AiE0390m	AiP12089	pAAV-AiE0390m-minBG-SYFP2-WPRE3-BGHpA	EPI	Astro	SYFP2	RO	Mich et al., 2025 bioRxiv
623024	C57BL/6J	AiE0390m	AiP12089	pAAV-AiE0390m-minBG-SYFP2-WPRE3-BGHpA	EPI	Astro	SYFP2	RO	Ben-Simon, et al. 2025 Cell
678872	C57BL/6J	AiE0390m	AiP12089	pAAV-AiE0390m-minBG-SYFP2-WPRE3-BGHpA	EPI	Astro	SYFP2	RO	Ben-Simon, et al. 2025 Cell
574637	C57BL/6J	AiE0390m	AiP12089	pAAV-AiE0390m-minBG-SYFP2-WPRE3-BGHpA	STPT	Astro	SYFP2	RO	Ben-Simon, et al. 2025 Cell
678872	C57BL/6J	AiE0390m	AiP12089	pAAV-AiE0390m-minBG-SYFP2-WPRE3-BGHpA	EPI	Astro	SYFP2	RO	Ben-Simon, et al. 2025 Cell
574637	C57BL/6J	AiE0390m	AiP12089	pAAV-AiE0390m-minBG-SYFP2-WPRE3-BGHpA	STPT	Astro	SYFP2	RO	Ben-Simon, et al. 2025 Cell
678872	C57BL/6J	AiE0390m	AiP12089	pAAV-AiE0390m-minBG-SYFP2-WPRE3-BGHpA	EPI	Astro	SYFP2	RO	Ben-Simon, et al. 2025 Cell
574637	C57BL/6J	AiE0390m	AiP12089	pAAV-AiE0390m-minBG-SYFP2-WPRE3-BGHpA	STPT	Astro	SYFP2	RO	Ben-Simon, et al. 2025 Cell
671887	CD-1_IGS	AiE0390m	AiP12089	pAAV-AiE0390m-minBG-SYFP2-WPRE3-BGHpA	STPT	Astro	SYFP2	ICV	Ben-Simon, et al. 2025 Cell
636220	Scn1a +/+	AiE0390m	AiP14038	pAAV-390m-minRho-SYFP2-P2A-3XFLAG-10aa-H2B*-W	EPI	Astro	SYFP2	RO	Mich et al., 2025 bioRxiv
636222	Scn1a-R613X	AiE0390m	AiP14038	pAAV-390m-minRho-SYFP2-P2A-3XFLAG-10aa-H2B*-W	EPI	Astro	SYFP2	RO	Mich et al., 2025 bioRxiv
637351	Scn1a-R613X	AiE0390m	AiP14038	pAAV-390m-minRho-SYFP2-P2A-3XFLAG-10aa-H2B*-W	EPI, IHC	Astro	SYFP2	RO	Mich et al., 2025 bioRxiv
637352	Scn1a-R613X	AiE0390m	AiP14038	pAAV-390m-minRho-SYFP2-P2A-3XFLAG-10aa-H2B*-W	EPI, IHC	Astro	SYFP2	RO	Mich et al., 2025 bioRxiv
637350	Scn1a +/+	AiE0390m	AiP14038	pAAV-390m-minRho-SYFP2-P2A-3XFLAG-10aa-H2B*-W	EPI, IHC	Astro	SYFP2	RO	Mich et al., 2025 bioRxiv
637354	Scn1a +/+	AiE0390m	AiP14038	pAAV-390m-minRho-SYFP2-P2A-3XFLAG-10aa-H2B*-W	EPI, IHC	Astro	SYFP2	RO	Mich et al., 2025 bioRxiv
751716	Ai14(RCL-tdT	AiE0390m_3xC	AiP14801	pAAV-AiE0390m_3xC2-minBG-iCre(R297T)-BGHpA	IHC	Astro	iCre(R297	RO	Mich et al., 2025 bioRxiv
751909	Ai14(RCL-tdT	AiE0390m_3xC	AiP14801	pAAV-AiE0390m_3xC2-minBG-iCre(R297T)-BGHpA	IHC	Astro	iCre(R297	RO	Mich et al., 2025 bioRxiv
749614	Ai14(RCL-tdT	AiE0390m_3xC	AiP14801	pAAV-AiE0390m_3xC2-minBG-iCre(R297T)-BGHpA	EPI, IHC	Astro	iCre(R297	RO	Ben-Simon, et al. 2025 Cell
626921	C57BL/6J	AiE0390m_3xC	AiP12558	pAAV-AiE0390m_3xC2-minBG-SYFP2-WPRE3-BGHpA	EPI, IHC	Astro	SYFP2	RO	Mich et al., 2025 bioRxiv
629462	C57BL/6J	AiE0390m_3xC	AiP12558	pAAV-AiE0390m_3xC2-minBG-SYFP2-WPRE3-BGHpA	EPI, IHC	Astro	SYFP2	RO	Mich et al., 2025 bioRxiv
651223	C57BL/6J	AiE0390m_3xC	AiP12558	pAAV-AiE0390m_3xC2-minBG-SYFP2-WPRE3-BGHpA	scRNA-seq	Astro	SYFP2	RO	Mich et al., 2025 bioRxiv
630480	C57BL/6J	AiE0390m_3xC	AiP12558	pAAV-AiE0390m_3xC2-minBG-SYFP2-WPRE3-BGHpA	scRNA-seq	Astro	SYFP2	RO	Mich et al., 2025 bioRxiv
574636	C57BL/6J	AiE0390m_3xC	AiP12558	pAAV-AiE0390m_3xC2-minBG-SYFP2-WPRE3-BGHpA	STPT	Astro	SYFP2	RO	Ben-Simon, et al. 2025 Cell
678873	C57BL/6J	AiE0390m_3xC	AiP12558	pAAV-AiE0390m_3xC2-minBG-SYFP2-WPRE3-BGHpA	EPI	Astro	SYFP2	RO	Ben-Simon, et al. 2025 Cell
639179	C57BL/6J	AiE0390m_3xC	AiP12558	pAAV-AiE0390m_3xC2-minBG-SYFP2-WPRE3-BGHpA	EPI	Astro	SYFP2	RO	Ben-Simon, et al. 2025 Cell
622082	C57BL/6J	AiE0391h	AiP12505	pAAV-AiE0391h-minBG-SYFP2-WPRE3-BGHpA	EPI, IHC	Oligo	SYFP2	RO	Mich et al., 2025 bioRxiv
626924	C57BL/6J	AiE0391h	AiP12505	pAAV-AiE0391h-minBG-SYFP2-WPRE3-BGHpA	EPI, IHC	Oligo	SYFP2	RO	Mich et al., 2025 bioRxiv
617306	C57BL/6J	AiE0391h	AiP12505	pAAV-AiE0391h-minBG-SYFP2-WPRE3-BGHpA	scRNA-seq	Oligo	SYFP2	RO	Mich et al., 2025 bioRxiv
551396	C57BL/6J	AiE0391h	AiP12505	pAAV-AiE0391h-minBG-SYFP2-WPRE3-BGHpA	EPI, IHC	Oligo	SYFP2	RO	Mich et al., 2025 bioRxiv
634957	C57BL/6J	AiE0391h	AiP12505	pAAV-AiE0391h-minBG-SYFP2-WPRE3-BGHpA	STPT	Oligo	SYFP2	RO	Ben-Simon, et al. 2025 Cell
620746	C57BL/6J	AiE0391h	AiP12505	pAAV-AiE0391h-minBG-SYFP2-WPRE3-BGHpA	EPI	Oligo	SYFP2	RO	Ben-Simon, et al. 2025 Cell
500568	C57BL/6J	AiE0391m	AiP12090	pAAV-AiE0391m-minBG-SYFP2-WPRE3-BGHpA	EPI	Oligo	SYFP2	RO	Mich et al., 2025 bioRxiv
514398	C57BL/6J	AiE0392h	AiP12154	pAAV-AiE0392h-minBG-SYFP2-WPRE3-BGHpA	EPI	Oligo	SYFP2	RO	Mich et al., 2025 bioRxiv
514399	C57BL/6J	AiE0393h	AiP12155	pAAV-AiE0393h-minBG-SYFP2-WPRE3-BGHpA	EPI	Oligo	SYFP2	RO	Mich et al., 2025 bioRxiv
502937	C57BL/6J	AiE0393m	AiP12104	pAAV-AiE0393m-minBG-SYFP2-WPRE3-BGHpA	EPI	Oligo	SYFP2	RO	Mich et al., 2025 bioRxiv
567942	C57BL/6J	AiE0394h	AiP12156	pAAV-AiE0394h-minBG-SYFP2-WPRE3-BGHpA	EPI	Oligo	SYFP2	RO	Mich et al., 2025 bioRxiv
567943	C57BL/6J	AiE0394m	AiP12497	pAAV-AiE0394m-minBG-SYFP2-WPRE3-BGHpA	EPI	Oligo	SYFP2	RO	Mich et al., 2025 bioRxiv
622083	C57BL/6J	AiE0395h	AiP12157	pAAV-AiE0395h-minBG-SYFP2-WPRE3-BGHpA	EPI, IHC	Oligo	SYFP2	RO	Mich et al., 2025 bioRxiv
621238	C57BL/6J	AiE0395h	AiP12823	pAAV-AiE0395h-minRho-SYFP2-10aa-H2Bmod-WPRE3-(	EPI	Oligo	SYFP2	RO	Mich et al., 2025 bioRxiv
626925	C57BL/6J	AiE0395h	AiP12157	pAAV-AiE0395h-minBG-SYFP2-WPRE3-BGHpA	EPI, IHC	Oligo	SYFP2	RO	Mich et al., 2025 bioRxiv
629464	C57BL/6J	AiE0395h	AiP12157	pAAV-AiE0395h-minBG-SYFP2-WPRE3-BGHpA	EPI, IHC	Oligo	SYFP2	RO	Mich et al., 2025 bioRxiv
617307	C57BL/6J	AiE0395h	AiP12157	pAAV-AiE0395h-minBG-SYFP2-WPRE3-BGHpA	scRNA-seq	Oligo	SYFP2	RO	Mich et al., 2025 bioRxiv
562430	C57BL/6J	AiE0395h	AiP12157	pAAV-AiE0395h-minBG-SYFP2-WPRE3-BGHpA	scRNA-seq	Oligo	SYFP2	RO	Mich et al., 2025 bioRxiv
641432	C57BL/6J	AiE0395h	AiP12157	pAAV-AiE0395h-minBG-SYFP2-WPRE3-BGHpA	scRNA-seq	Oligo	SYFP2	RO	Mich et al., 2025 bioRxiv
515295	C57BL/6J	AiE0395h	AiP12157	pAAV-AiE0395h-minBG-SYFP2-WPRE3-BGHpA	EPI	Oligo	SYFP2	RO	Mich et al., 2025 bioRxiv
620747	C57BL/6J	AiE0395h	AiP12157	pAAV-AiE0395h-minBG-SYFP2-WPRE3-BGHpA	EPI	Oligo	SYFP2	RO	Ben-Simon, et al. 2025 Cell
634958	C57BL/6J	AiE0395h	AiP12157	pAAV-AiE0395h-minBG-SYFP2-WPRE3-BGHpA	STPT	Oligo	SYFP2	RO	Ben-Simon, et al. 2025 Cell
636677	C57BL/6J	AiE0395m	AiP12498	pAAV-AiE0395m-minBG-SYFP2-WPRE3-BGHpA	EPI, IHC	Oligo	SYFP2	RO	Mich et al., 2025 bioRxiv
567944	C57BL/6J	AiE0395m	AiP12498	pAAV-AiE0395m-minBG-SYFP2-WPRE3-BGHpA	EPI, IHC	Oligo	SYFP2	RO	Mich et al., 2025 bioRxiv
616882	C57BL/6J	AiE0395m	AiP12498	pAAV-AiE0395m-minBG-SYFP2-WPRE3-BGHpA	STPT	Oligo	SYFP2	RO	Ben-Simon, et al. 2025 Cell
621446	C57BL/6J	AiE0395m	AiP12498	pAAV-AiE0395m-minBG-SYFP2-WPRE3-BGHpA	EPI	Oligo	SYFP2	RO	Ben-Simon, et al. 2025 Cell
622084	C57BL/6J	AiE0396h	AiP12158	pAAV-AiE0396h-minBG-SYFP2-WPRE3-BGHpA	EPI, IHC	Oligo	SYFP2	RO	Mich et al., 2025 bioRxiv
626926	C57BL/6J	AiE0396h	AiP12158	pAAV-AiE0396h-minBG-SYFP2-WPRE3-BGHpA	EPI, IHC	Oligo	SYFP2	RO	Mich et al., 2025 bioRxiv
622118	C57BL/6J	AiE0396h	AiP12158	pAAV-AiE0396h-minBG-SYFP2-WPRE3-BGHpA	scRNA-seq	Oligo	SYFP2	RO	Mich et al., 2025 bioRxiv
567945	C57BL/6J	AiE0396h	AiP12158	pAAV-AiE0396h-minBG-SYFP2-WPRE3-BGHpA	EPI, IHC	Oligo	SYFP2	RO	Mich et al., 2025 bioRxiv
622617	C57BL/6J	AiE0396h	AiP12158	pAAV-AiE0396h-minBG-SYFP2-WPRE3-BGHpA	EPI	Oligo	SYFP2	RO	Ben-Simon, et al. 2025 Cell
601540	C57BL/6J	AiE0396m	AiP12099	pAAV-AiE0396m-minBG-SYFP2-WPRE3-BGHpA	scRNA-seq	Oligo	SYFP2	RO	Mich et al., 2025 bioRxiv
501913	C57BL/6J	AiE0396m	AiP12099	pAAV-AiE0396m-minBG-SYFP2-WPRE3-BGHpA	EPI	Oligo	SYFP2	RO	Mich et al., 2025 bioRxiv
621447	C57BL/6J	AiE0396m	AiP12099	pAAV-AiE0396m-minBG-SYFP2-WPRE3-BGHpA	EPI	Oligo	SYFP2	RO	Ben-Simon, et al. 2025 Cell
515296	C57BL/6J	AiE0397h	AiP12159	pAAV-AiE0397h-minBG-SYFP2-WPRE3-BGHpA	EPI	Oligo	SYFP2	RO	Mich et al., 2025 bioRxiv
622618	C57BL/6J	AiE0397h	AiP12159	pAAV-AiE0397h-minBG-SYFP2-WPRE3-BGHpA	EPI	Oligo	SYFP2	RO	Ben-Simon, et al. 2025 Cell
642125	C57BL/6J	AiE0397m	AiP12123	pAAV-AiE0397m-minBG-SYFP2-WPRE3-BGHpA	scRNA-seq	Oligo	SYFP2	RO	Mich et al., 2025 bioRxiv

570672	C57BL/6J	AiE0397m	AiP12123	pAAV-AiE0397m-minBG-SYFP2-WPRE3-BGHpA	EPI, IHC	Oligo	SYFP2	RO	Mich et al., 2025 bioRxiv
616881	C57BL/6J	AiE0397m	AiP12123	pAAV-AiE0397m-minBG-SYFP2-WPRE3-BGHpA	STPT	Oligo	SYFP2	RO	Ben-Simon, et al. 2025 Cell
621448	C57BL/6J	AiE0397m	AiP12123	pAAV-AiE0397m-minBG-SYFP2-WPRE3-BGHpA	EPI	Oligo	SYFP2	RO	Ben-Simon, et al. 2025 Cell
637261	C57BL/6J	AiE0397m	AiP12123	pAAV-AiE0397m-minBG-SYFP2-WPRE3-BGHpA	STPT	Oligo	SYFP2	RO	Ben-Simon, et al. 2025 Cell
515297	C57BL/6J	AiE0398h	AiP12160	pAAV-AiE0398h-minBG-SYFP2-WPRE3-BGHpA	EPI	Oligo	SYFP2	RO	Mich et al., 2025 bioRxiv
622619	C57BL/6J	AiE0398h	AiP12160	pAAV-AiE0398h-minBG-SYFP2-WPRE3-BGHpA	EPI	Oligo	SYFP2	RO	Ben-Simon, et al. 2025 Cell
500569	C57BL/6J	AiE0398m	AiP12091	pAAV-AiE0398m-minBG-SYFP2-WPRE3-BGHpA	EPI	Oligo	SYFP2	RO	Mich et al., 2025 bioRxiv
621449	C57BL/6J	AiE0398m	AiP12091	pAAV-AiE0398m-minBG-SYFP2-WPRE3-BGHpA	EPI	Oligo	SYFP2	RO	Ben-Simon, et al. 2025 Cell
570673	C57BL/6J	AiE0399h	AiP12161	pAAV-AiE0399h-minBG-SYFP2-WPRE3-BGHpA	EPI	Oligo	SYFP2	RO	Mich et al., 2025 bioRxiv
502938	C57BL/6J	AiE0399m	AiP12105	pAAV-AiE0399m-minBG-SYFP2-WPRE3-BGHpA	EPI	Oligo	SYFP2	RO	Mich et al., 2025 bioRxiv
622085	C57BL/6J	AiE0400h	AiP12162	pAAV-AiE0400h-minBG-SYFP2-WPRE3-BGHpA	EPI, IHC	Oligo	SYFP2	RO	Mich et al., 2025 bioRxiv
626927	C57BL/6J	AiE0400h	AiP12162	pAAV-AiE0400h-minBG-SYFP2-WPRE3-BGHpA	EPI, IHC	Oligo	SYFP2	RO	Mich et al., 2025 bioRxiv
622119	C57BL/6J	AiE0400h	AiP12162	pAAV-AiE0400h-minBG-SYFP2-WPRE3-BGHpA	scRNA-seq	Oligo	SYFP2	RO	Mich et al., 2025 bioRxiv
570674	C57BL/6J	AiE0400h	AiP12162	pAAV-AiE0400h-minBG-SYFP2-WPRE3-BGHpA	EPI, IHC	Oligo	SYFP2	RO	Mich et al., 2025 bioRxiv
621151	C57BL/6J	AiE0400h	AiP12162	pAAV-AiE0400h-minBG-SYFP2-WPRE3-BGHpA	EPI	Oligo	SYFP2	RO	Ben-Simon, et al. 2025 Cell
616880	C57BL/6J	AiE0400h	AiP12162	pAAV-AiE0400h-minBG-SYFP2-WPRE3-BGHpA	STPT	Oligo	SYFP2	RO	Ben-Simon, et al. 2025 Cell
671883	CD-1_IGS	AiE0400h	AiP12162	pAAV-AiE0400h-minBG-SYFP2-WPRE3-BGHpA	STPT	Oligo	SYFP2	ICV	Ben-Simon, et al. 2025 Cell
601541	C57BL/6J	AiE0400m	AiP12106	pAAV-AiE0400m-minBG-SYFP2-WPRE3-BGHpA	scRNA-seq	Oligo	SYFP2	RO	Mich et al., 2025 bioRxiv
502939	C57BL/6J	AiE0400m	AiP12106	pAAV-AiE0400m-minBG-SYFP2-WPRE3-BGHpA	EPI	Oligo	SYFP2	RO	Mich et al., 2025 bioRxiv
621836	C57BL/6J	AiE0400m	AiP12106	pAAV-AiE0400m-minBG-SYFP2-WPRE3-BGHpA	EPI	Oligo	SYFP2	RO	Ben-Simon, et al. 2025 Cell
616884	C57BL/6J	AiE0400m	AiP12106	pAAV-AiE0400m-minBG-SYFP2-WPRE3-BGHpA	STPT	Oligo	SYFP2	RO	Ben-Simon, et al. 2025 Cell
637264	C57BL/6J	AiE0400m	AiP12106	pAAV-AiE0400m-minBG-SYFP2-WPRE3-BGHpA	STPT	Oligo	SYFP2	RO	Ben-Simon, et al. 2025 Cell
626928	C57BL/6J	AiE0401h	AiP12677	pAAV-AiE0401h-minBG-SYFP2-WPRE3-BGHpA	EPI, IHC	Oligo	SYFP2	RO	Mich et al., 2025 bioRxiv
629465	C57BL/6J	AiE0401h	AiP12677	pAAV-AiE0401h-minBG-SYFP2-WPRE3-BGHpA	EPI, IHC	Oligo	SYFP2	RO	Mich et al., 2025 bioRxiv
619575	C57BL/6J	AiE0401h	AiP12677	pAAV-AiE0401h-minBG-SYFP2-WPRE3-BGHpA	scRNA-seq	Oligo	SYFP2	RO	Mich et al., 2025 bioRxiv
570675	C57BL/6J	AiE0401h	AiP12677	pAAV-AiE0401h-minBG-SYFP2-WPRE3-BGHpA	EPI, IHC	Oligo	SYFP2	RO	Mich et al., 2025 bioRxiv
670101	C57BL/6J	AiE0401h	AiP12677	pAAV-AiE0401h-minBG-SYFP2-WPRE3-BGHpA	EPI	Oligo	SYFP2	RO	Ben-Simon, et al. 2025 Cell
616879	C57BL/6J	AiE0401h	AiP12677	pAAV-AiE0401h-minBG-SYFP2-WPRE3-BGHpA	STPT	Oligo	SYFP2	RO	Ben-Simon, et al. 2025 Cell
671884	CD-1_IGS	AiE0401h	AiP12677	pAAV-AiE0401h-minBG-SYFP2-WPRE3-BGHpA	STPT	Oligo	SYFP2	ICV	Ben-Simon, et al. 2025 Cell
574340	C57BL/6J	AiE0401m	AiP12124	pAAV-AiE0401m-minBG-SYFP2-WPRE3-BGHpA	EPI	Oligo	SYFP2	RO	Mich et al., 2025 bioRxiv
575095	C57BL/6J	AiE0402h	AiP12163	pAAV-AiE0402h-minBG-SYFP2-WPRE3-BGHpA	EPI	Oligo	SYFP2	RO	Mich et al., 2025 bioRxiv
500570	C57BL/6J	AiE0402m	AiP12092	pAAV-AiE0402m-minBG-SYFP2-WPRE3-BGHpA	EPI	Oligo	SYFP2	RO	Mich et al., 2025 bioRxiv
621837	C57BL/6J	AiE0402m	AiP12092	pAAV-AiE0402m-minBG-SYFP2-WPRE3-BGHpA	EPI	Oligo	SYFP2	RO	Ben-Simon, et al. 2025 Cell
622086	C57BL/6J	AiE0403h	AiP12499	pAAV-AiE0403h-minBG-SYFP2-WPRE3-BGHpA	EPI, IHC	Oligo	SYFP2	RO	Mich et al., 2025 bioRxiv
629467	C57BL/6J	AiE0403h	AiP12499	pAAV-AiE0403h-minBG-SYFP2-WPRE3-BGHpA	EPI, IHC	Oligo	SYFP2	RO	Mich et al., 2025 bioRxiv
619576	C57BL/6J	AiE0403h	AiP12499	pAAV-AiE0403h-minBG-SYFP2-WPRE3-BGHpA	scRNA-seq	Oligo	SYFP2	RO	Mich et al., 2025 bioRxiv
551391	C57BL/6J	AiE0403h	AiP12499	pAAV-AiE0403h-minBG-SYFP2-WPRE3-BGHpA	EPI, IHC	Oligo	SYFP2	RO	Mich et al., 2025 bioRxiv
621152	C57BL/6J	AiE0403h	AiP12499	pAAV-AiE0403h-minBG-SYFP2-WPRE3-BGHpA	EPI	Oligo	SYFP2	RO	Ben-Simon, et al. 2025 Cell
634959	C57BL/6J	AiE0403h	AiP12499	pAAV-AiE0403h-minBG-SYFP2-WPRE3-BGHpA	STPT	Oligo	SYFP2	RO	Ben-Simon, et al. 2025 Cell
575092	C57BL/6J	AiE0403m	AiP12125	pAAV-AiE0403m-minBG-SYFP2-WPRE3-BGHpA	EPI	Oligo	SYFP2	RO	Mich et al., 2025 bioRxiv
515298	C57BL/6J	AiE0404h	AiP12164	pAAV-AiE0404h-minBG-SYFP2-WPRE3-BGHpA	EPI	Oligo	SYFP2	RO	Mich et al., 2025 bioRxiv
621153	C57BL/6J	AiE0404h	AiP12164	pAAV-AiE0404h-minBG-SYFP2-WPRE3-BGHpA	EPI	Oligo	SYFP2	RO	Ben-Simon, et al. 2025 Cell
650133	C57BL/6J	AiE0404h	AiP12164	pAAV-AiE0404h-minBG-SYFP2-WPRE3-BGHpA	STPT	Oligo	SYFP2	RO	Ben-Simon, et al. 2025 Cell
576008	C57BL/6J	AiE0404m	AiP12500	pAAV-AiE0404m-minBG-SYFP2-WPRE3-BGHpA	EPI	Oligo	SYFP2	RO	Mich et al., 2025 bioRxiv
575096	C57BL/6J	AiE0405h	AiP12165	pAAV-AiE0405h-minBG-SYFP2-WPRE3-BGHpA	EPI	Oligo	SYFP2	RO	Mich et al., 2025 bioRxiv
601542	C57BL/6J	AiE0405m	AiP12107	pAAV-AiE0405m-minBG-SYFP2-WPRE3-BGHpA	scRNA-seq	Oligo	SYFP2	RO	Mich et al., 2025 bioRxiv
502940	C57BL/6J	AiE0405m	AiP12107	pAAV-AiE0405m-minBG-SYFP2-WPRE3-BGHpA	EPI	Oligo	SYFP2	RO	Mich et al., 2025 bioRxiv
616885	C57BL/6J	AiE0405m	AiP12107	pAAV-AiE0405m-minBG-SYFP2-WPRE3-BGHpA	STPT	Oligo	SYFP2	RO	Ben-Simon, et al. 2025 Cell
621838	C57BL/6J	AiE0405m	AiP12107	pAAV-AiE0405m-minBG-SYFP2-WPRE3-BGHpA	EPI	Oligo	SYFP2	RO	Ben-Simon, et al. 2025 Cell
575097	C57BL/6J	AiE0406h	AiP12166	pAAV-AiE0406h-minBG-SYFP2-WPRE3-BGHpA	EPI	Oligo	SYFP2	RO	Mich et al., 2025 bioRxiv
502941	C57BL/6J	AiE0406m	AiP12108	pAAV-AiE0406m-minBG-SYFP2-WPRE3-BGHpA	EPI	Oligo	SYFP2	RO	Mich et al., 2025 bioRxiv
515299	C57BL/6J	AiE0407h	AiP12167	pAAV-AiE0407h-minBG-SYFP2-WPRE3-BGHpA	EPI	Oligo	SYFP2	RO	Mich et al., 2025 bioRxiv
621154	C57BL/6J	AiE0407h	AiP12167	pAAV-AiE0407h-minBG-SYFP2-WPRE3-BGHpA	EPI	Oligo	SYFP2	RO	Ben-Simon, et al. 2025 Cell
637257	C57BL/6J	AiE0407h	AiP12167	pAAV-AiE0407h-minBG-SYFP2-WPRE3-BGHpA	STPT	Oligo	SYFP2	RO	Ben-Simon, et al. 2025 Cell
616883	C57BL/6J	AiE0407h	AiP12167	pAAV-AiE0407h-minBG-SYFP2-WPRE3-BGHpA	STPT	Oligo	SYFP2	RO	Ben-Simon, et al. 2025 Cell
575093	C57BL/6J	AiE0407m	AiP12126	pAAV-AiE0407m-minBG-SYFP2-WPRE3-BGHpA	EPI	Oligo	SYFP2	RO	Mich et al., 2025 bioRxiv
515300	C57BL/6J	AiE0408h	AiP12168	pAAV-AiE0408h-minBG-SYFP2-WPRE3-BGHpA	EPI	Oligo	SYFP2	RO	Mich et al., 2025 bioRxiv
575094	C57BL/6J	AiE0408m	AiP12127	pAAV-AiE0408m-minBG-SYFP2-WPRE3-BGHpA	EPI	Oligo	SYFP2	RO	Mich et al., 2025 bioRxiv
622087	C57BL/6J	AiE0409h	AiP13062	pAAV-AiE0409h-minBG-SYFP2-WPRE3-BGHpA	EPI, IHC	Oligo	SYFP2	RO	Mich et al., 2025 bioRxiv
629466	C57BL/6J	AiE0409h	AiP13062	pAAV-AiE0409h-minBG-SYFP2-WPRE3-BGHpA	EPI, IHC	Oligo	SYFP2	RO	Mich et al., 2025 bioRxiv
619577	C57BL/6J	AiE0409h	AiP13062	pAAV-AiE0409h-minBG-SYFP2-WPRE3-BGHpA	scRNA-seq	Oligo	SYFP2	RO	Mich et al., 2025 bioRxiv
641433	C57BL/6J	AiE0409h	AiP13062	pAAV-AiE0409h-minBG-SYFP2-WPRE3-BGHpA	scRNA-seq	Oligo	SYFP2	RO	Mich et al., 2025 bioRxiv
577081	C57BL/6J	AiE0409h	AiP13062	pAAV-AiE0409h-minBG-SYFP2-WPRE3-BGHpA	EPI	Oligo	SYFP2	RO	Mich et al., 2025 bioRxiv
621155	C57BL/6J	AiE0409h	AiP13062	pAAV-AiE0409h-minBG-SYFP2-WPRE3-BGHpA	EPI	Oligo	SYFP2	RO	Ben-Simon, et al. 2025 Cell
576143	C57BL/6J	AiE0409h	AiP13062	pAAV-AiE0409h-minBG-SYFP2-WPRE3-BGHpA	EPI	Oligo	SYFP2	RO	Ben-Simon, et al. 2025 Cell
622126	C57BL/6J	AiE0409h	AiP13062	pAAV-AiE0409h-minBG-SYFP2-WPRE3-BGHpA	STPT	Oligo	SYFP2	RO	Ben-Simon, et al. 2025 Cell
501908	C57BL/6J	AiE0409m	AiP12093	pAAV-AiE0409m-minBG-SYFP2-WPRE3-BGHpA	EPI	Oligo	SYFP2	RO	Mich et al., 2025 bioRxiv
577082	C57BL/6J	AiE0410h	AiP13063	pAAV-AiE0410h-minBG-SYFP2-WPRE3-BGHpA	EPI	Oligo	SYFP2	RO	Mich et al., 2025 bioRxiv
573437	C57BL/6J	AiE0410h	AiP13063	pAAV-AiE0410h-minBG-SYFP2-WPRE3-BGHpA	EPI	Oligo	SYFP2	RO	Ben-Simon, et al. 2025 Cell
621156	C57BL/6J	AiE0410h	AiP13063	pAAV-AiE0410h-minBG-SYFP2-WPRE3-BGHpA	EPI	Oligo	SYFP2	RO	Ben-Simon, et al. 2025 Cell
622127	C57BL/6J	AiE0410h	AiP13063	pAAV-AiE0410h-minBG-SYFP2-WPRE3-BGHpA	STPT	Oligo	SYFP2	RO	Ben-Simon, et al. 2025 Cell
708281	C57BL/6J	AiE0410h_3xC2	AiP14256	pAAV-AiE0410h_3xC2-minBG-SYFP2-WPRE3-BGHpA	EPI	Oligo	SYFP2	RO	Ben-Simon, et al. 2025 Cell
717603	Ai14(RCL-tdT	AiE0410m	AiP13997	pAAV-AiE0410m-minBG-iCre(R297T)-BGHpA	EPI	Oligo	iCre(R297	RO	Ben-Simon, et al. 2025 Cell
717603	Ai14(RCL-tdT	AiE0410m	AiP13997	pAAV-AiE0410m-minBG-iCre(R297T)-BGHpA	EPI	Oligo	iCre(R297	RO	Ben-Simon, et al. 2025 Cell
738666	Ai14(RCL-tdT	AiE0410m	AiP14945	pAAV-AiE0410m-minBG-iCre(R297T)-3XmiR126TS-BGH	STPT, IHC	Oligo	iCre(R297	RO	Ben-Simon, et al. 2025 Cell
717606	Ai14(RCL-tdT	AiE0410m	AiP14945	pAAV-AiE0410m-minBG-iCre(R297T)-3XmiR126TS-BGH	EPI, IHC	Oligo	iCre(R297	RO	Ben-Simon, et al. 2025 Cell
720915	Ai14(RCL-tdT	AiE0410m	AiP14946	pAAV-AiE0410m-minBG-iCre(R297T)-3XmiR221TS-BGH	EPI	Oligo	iCre(R297	RO	Ben-Simon, et al. 2025 Cell
608408	C57BL/6J	AiE0410m	AiP13636	pAAV-AiE0410m-minBG-SYFP2-P2A-3XFLAG-10aa-H2B-	EPI	Oligo	SYFP2	RO	Mich et al., 2025 bioRxiv
621235	C57BL/6J	AiE0410m	AiP13636	pAAV-AiE0410m-minBG-SYFP2-P2A-3XFLAG-10aa-H2B-	EPI	Oligo	SYFP2	RO	Mich et al., 2025 bioRxiv
621241	C57BL/6J	AiE0410m	AiP12820	pAAV-AiE0410m-minRho-SYFP2-10aa-H2Bmod-WPRE3-	EPI	Oligo	SYFP2	RO	Mich et al., 2025 bioRxiv
626922	C57BL/6J	AiE0410m	AiP12109	pAAV-AiE0410m-minBG-SYFP2-WPRE3-BGHpA	EPI, IHC	Oligo	SYFP2	RO	Mich et al., 2025 bioRxiv
629463	C57BL/6J	AiE0410m	AiP12109	pAAV-AiE0410m-minBG-SYFP2-WPRE3-BGHpA	EPI, IHC	Oligo	SYFP2	RO	Mich et al., 2025 bioRxiv
637135	C57BL/6J	AiE0410m	AiP12109	pAAV-AiE0410m-minBG-SYFP2-WPRE3-BGHpA	EPI, IHC	Oligo	SYFP2	RO	Mich et al., 2025 bioRxiv
647358	C57BL/6J	AiE0410m	AiP12109	pAAV-AiE0410m-minBG-SYFP2-WPRE3-BGHpA	EPI, IHC	Oligo	SYFP2	RO	Mich et al., 2025 bioRxiv
647359	C57BL/6J	AiE0410m	AiP14295	pAAV-TeIN-LITR-AiE0410m-minBG-SYFP2-P2A-3XFLAG-	EPI, IHC	Oligo	SYFP2	RO	Mich et al., 2025 bioRxiv
648488	C57BL/6J	AiE0410m	AiP14295	pAAV-TeIN-LITR-AiE0410m-minBG-SYFP2-P2A-3XFLAG-	EPI, IHC	Oligo	SYFP2	RO	Mich et al., 2025 bioRxiv
617304	C57BL/6J	AiE0410m	AiP12109	pAAV-AiE0410m-minBG-SYFP2-WPRE3-BGHpA	scRNA-seq	Oligo	SYFP2	RO	Mich et al., 2025 bioRxiv
556486	C57BL/6J	AiE0410m	AiP12109	pAAV-AiE0410m-minBG-SYFP2-WPRE3-BGHpA	scRNA-seq	Oligo	SYFP2	RO	Mich et al., 2025 bioRxiv
556486	C57BL/6J	AiE0410m	AiP12109	pAAV-AiE0410m-minBG-SYFP2-WPRE3-BGHpA	scRNA-seq	Oligo	SYFP2	RO	Mich et al., 2025 bioRxiv
502942	C57BL/6J	AiE0410m	AiP12109	pAAV-AiE0410m-minBG-SYFP2-WPRE3-BGHpA	EPI	Oligo	SYFP2	RO	Mich et al., 2025 bioRxiv

574070	C57BL/6J	AiE0410m	AiP12109	pAAV-AiE0410m-minBG-SYFP2-WPRE3-BGHpA	STPT	Oligo	SYFP2	RO	Ben-Simon, et al. 2025 Cell
639180	C57BL/6J	AiE0410m	AiP12109	pAAV-AiE0410m-minBG-SYFP2-WPRE3-BGHpA	EPI	Oligo	SYFP2	RO	Ben-Simon, et al. 2025 Cell
711350	C57BL/6J	AiE0410m	AiP12109	pAAV-AiE0410m-minBG-SYFP2-WPRE3-BGHpA	EPI	Oligo	SYFP2	RO	Ben-Simon, et al. 2025 Cell
693219	C57BL/6J	AiE0410m	AiP13636	pAAV-AiE0410m-minBG-SYFP2-P2A-3XFLAG-10aa-H2B-'	STPT	Oligo	SYFP2	RO	Ben-Simon, et al. 2025 Cell
610230	C57BL/6J	AiE0410m	AiP13636	pAAV-AiE0410m-minBG-SYFP2-P2A-3XFLAG-10aa-H2B-'	EPI	Oligo	SYFP2	RO	Ben-Simon, et al. 2025 Cell
693219	C57BL/6J	AiE0410m	AiP13636	pAAV-AiE0410m-minBG-SYFP2-P2A-3XFLAG-10aa-H2B-'	STPT	Oligo	SYFP2	RO	Ben-Simon, et al. 2025 Cell
610230	C57BL/6J	AiE0410m	AiP13636	pAAV-AiE0410m-minBG-SYFP2-P2A-3XFLAG-10aa-H2B-'	EPI	Oligo	SYFP2	RO	Ben-Simon, et al. 2025 Cell
693219	C57BL/6J	AiE0410m	AiP13636	pAAV-AiE0410m-minBG-SYFP2-P2A-3XFLAG-10aa-H2B-'	STPT	Oligo	SYFP2	RO	Ben-Simon, et al. 2025 Cell
693219	C57BL/6J	AiE0410m	AiP13636	pAAV-AiE0410m-minBG-SYFP2-P2A-3XFLAG-10aa-H2B-'	STPT	Oligo	SYFP2	RO	Ben-Simon, et al. 2025 Cell
693219	C57BL/6J	AiE0410m	AiP13636	pAAV-AiE0410m-minBG-SYFP2-P2A-3XFLAG-10aa-H2B-'	STPT	Oligo	SYFP2	RO	Ben-Simon, et al. 2025 Cell
610230	C57BL/6J	AiE0410m	AiP13636	pAAV-AiE0410m-minBG-SYFP2-P2A-3XFLAG-10aa-H2B-'	EPI	Oligo	SYFP2	RO	Ben-Simon, et al. 2025 Cell
693219	C57BL/6J	AiE0410m	AiP13636	pAAV-AiE0410m-minBG-SYFP2-P2A-3XFLAG-10aa-H2B-'	STPT	Oligo	SYFP2	RO	Ben-Simon, et al. 2025 Cell
610230	C57BL/6J	AiE0410m	AiP13636	pAAV-AiE0410m-minBG-SYFP2-P2A-3XFLAG-10aa-H2B-'	EPI	Oligo	SYFP2	RO	Ben-Simon, et al. 2025 Cell
610230	C57BL/6J	AiE0410m	AiP13636	pAAV-AiE0410m-minBG-SYFP2-P2A-3XFLAG-10aa-H2B-'	EPI	Oligo	SYFP2	RO	Ben-Simon, et al. 2025 Cell
610230	C57BL/6J	AiE0410m	AiP13636	pAAV-AiE0410m-minBG-SYFP2-P2A-3XFLAG-10aa-H2B-'	EPI	Oligo	SYFP2	RO	Ben-Simon, et al. 2025 Cell
693219	C57BL/6J	AiE0410m	AiP13636	pAAV-AiE0410m-minBG-SYFP2-P2A-3XFLAG-10aa-H2B-'	STPT	Oligo	SYFP2	RO	Ben-Simon, et al. 2025 Cell
610230	C57BL/6J	AiE0410m	AiP13636	pAAV-AiE0410m-minBG-SYFP2-P2A-3XFLAG-10aa-H2B-'	EPI	Oligo	SYFP2	RO	Ben-Simon, et al. 2025 Cell
631111	C57BL/6J	AiE0410m	AiP13636	pAAV-AiE0410m-minBG-SYFP2-P2A-3XFLAG-10aa-H2B-'	EPI	Oligo	SYFP2	ICV	Ben-Simon, et al. 2025 Cell
693219	C57BL/6J	AiE0410m	AiP13636	pAAV-AiE0410m-minBG-SYFP2-P2A-3XFLAG-10aa-H2B-'	STPT	Oligo	SYFP2	RO	Ben-Simon, et al. 2025 Cell
610230	C57BL/6J	AiE0410m	AiP13636	pAAV-AiE0410m-minBG-SYFP2-P2A-3XFLAG-10aa-H2B-'	EPI	Oligo	SYFP2	RO	Ben-Simon, et al. 2025 Cell
671886	CD-1_IGS	AiE0410m	AiP12109	pAAV-AiE0410m-minBG-SYFP2-WPRE3-BGHpA	STPT	Oligo	SYFP2	ICV	Ben-Simon, et al. 2025 Cell
676096	CD-1_IGS	AiE0410m	AiP13636	pAAV-AiE0410m-minBG-SYFP2-P2A-3XFLAG-10aa-H2B-'	EPI	Oligo	SYFP2	ICV	Ben-Simon, et al. 2025 Cell
619578	C57BL/6J	AiE0410m_3xC	AiP12556	pAAV-AiE0410m_3xC2-minBG-SYFP2-WPRE3-BGHpA	scRNA-seq	Oligo	SYFP2	RO	Mich et al., 2025 bioRxiv
621842	C57BL/6J	AiE0410m_3xC	AiP12556	pAAV-AiE0410m_3xC2-minBG-SYFP2-WPRE3-BGHpA	EPI	Oligo	SYFP2	RO	Ben-Simon, et al. 2025 Cell
711351	C57BL/6J	AiE0410m_3xC	AiP12556	pAAV-AiE0410m_3xC2-minBG-SYFP2-WPRE3-BGHpA	EPI	Oligo	SYFP2	RO	Ben-Simon, et al. 2025 Cell
579922	C57BL/6J	AiE0410m_3xC	AiP12556	pAAV-AiE0410m_3xC2-minBG-SYFP2-WPRE3-BGHpA	STPT	Oligo	SYFP2	RO	Ben-Simon, et al. 2025 Cell
524230	C57BL/6J	AiE0495m	AiP12268	pAAV-AiE0495m-minBG-SYFP2-WPRE3-BGHpA	EPI	Astro	SYFP2	RO	Mich et al., 2025 bioRxiv
591408	C57BL/6J	AiE0496m	AiP12939	pAAV-AiE0496m-minBG-SYFP2-WPRE3-BGHpA	EPI	Astro	SYFP2	RO	Mich et al., 2025 bioRxiv
623025	C57BL/6J	AiE0496m	AiP12939	pAAV-AiE0496m-minBG-SYFP2-WPRE3-BGHpA	EPI	Astro	SYFP2	RO	Ben-Simon, et al. 2025 Cell
575098	C57BL/6J	AiE0497m	AiP12243	pAAV-AiE0497m-minBG-SYFP2-WPRE3-BGHpA	EPI	Astro	SYFP2	RO	Mich et al., 2025 bioRxiv
674240	C57BL/6J	AiE0497m	AiP12243	pAAV-AiE0497m-minBG-SYFP2-WPRE3-BGHpA	EPI	Astro	SYFP2	RO	Ben-Simon, et al. 2025 Cell
674240	C57BL/6J	AiE0497m	AiP12243	pAAV-AiE0497m-minBG-SYFP2-WPRE3-BGHpA	EPI	Astro	SYFP2	RO	Ben-Simon, et al. 2025 Cell
622081	C57BL/6J	AiE0641m	AiP12845	pAAV-AiE0641m-minBG-SYFP2-WPRE3-BGHpA	EPI, IHC	Oligo	SYFP2	RO	Mich et al., 2025 bioRxiv
626923	C57BL/6J	AiE0641m	AiP12845	pAAV-AiE0641m-minBG-SYFP2-WPRE3-BGHpA	EPI, IHC	Oligo	SYFP2	RO	Mich et al., 2025 bioRxiv
601543	C57BL/6J	AiE0641m	AiP12845	pAAV-AiE0641m-minBG-SYFP2-WPRE3-BGHpA	scRNA-seq	Oligo	SYFP2	RO	Mich et al., 2025 bioRxiv
617305	C57BL/6J	AiE0641m	AiP12845	pAAV-AiE0641m-minBG-SYFP2-WPRE3-BGHpA	scRNA-seq	Oligo	SYFP2	RO	Mich et al., 2025 bioRxiv
563436	C57BL/6J	AiE0641m	AiP12845	pAAV-AiE0641m-minBG-SYFP2-WPRE3-BGHpA	EPI, IHC	Oligo	SYFP2	RO	Mich et al., 2025 bioRxiv
580147	C57BL/6J	AiE0641m	AiP12845	pAAV-AiE0641m-minBG-SYFP2-WPRE3-BGHpA	STPT	Oligo	SYFP2	RO	Ben-Simon, et al. 2025 Cell
621841	C57BL/6J	AiE0641m	AiP12845	pAAV-AiE0641m-minBG-SYFP2-WPRE3-BGHpA	EPI	Oligo	SYFP2	RO	Ben-Simon, et al. 2025 Cell
671885	CD-1_IGS	AiE0641m	AiP12845	pAAV-AiE0641m-minBG-SYFP2-WPRE3-BGHpA	STPT	Oligo	SYFP2	ICV	Ben-Simon, et al. 2025 Cell
656791	C57BL/6J	AiE0641m_3xC	AiP14004	pAAV-AiE0641m_3xC2-minBG-SYFP2-WPRE3-BGHpA	EPI	Oligo	SYFP2	RO	Ben-Simon, et al. 2025 Cell
563437	C57BL/6J	AiE0642m	AiP12846	pAAV-AiE0642m-minBG-SYFP2-WPRE3-BGHpA	EPI	Astro	SYFP2	RO	Mich et al., 2025 bioRxiv
572498	C57BL/6J	AiE0733m	AiP13099	pAAV-AiE0733m-minBG-SYFP2-WPRE3-BGHpA	EPI	Oligo	SYFP2	RO	Mich et al., 2025 bioRxiv
570706	C57BL/6J	AiE0733m	AiP13099	pAAV-AiE0733m-minBG-SYFP2-WPRE3-BGHpA	EPI	Oligo	SYFP2	RO	Ben-Simon, et al. 2025 Cell
637134	C57BL/6J	AiE2117m	AiP1346	pAAV-AiE2117m-minBG-SYFP2-WPRE3-BGHpA	EPI, IHC	Astro	SYFP2	RO	Mich et al., 2025 bioRxiv
622133	C57BL/6J	AiE2117m	AiP1346	pAAV-AiE2117m-minBG-SYFP2-WPRE3-BGHpA	STPT	Astro	SYFP2	RO	Ben-Simon, et al. 2025 Cell
622133	C57BL/6J	AiE2117m	AiP1346	pAAV-AiE2117m-minBG-SYFP2-WPRE3-BGHpA	STPT	Astro	SYFP2	RO	Ben-Simon, et al. 2025 Cell
622133	C57BL/6J	AiE2117m	AiP1346	pAAV-AiE2117m-minBG-SYFP2-WPRE3-BGHpA	STPT	Astro	SYFP2	RO	Ben-Simon, et al. 2025 Cell
622133	C57BL/6J	AiE2117m	AiP1346	pAAV-AiE2117m-minBG-SYFP2-WPRE3-BGHpA	STPT	Astro	SYFP2	RO	Ben-Simon, et al. 2025 Cell
609039	C57BL/6J	AiE2117m	AiP1346	pAAV-AiE2117m-minBG-SYFP2-WPRE3-BGHpA	EPI	Astro	SYFP2	RO	Ben-Simon, et al. 2025 Cell
609039	C57BL/6J	AiE2117m	AiP1346	pAAV-AiE2117m-minBG-SYFP2-WPRE3-BGHpA	EPI	Astro	SYFP2	RO	Ben-Simon, et al. 2025 Cell
609039	C57BL/6J	AiE2117m	AiP1346	pAAV-AiE2117m-minBG-SYFP2-WPRE3-BGHpA	EPI	Astro	SYFP2	RO	Ben-Simon, et al. 2025 Cell
609039	C57BL/6J	AiE2117m	AiP1346	pAAV-AiE2117m-minBG-SYFP2-WPRE3-BGHpA	EPI	Astro	SYFP2	RO	Ben-Simon, et al. 2025 Cell
622133	C57BL/6J	AiE2117m	AiP1346	pAAV-AiE2117m-minBG-SYFP2-WPRE3-BGHpA	STPT	Astro	SYFP2	RO	Ben-Simon, et al. 2025 Cell
609039	C57BL/6J	AiE2117m	AiP1346	pAAV-AiE2117m-minBG-SYFP2-WPRE3-BGHpA	EPI	Astro	SYFP2	RO	Ben-Simon, et al. 2025 Cell
609039	C57BL/6J	AiE2117m	AiP1346	pAAV-AiE2117m-minBG-SYFP2-WPRE3-BGHpA	EPI	Astro	SYFP2	RO	Ben-Simon, et al. 2025 Cell
622133	C57BL/6J	AiE2117m	AiP1346	pAAV-AiE2117m-minBG-SYFP2-WPRE3-BGHpA	STPT	Astro	SYFP2	RO	Ben-Simon, et al. 2025 Cell
622133	C57BL/6J	AiE2117m	AiP1346	pAAV-AiE2117m-minBG-SYFP2-WPRE3-BGHpA	STPT	Astro	SYFP2	RO	Ben-Simon, et al. 2025 Cell
609039	C57BL/6J	AiE2117m	AiP1346	pAAV-AiE2117m-minBG-SYFP2-WPRE3-BGHpA	EPI	Astro	SYFP2	RO	Ben-Simon, et al. 2025 Cell
637140	C57BL/6J	AiE2118m	AiP1347	pAAV-AiE2118m-minBG-SYFP2-WPRE3-BGHpA	EPI, IHC	Astro	SYFP2	RO	Mich et al., 2025 bioRxiv
642136	C57BL/6J	AiE2118m	AiP1347	pAAV-AiE2118m-minBG-SYFP2-WPRE3-BGHpA	EPI, IHC	Astro	SYFP2	RO	Mich et al., 2025 bioRxiv
689258	C57BL/6J	AiE2118m	AiP1347	pAAV-AiE2118m-minBG-SYFP2-WPRE3-BGHpA	EPI	Astro	SYFP2	RO	Ben-Simon, et al. 2025 Cell
617533	C57BL/6J	AiE2118m	AiP1347	pAAV-AiE2118m-minBG-SYFP2-WPRE3-BGHpA	STPT	Astro	SYFP2	RO	Ben-Simon, et al. 2025 Cell
604287	C57BL/6J	AiE2118m	AiP1347	pAAV-AiE2118m-minBG-SYFP2-WPRE3-BGHpA	EPI	Astro	SYFP2	RO	Ben-Simon, et al. 2025 Cell
703995	C57BL/6J	AiE2118m	AiP1347	pAAV-AiE2118m-minBG-SYFP2-WPRE3-BGHpA	EPI	Astro	SYFP2	RO	Ben-Simon, et al. 2025 Cell
604287	C57BL/6J	AiE2118m	AiP1347	pAAV-AiE2118m-minBG-SYFP2-WPRE3-BGHpA	EPI	Astro	SYFP2	RO	Ben-Simon, et al. 2025 Cell
617533	C57BL/6J	AiE2118m	AiP1347	pAAV-AiE2118m-minBG-SYFP2-WPRE3-BGHpA	STPT	Astro	SYFP2	RO	Ben-Simon, et al. 2025 Cell
604287	C57BL/6J	AiE2118m	AiP1347	pAAV-AiE2118m-minBG-SYFP2-WPRE3-BGHpA	EPI	Astro	SYFP2	RO	Ben-Simon, et al. 2025 Cell
604287	C57BL/6J	AiE2118m	AiP1347	pAAV-AiE2118m-minBG-SYFP2-WPRE3-BGHpA	EPI	Astro	SYFP2	RO	Ben-Simon, et al. 2025 Cell
617533	C57BL/6J	AiE2118m	AiP1347	pAAV-AiE2118m-minBG-SYFP2-WPRE3-BGHpA	STPT	Astro	SYFP2	RO	Ben-Simon, et al. 2025 Cell
638242	C57BL/6J	AiE2118m	AiP1347	pAAV-AiE2118m-minBG-SYFP2-WPRE3-BGHpA	STPT	Astro	SYFP2	RO	Ben-Simon, et al. 2025 Cell
617533	C57BL/6J	AiE2118m	AiP1347	pAAV-AiE2118m-minBG-SYFP2-WPRE3-BGHpA	STPT	Astro	SYFP2	RO	Ben-Simon, et al. 2025 Cell
703995	C57BL/6J	AiE2118m	AiP1347	pAAV-AiE2118m-minBG-SYFP2-WPRE3-BGHpA	EPI	Astro	SYFP2	RO	Ben-Simon, et al. 2025 Cell
689258	C57BL/6J	AiE2118m	AiP1347	pAAV-AiE2118m-minBG-SYFP2-WPRE3-BGHpA	EPI	Astro	SYFP2	RO	Ben-Simon, et al. 2025 Cell
617533	C57BL/6J	AiE2118m	AiP1347	pAAV-AiE2118m-minBG-SYFP2-WPRE3-BGHpA	STPT	Astro	SYFP2	RO	Ben-Simon, et al. 2025 Cell
617533	C57BL/6J	AiE2118m	AiP1347	pAAV-AiE2118m-minBG-SYFP2-WPRE3-BGHpA	STPT	Astro	SYFP2	RO	Ben-Simon, et al. 2025 Cell
617533	C57BL/6J	AiE2118m	AiP1347	pAAV-AiE2118m-minBG-SYFP2-WPRE3-BGHpA	STPT	Astro	SYFP2	RO	Ben-Simon, et al. 2025 Cell
638242	C57BL/6J	AiE2118m	AiP1347	pAAV-AiE2118m-minBG-SYFP2-WPRE3-BGHpA	STPT	Astro	SYFP2	RO	Ben-Simon, et al. 2025 Cell
617533	C57BL/6J	AiE2118m	AiP1347	pAAV-AiE2118m-minBG-SYFP2-WPRE3-BGHpA	STPT	Astro	SYFP2	RO	Ben-Simon, et al. 2025 Cell
638242	C57BL/6J	AiE2118m	AiP1347	pAAV-AiE2118m-minBG-SYFP2-WPRE3-BGHpA	STPT	Astro	SYFP2	RO	Ben-Simon, et al. 2025 Cell
617533	C57BL/6J	AiE2118m	AiP1347	pAAV-AiE2118m-minBG-SYFP2-WPRE3-BGHpA	STPT	Astro	SYFP2	RO	Ben-Simon, et al. 2025 Cell
638242	C57BL/6J	AiE2118m	AiP1347	pAAV-AiE2118m-minBG-SYFP2-WPRE3-BGHpA	STPT	Astro	SYFP2	RO	Ben-Simon, et al. 2025 Cell
689258	C57BL/6J	AiE2118m	AiP1347	pAAV-AiE2118m-minBG-SYFP2-WPRE3-BGHpA	EPI	Astro	SYFP2	RO	Ben-Simon, et al. 2025 Cell
604287	C57BL/6J	AiE2118m	AiP1347	pAAV-AiE2118m-minBG-SYFP2-WPRE3-BGHpA	EPI	Astro	SYFP2	RO	Ben-Simon, et al. 2025 Cell
703995	C57BL/6J	AiE2118m	AiP1347	pAAV-AiE2118m-minBG-SYFP2-WPRE3-BGHpA	EPI	Astro	SYFP2	RO	Ben-Simon, et al. 2025 Cell
604287	C57BL/6J	AiE2118m	AiP1347	pAAV-AiE2118m-minBG-SYFP2-WPRE3-BGHpA	EPI	Astro	SYFP2	RO	Ben-Simon, et al. 2025 Cell
638242	C57BL/6J	AiE2118m	AiP1347	pAAV-AiE2118m-minBG-SYFP2-WPRE3-BGHpA	STPT	Astro	SYFP2	RO	Ben-Simon, et al. 2025 Cell
689258	C57BL/6J	AiE2118m	AiP1347	pAAV-AiE2118m-minBG-SYFP2-WPRE3-BGHpA	EPI	Astro	SYFP2	RO	Ben-Simon, et al. 2025 Cell
604287	C57BL/6J	AiE2118m	AiP1347	pAAV-AiE2118m-minBG-SYFP2-WPRE3-BGHpA	EPI	Astro	SYFP2	RO	Ben-Simon, et al. 2025 Cell
638242	C57BL/6J	AiE2118m	AiP1347	pAAV-AiE2118m-minBG-SYFP2-WPRE3-BGHpA	STPT	Astro	SYFP2	RO	Ben-Simon, et al. 2025 Cell

638242	C57BL/6J	AiE2118m	AiP1347	pAAV-AiE2118m-minBG-SYFP2-WPRE3-BGHpA	STPT	Astro	SYFP2	RO	Ben-Simon, et al. 2025 Cell
703995	C57BL/6J	AiE2118m	AiP1347	pAAV-AiE2118m-minBG-SYFP2-WPRE3-BGHpA	EPI	Astro	SYFP2	RO	Ben-Simon, et al. 2025 Cell
703995	C57BL/6J	AiE2118m	AiP1347	pAAV-AiE2118m-minBG-SYFP2-WPRE3-BGHpA	EPI	Astro	SYFP2	RO	Ben-Simon, et al. 2025 Cell
703995	C57BL/6J	AiE2118m	AiP1347	pAAV-AiE2118m-minBG-SYFP2-WPRE3-BGHpA	EPI	Astro	SYFP2	RO	Ben-Simon, et al. 2025 Cell
638242	C57BL/6J	AiE2118m	AiP1347	pAAV-AiE2118m-minBG-SYFP2-WPRE3-BGHpA	STPT	Astro	SYFP2	RO	Ben-Simon, et al. 2025 Cell
617533	C57BL/6J	AiE2118m	AiP1347	pAAV-AiE2118m-minBG-SYFP2-WPRE3-BGHpA	STPT	Astro	SYFP2	RO	Ben-Simon, et al. 2025 Cell
617533	C57BL/6J	AiE2118m	AiP1347	pAAV-AiE2118m-minBG-SYFP2-WPRE3-BGHpA	STPT	Astro	SYFP2	RO	Ben-Simon, et al. 2025 Cell
638242	C57BL/6J	AiE2118m	AiP1347	pAAV-AiE2118m-minBG-SYFP2-WPRE3-BGHpA	STPT	Astro	SYFP2	RO	Ben-Simon, et al. 2025 Cell
638242	C57BL/6J	AiE2118m	AiP1347	pAAV-AiE2118m-minBG-SYFP2-WPRE3-BGHpA	STPT	Astro	SYFP2	RO	Ben-Simon, et al. 2025 Cell
604287	C57BL/6J	AiE2118m	AiP1347	pAAV-AiE2118m-minBG-SYFP2-WPRE3-BGHpA	EPI	Astro	SYFP2	RO	Ben-Simon, et al. 2025 Cell
638242	C57BL/6J	AiE2118m	AiP1347	pAAV-AiE2118m-minBG-SYFP2-WPRE3-BGHpA	STPT	Astro	SYFP2	RO	Ben-Simon, et al. 2025 Cell
617533	C57BL/6J	AiE2118m	AiP1347	pAAV-AiE2118m-minBG-SYFP2-WPRE3-BGHpA	STPT	Astro	SYFP2	RO	Ben-Simon, et al. 2025 Cell
638242	C57BL/6J	AiE2118m	AiP1347	pAAV-AiE2118m-minBG-SYFP2-WPRE3-BGHpA	STPT	Astro	SYFP2	RO	Ben-Simon, et al. 2025 Cell
617533	C57BL/6J	AiE2118m	AiP1347	pAAV-AiE2118m-minBG-SYFP2-WPRE3-BGHpA	STPT	Astro	SYFP2	RO	Ben-Simon, et al. 2025 Cell
638242	C57BL/6J	AiE2118m	AiP1347	pAAV-AiE2118m-minBG-SYFP2-WPRE3-BGHpA	STPT	Astro	SYFP2	RO	Ben-Simon, et al. 2025 Cell
638242	C57BL/6J	AiE2118m	AiP1347	pAAV-AiE2118m-minBG-SYFP2-WPRE3-BGHpA	STPT	Astro	SYFP2	RO	Ben-Simon, et al. 2025 Cell
604287	C57BL/6J	AiE2118m	AiP1347	pAAV-AiE2118m-minBG-SYFP2-WPRE3-BGHpA	EPI	Astro	SYFP2	RO	Ben-Simon, et al. 2025 Cell
617533	C57BL/6J	AiE2118m	AiP1347	pAAV-AiE2118m-minBG-SYFP2-WPRE3-BGHpA	STPT	Astro	SYFP2	RO	Ben-Simon, et al. 2025 Cell
753053	C57BL/6J	AiE2118m	AiP14191	pAAV-AiE2118m-minBG-SYFP2-4XmiR124T-WPRE3-BGH	EPI	Astro	SYFP2	RO	Ben-Simon, et al. 2025 Cell
703996	C57BL/6J	AiE2118m	AiP14698	pAAV-AiE2118m-minBG-SYFP2-4XmiR204T-WPRE3-BGH	EPI	Astro	SYFP2	RO	Ben-Simon, et al. 2025 Cell
703996	C57BL/6J	AiE2118m	AiP14698	pAAV-AiE2118m-minBG-SYFP2-4XmiR204T-WPRE3-BGH	EPI	Astro	SYFP2	RO	Ben-Simon, et al. 2025 Cell
703996	C57BL/6J	AiE2118m	AiP14698	pAAV-AiE2118m-minBG-SYFP2-4XmiR204T-WPRE3-BGH	EPI	Astro	SYFP2	RO	Ben-Simon, et al. 2025 Cell
703996	C57BL/6J	AiE2118m	AiP14698	pAAV-AiE2118m-minBG-SYFP2-4XmiR204T-WPRE3-BGH	EPI	Astro	SYFP2	RO	Ben-Simon, et al. 2025 Cell
703997	C57BL/6J	AiE2118m	AiP14699	pAAV-AiE2118m-minBG-SYFP2-4XmiR708T-WPRE3-BGH	EPI	Astro	SYFP2	RO	Ben-Simon, et al. 2025 Cell
613554	C57BL/6J	AiE2119m	AiP1421	pAAV-AiE2119m-minBG-SYFP2-WPRE3-BGHpA	STPT	Astro	SYFP2	RO	Ben-Simon, et al. 2025 Cell
613554	C57BL/6J	AiE2119m	AiP1421	pAAV-AiE2119m-minBG-SYFP2-WPRE3-BGHpA	STPT	Astro	SYFP2	RO	Ben-Simon, et al. 2025 Cell
600132	C57BL/6J	AiE2119m	AiP1421	pAAV-AiE2119m-minBG-SYFP2-WPRE3-BGHpA	EPI	Astro	SYFP2	RO	Ben-Simon, et al. 2025 Cell
613554	C57BL/6J	AiE2119m	AiP1421	pAAV-AiE2119m-minBG-SYFP2-WPRE3-BGHpA	STPT	Astro	SYFP2	RO	Ben-Simon, et al. 2025 Cell
613554	C57BL/6J	AiE2119m	AiP1421	pAAV-AiE2119m-minBG-SYFP2-WPRE3-BGHpA	STPT	Astro	SYFP2	RO	Ben-Simon, et al. 2025 Cell
600132	C57BL/6J	AiE2119m	AiP1421	pAAV-AiE2119m-minBG-SYFP2-WPRE3-BGHpA	EPI	Astro	SYFP2	RO	Ben-Simon, et al. 2025 Cell
600132	C57BL/6J	AiE2119m	AiP1421	pAAV-AiE2119m-minBG-SYFP2-WPRE3-BGHpA	EPI	Astro	SYFP2	RO	Ben-Simon, et al. 2025 Cell
613554	C57BL/6J	AiE2119m	AiP1421	pAAV-AiE2119m-minBG-SYFP2-WPRE3-BGHpA	STPT	Astro	SYFP2	RO	Ben-Simon, et al. 2025 Cell
600132	C57BL/6J	AiE2119m	AiP1421	pAAV-AiE2119m-minBG-SYFP2-WPRE3-BGHpA	EPI	Astro	SYFP2	RO	Ben-Simon, et al. 2025 Cell
600132	C57BL/6J	AiE2119m	AiP1421	pAAV-AiE2119m-minBG-SYFP2-WPRE3-BGHpA	EPI	Astro	SYFP2	RO	Ben-Simon, et al. 2025 Cell
642132	C57BL/6J	AiE2120m	AiP1349	pAAV-AiE2120m-minBG-SYFP2-WPRE3-BGHpA	EPI, IHC	Astro	SYFP2	RO	Mich et al., 2025 bioRxiv
642137	C57BL/6J	AiE2120m	AiP1349	pAAV-AiE2120m-minBG-SYFP2-WPRE3-BGHpA	EPI, IHC	Astro	SYFP2	RO	Mich et al., 2025 bioRxiv
622134	C57BL/6J	AiE2120m	AiP1349	pAAV-AiE2120m-minBG-SYFP2-WPRE3-BGHpA	STPT	Astro	SYFP2	RO	Ben-Simon, et al. 2025 Cell
606959	C57BL/6J	AiE2120m	AiP1349	pAAV-AiE2120m-minBG-SYFP2-WPRE3-BGHpA	EPI	Astro	SYFP2	RO	Ben-Simon, et al. 2025 Cell
671881	CD-1_IGS	AiE2120m	AiP1349	pAAV-AiE2120m-minBG-SYFP2-WPRE3-BGHpA	STPT	Astro	SYFP2	ICV	Ben-Simon, et al. 2025 Cell
642133	C57BL/6J	AiE2121m	AiP1457	pAAV-AiE2121m-minBG-SYFP2-WPRE3-BGHpA	EPI, IHC	Astro	SYFP2	RO	Mich et al., 2025 bioRxiv
642135	C57BL/6J	AiE2121m	AiP1457	pAAV-AiE2121m-minBG-SYFP2-WPRE3-BGHpA	EPI, IHC	Astro	SYFP2	RO	Mich et al., 2025 bioRxiv
604282	C57BL/6J	AiE2121m	AiP1457	pAAV-AiE2121m-minBG-SYFP2-WPRE3-BGHpA	EPI	Astro	SYFP2	RO	Ben-Simon, et al. 2025 Cell
615684	C57BL/6J	AiE2121m	AiP1457	pAAV-AiE2121m-minBG-SYFP2-WPRE3-BGHpA	STPT	Astro	SYFP2	RO	Ben-Simon, et al. 2025 Cell
604282	C57BL/6J	AiE2121m	AiP1457	pAAV-AiE2121m-minBG-SYFP2-WPRE3-BGHpA	EPI	Astro	SYFP2	RO	Ben-Simon, et al. 2025 Cell
615684	C57BL/6J	AiE2121m	AiP1457	pAAV-AiE2121m-minBG-SYFP2-WPRE3-BGHpA	STPT	Astro	SYFP2	RO	Ben-Simon, et al. 2025 Cell
604282	C57BL/6J	AiE2121m	AiP1457	pAAV-AiE2121m-minBG-SYFP2-WPRE3-BGHpA	EPI	Astro	SYFP2	RO	Ben-Simon, et al. 2025 Cell
615684	C57BL/6J	AiE2121m	AiP1457	pAAV-AiE2121m-minBG-SYFP2-WPRE3-BGHpA	STPT	Astro	SYFP2	RO	Ben-Simon, et al. 2025 Cell
615684	C57BL/6J	AiE2121m	AiP1457	pAAV-AiE2121m-minBG-SYFP2-WPRE3-BGHpA	STPT	Astro	SYFP2	RO	Ben-Simon, et al. 2025 Cell
604282	C57BL/6J	AiE2121m	AiP1457	pAAV-AiE2121m-minBG-SYFP2-WPRE3-BGHpA	EPI	Astro	SYFP2	RO	Ben-Simon, et al. 2025 Cell
604282	C57BL/6J	AiE2121m	AiP1457	pAAV-AiE2121m-minBG-SYFP2-WPRE3-BGHpA	EPI	Astro	SYFP2	RO	Ben-Simon, et al. 2025 Cell
604282	C57BL/6J	AiE2121m	AiP1457	pAAV-AiE2121m-minBG-SYFP2-WPRE3-BGHpA	EPI	Astro	SYFP2	RO	Ben-Simon, et al. 2025 Cell
604282	C57BL/6J	AiE2121m	AiP1457	pAAV-AiE2121m-minBG-SYFP2-WPRE3-BGHpA	EPI	Astro	SYFP2	RO	Ben-Simon, et al. 2025 Cell
615684	C57BL/6J	AiE2121m	AiP1457	pAAV-AiE2121m-minBG-SYFP2-WPRE3-BGHpA	STPT	Astro	SYFP2	RO	Ben-Simon, et al. 2025 Cell
615684	C57BL/6J	AiE2121m	AiP1457	pAAV-AiE2121m-minBG-SYFP2-WPRE3-BGHpA	STPT	Astro	SYFP2	RO	Ben-Simon, et al. 2025 Cell
604282	C57BL/6J	AiE2121m	AiP1457	pAAV-AiE2121m-minBG-SYFP2-WPRE3-BGHpA	EPI	Astro	SYFP2	RO	Ben-Simon, et al. 2025 Cell
615684	C57BL/6J	AiE2121m	AiP1457	pAAV-AiE2121m-minBG-SYFP2-WPRE3-BGHpA	STPT	Astro	SYFP2	RO	Ben-Simon, et al. 2025 Cell
615684	C57BL/6J	AiE2121m	AiP1457	pAAV-AiE2121m-minBG-SYFP2-WPRE3-BGHpA	STPT	Astro	SYFP2	RO	Ben-Simon, et al. 2025 Cell
604282	C57BL/6J	AiE2121m	AiP1457	pAAV-AiE2121m-minBG-SYFP2-WPRE3-BGHpA	EPI	Astro	SYFP2	RO	Ben-Simon, et al. 2025 Cell
604282	C57BL/6J	AiE2121m	AiP1457	pAAV-AiE2121m-minBG-SYFP2-WPRE3-BGHpA	EPI	Astro	SYFP2	RO	Ben-Simon, et al. 2025 Cell
615684	C57BL/6J	AiE2121m	AiP1457	pAAV-AiE2121m-minBG-SYFP2-WPRE3-BGHpA	STPT	Astro	SYFP2	RO	Ben-Simon, et al. 2025 Cell
604282	C57BL/6J	AiE2121m	AiP1457	pAAV-AiE2121m-minBG-SYFP2-WPRE3-BGHpA	EPI	Astro	SYFP2	RO	Ben-Simon, et al. 2025 Cell
615684	C57BL/6J	AiE2121m	AiP1457	pAAV-AiE2121m-minBG-SYFP2-WPRE3-BGHpA	STPT	Astro	SYFP2	RO	Ben-Simon, et al. 2025 Cell
615684	C57BL/6J	AiE2121m	AiP1457	pAAV-AiE2121m-minBG-SYFP2-WPRE3-BGHpA	STPT	Astro	SYFP2	RO	Ben-Simon, et al. 2025 Cell
637139	C57BL/6J	AiE2122m	AiP1351	pAAV-AiE2122m-minBG-SYFP2-WPRE3-BGHpA	EPI, IHC	Astro	SYFP2	RO	Mich et al., 2025 bioRxiv
706183	C57BL/6J	AiE2122m	AiP1351	pAAV-AiE2122m-minBG-SYFP2-WPRE3-BGHpA	EPI	Astro	SYFP2	RO	Ben-Simon, et al. 2025 Cell
622135	C57BL/6J	AiE2122m	AiP1351	pAAV-AiE2122m-minBG-SYFP2-WPRE3-BGHpA	STPT	Astro	SYFP2	RO	Ben-Simon, et al. 2025 Cell
622135	C57BL/6J	AiE2122m	AiP1351	pAAV-AiE2122m-minBG-SYFP2-WPRE3-BGHpA	STPT	Astro	SYFP2	RO	Ben-Simon, et al. 2025 Cell
706183	C57BL/6J	AiE2122m	AiP1351	pAAV-AiE2122m-minBG-SYFP2-WPRE3-BGHpA	EPI	Astro	SYFP2	RO	Ben-Simon, et al. 2025 Cell
706183	C57BL/6J	AiE2122m	AiP1351	pAAV-AiE2122m-minBG-SYFP2-WPRE3-BGHpA	EPI	Astro	SYFP2	RO	Ben-Simon, et al. 2025 Cell
609040	C57BL/6J	AiE2122m	AiP1351	pAAV-AiE2122m-minBG-SYFP2-WPRE3-BGHpA	EPI	Astro	SYFP2	RO	Ben-Simon, et al. 2025 Cell
622135	C57BL/6J	AiE2122m	AiP1351	pAAV-AiE2122m-minBG-SYFP2-WPRE3-BGHpA	STPT	Astro	SYFP2	RO	Ben-Simon, et al. 2025 Cell
609040	C57BL/6J	AiE2122m	AiP1351	pAAV-AiE2122m-minBG-SYFP2-WPRE3-BGHpA	EPI	Astro	SYFP2	RO	Ben-Simon, et al. 2025 Cell
622135	C57BL/6J	AiE2122m	AiP1351	pAAV-AiE2122m-minBG-SYFP2-WPRE3-BGHpA	STPT	Astro	SYFP2	RO	Ben-Simon, et al. 2025 Cell
613555	C57BL/6J	AiE2123m	AiP1422	pAAV-AiE2123m-minBG-SYFP2-WPRE3-BGHpA	STPT	Astro	SYFP2	RO	Ben-Simon, et al. 2025 Cell
613555	C57BL/6J	AiE2123m	AiP1422	pAAV-AiE2123m-minBG-SYFP2-WPRE3-BGHpA	STPT	Astro	SYFP2	RO	Ben-Simon, et al. 2025 Cell
613555	C57BL/6J	AiE2123m	AiP1422	pAAV-AiE2123m-minBG-SYFP2-WPRE3-BGHpA	STPT	Astro	SYFP2	RO	Ben-Simon, et al. 2025 Cell
600471	C57BL/6J	AiE2123m	AiP1422	pAAV-AiE2123m-minBG-SYFP2-WPRE3-BGHpA	EPI	Astro	SYFP2	RO	Ben-Simon, et al. 2025 Cell
600471	C57BL/6J	AiE2123m	AiP1422	pAAV-AiE2123m-minBG-SYFP2-WPRE3-BGHpA	EPI	Astro	SYFP2	RO	Ben-Simon, et al. 2025 Cell
600471	C57BL/6J	AiE2123m	AiP1422	pAAV-AiE2123m-minBG-SYFP2-WPRE3-BGHpA	EPI	Astro	SYFP2	RO	Ben-Simon, et al. 2025 Cell
600471	C57BL/6J	AiE2123m	AiP1422	pAAV-AiE2123m-minBG-SYFP2-WPRE3-BGHpA	EPI	Astro	SYFP2	RO	Ben-Simon, et al. 2025 Cell
600471	C57BL/6J	AiE2123m	AiP1422	pAAV-AiE2123m-minBG-SYFP2-WPRE3-BGHpA	EPI	Astro	SYFP2	RO	Ben-Simon, et al. 2025 Cell
600471	C57BL/6J	AiE2123m	AiP1422	pAAV-AiE2123m-minBG-SYFP2-WPRE3-BGHpA	EPI	Astro	SYFP2	RO	Ben-Simon, et al. 2025 Cell
613555	C57BL/6J	AiE2123m	AiP1422	pAAV-AiE2123m-minBG-SYFP2-WPRE3-BGHpA	STPT	Astro	SYFP2	RO	Ben-Simon, et al. 2025 Cell
600471	C57BL/6J	AiE2123m	AiP1422	pAAV-AiE2123m-minBG-SYFP2-WPRE3-BGHpA	EPI	Astro	SYFP2	RO	Ben-Simon, et al. 2025 Cell
600471	C57BL/6J	AiE2123m	AiP1422	pAAV-AiE2123m-minBG-SYFP2-WPRE3-BGHpA	EPI	Astro	SYFP2	RO	Ben-Simon, et al. 2025 Cell
613555	C57BL/6J	AiE2123m	AiP1422	pAAV-AiE2123m-minBG-SYFP2-WPRE3-BGHpA	STPT	Astro	SYFP2	RO	Ben-Simon, et al. 2025 Cell
600471	C57BL/6J	AiE2123m	AiP1422	pAAV-AiE2123m-minBG-SYFP2-WPRE3-BGHpA	EPI	Astro	SYFP2	RO	Ben-Simon, et al. 2025 Cell
613555	C57BL/6J	AiE2123m	AiP1422	pAAV-AiE2123m-minBG-SYFP2-WPRE3-BGHpA	STPT	Astro	SYFP2	RO	Ben-Simon, et al. 2025 Cell
613555	C57BL/6J	AiE2123m	AiP1422	pAAV-AiE2123m-minBG-SYFP2-WPRE3-BGHpA	STPT	Astro	SYFP2	RO	Ben-Simon, et al. 2025 Cell
600471	C57BL/6J	AiE2123m	AiP1422	pAAV-AiE2123m-minBG-SYFP2-WPRE3-BGHpA	EPI	Astro	SYFP2	RO	Ben-Simon, et al. 2025 Cell

613555	C57BL/6J	AiE2123m	AiP1422	pAAV-AiE2123m-minBG-SYFP2-WPRE3-BGHpA	STPT	Astro	SYFP2	RO	Ben-Simon, et al. 2025 Cell
613555	C57BL/6J	AiE2123m	AiP1422	pAAV-AiE2123m-minBG-SYFP2-WPRE3-BGHpA	STPT	Astro	SYFP2	RO	Ben-Simon, et al. 2025 Cell
613555	C57BL/6J	AiE2123m	AiP1422	pAAV-AiE2123m-minBG-SYFP2-WPRE3-BGHpA	STPT	Astro	SYFP2	RO	Ben-Simon, et al. 2025 Cell
600471	C57BL/6J	AiE2123m	AiP1422	pAAV-AiE2123m-minBG-SYFP2-WPRE3-BGHpA	EPI	Astro	SYFP2	RO	Ben-Simon, et al. 2025 Cell
613555	C57BL/6J	AiE2123m	AiP1422	pAAV-AiE2123m-minBG-SYFP2-WPRE3-BGHpA	STPT	Astro	SYFP2	RO	Ben-Simon, et al. 2025 Cell
651228	C57BL/6J	AiE2160m	AiP1389	pAAV-AiE2160m-minBG-SYFP2-WPRE3-BGHpA	scRNA-seq	Astro	SYFP2	RO	Mich et al., 2025 bioRxiv
651229	C57BL/6J	AiE2160m	AiP1389	pAAV-AiE2160m-minBG-SYFP2-WPRE3-BGHpA	scRNA-seq	Astro	SYFP2	RO	Mich et al., 2025 bioRxiv
622138	C57BL/6J	AiE2160m	AiP1389	pAAV-AiE2160m-minBG-SYFP2-WPRE3-BGHpA	STPT	Astro	SYFP2	RO	Ben-Simon, et al. 2025 Cell
671882	C57BL/6J	AiE2160m	AiP1389	pAAV-AiE2160m-minBG-SYFP2-WPRE3-BGHpA	STPT	Astro	SYFP2	ICV	Ben-Simon, et al. 2025 Cell
606960	C57BL/6J	AiE2160m	AiP1389	pAAV-AiE2160m-minBG-SYFP2-WPRE3-BGHpA	EPI	Astro	SYFP2	RO	Ben-Simon, et al. 2025 Cell
622138	C57BL/6J	AiE2160m	AiP1389	pAAV-AiE2160m-minBG-SYFP2-WPRE3-BGHpA	STPT	Astro	SYFP2	RO	Ben-Simon, et al. 2025 Cell
606960	C57BL/6J	AiE2160m	AiP1389	pAAV-AiE2160m-minBG-SYFP2-WPRE3-BGHpA	EPI	Astro	SYFP2	RO	Ben-Simon, et al. 2025 Cell
622138	C57BL/6J	AiE2160m	AiP1389	pAAV-AiE2160m-minBG-SYFP2-WPRE3-BGHpA	STPT	Astro	SYFP2	RO	Ben-Simon, et al. 2025 Cell
606960	C57BL/6J	AiE2160m	AiP1389	pAAV-AiE2160m-minBG-SYFP2-WPRE3-BGHpA	EPI	Astro	SYFP2	RO	Ben-Simon, et al. 2025 Cell
629461	C57BL/6J	gfaABC1D	AiP13972	pAAV-GfaABC1D-SYFP2-P2A-3XFLAG-10aa-H2B*-WPRE	EPI, IHC	Astro	SYFP2	RO	Lee et al., 2008 Glia
627900	C57BL/6J	gfaABC1D	AiP13972	pAAV-GfaABC1D-SYFP2-P2A-3XFLAG-10aa-H2B*-WPRE	EPI	Astro	SYFP2	RO	Lee et al., 2008 Glia
636676	C57BL/6J	gfaABC1D	AiP13972	pAAV-GfaABC1D-SYFP2-P2A-3XFLAG-10aa-H2B*-WPRE	EPI, IHC	Astro	SYFP2	RO	Lee et al., 2008 Glia
745308	C57BL/6J	gfaABC1D	AiP13972	pAAV-GfaABC1D-SYFP2-P2A-3XFLAG-10aa-H2B*-WPRE	EPI, IHC	Astro	SYFP2	RO	Lee et al., 2008 Glia
745314	C57BL/6J	gfaABC1D	AiP13972	pAAV-GfaABC1D-SYFP2-P2A-3XFLAG-10aa-H2B*-WPRE	EPI, IHC	Astro	SYFP2	RO	Lee et al., 2008 Glia
630479	C57BL/6J	gfaABC1D	AiP13972	pAAV-GfaABC1D-SYFP2-P2A-3XFLAG-10aa-H2B*-WPRE	scRNA-seq	Astro	SYFP2	RO	Lee et al., 2008 Glia
651226	C57BL/6J	gfaABC1D	AiP13972	pAAV-GfaABC1D-SYFP2-P2A-3XFLAG-10aa-H2B*-WPRE	scRNA-seq	Astro	SYFP2	RO	Lee et al., 2008 Glia
637364	Scn1a +/-	gfaABC1D	AiP13972	pAAV-GfaABC1D-SYFP2-P2A-3XFLAG-10aa-H2B*-WPRE	EPI, IHC	Astro	SYFP2	RO	Lee et al., 2008 Glia
643123	Scn1a +/-	gfaABC1D	AiP13972	pAAV-GfaABC1D-SYFP2-P2A-3XFLAG-10aa-H2B*-WPRE	EPI, IHC	Astro	SYFP2	RO	Lee et al., 2008 Glia
637366	Scn1a +/+	gfaABC1D	AiP13972	pAAV-GfaABC1D-SYFP2-P2A-3XFLAG-10aa-H2B*-WPRE	EPI, IHC	Astro	SYFP2	RO	Lee et al., 2008 Glia
643124	Scn1a +/+	gfaABC1D	AiP13972	pAAV-GfaABC1D-SYFP2-P2A-3XFLAG-10aa-H2B*-WPRE	EPI, IHC	Astro	SYFP2	RO	Lee et al., 2008 Glia
637138	C57BL/6J	MBP promoter	AiP14084	pAAV-mMbp_promoter-SYFP2-P2A-3XFLAG-10aa-H2B*-	EPI, IHC	Oligo	SYFP2	RO	Gow et al., 1992 J. C. B.
642134	C57BL/6J	MBP promoter	AiP14084	pAAV-mMbp_promoter-SYFP2-P2A-3XFLAG-10aa-H2B*-	EPI, IHC	Oligo	SYFP2	RO	Gow et al., 1992 J. C. B.
644029	C57BL/6J	MBP promoter	AiP14084	pAAV-mMbp_promoter-SYFP2-P2A-3XFLAG-10aa-H2B*-	EPI, IHC	Oligo	SYFP2	RO	Gow et al., 1992 J. C. B.
638254	C57BL/6J	MBP promoter	AiP14084	pAAV-mMbp_promoter-SYFP2-P2A-3XFLAG-10aa-H2B*-	scRNA-seq	Oligo	SYFP2	RO	Gow et al., 1992 J. C. B.
651227	C57BL/6J	MBP promoter	AiP14084	pAAV-mMbp_promoter-SYFP2-P2A-3XFLAG-10aa-H2B*-	scRNA-seq	Oligo	SYFP2	RO	Gow et al., 1992 J. C. B.
622080	C57BL/6J	proB12	AiP12214	pAAV-ProB12-SYFP2-WPRE3-BGHpA	EPI, IHC	Astro	SYFP2	RO	Juttner et al., 2019 Nature Neuroscienc
625963	C57BL/6J	proB12	AiP12214	pAAV-ProB12-SYFP2-WPRE3-BGHpA	EPI, IHC	Astro	SYFP2	RO	Juttner et al., 2019 Nature Neuroscienc
636675	C57BL/6J	proB12	AiP12214	pAAV-ProB12-SYFP2-WPRE3-BGHpA	EPI, IHC	Astro	SYFP2	RO	Juttner et al., 2019 Nature Neuroscienc
616739	C57BL/6J	ProB12	AiP12214	pAAV-ProB12-SYFP2-WPRE3-BGHpA	scRNA-seq	Astro	SYFP2	RO	Juttner et al., 2019 Nature Neuroscienc

Table S2: List of mice used for characterizing the activity of astrocyte and oligodendrocyte-specific enhancer-AAV reporter vectors.

"Mouse ID" is a unique six-digit identifier for each mouse. "Genotype" describes the genotype. "Enhancer ID" is a unique label for each enhancer or promoter element tested (grouped by colors). "Vector ID" is a unique label for the enhancer-AAV DNA packaged into PHP.eB for testing. "Vector Full Name" is a descriptive name of the elements in each enhancer-AAV. "Data Modality" refers to the data collected from each mouse: EPI epifluorescence, IHC immunohistochemistry, STPT serial two-photon tomography, scRNA-seq single cell RNA-seq (SMARTerV4). "Targeted Cell Population" is Astrocytes or Oligodendrocytes. "Fluor" is SYFP2 or iCre(R297T) used to recombine tdTomato in Ai14 mouse line. "Delivery Method" is retro-orbital (RO) or intracerebroventricular (ICV). "Publication" refers to this work (Mich et al.), or if the mice were also reported on in a previous work (Ben-Simon et al.[35]), or whether the enhancer or promoter was previously described and used here as a positive control (Lee et al.[57], Gow et al.[59], Jüttner et al.[41]).

References

1. Khakh, B. S. & Sofroniew, M. V. Diversity of astrocyte functions and phenotypes in neural circuits. *Nat. Neurosci.* **18**, 942–952 (2015).
2. Zuchero, J. B. & Barres, B. A. Glia in mammalian development and disease. *Dev. Camb. Engl.* **142**, 3805–3809 (2015).
3. Volkenhoff, A. *et al.* Glial Glycolysis Is Essential for Neuronal Survival in Drosophila. *Cell Metab.* **22**, 437–447 (2015).
4. García-Cáceres, C. *et al.* Astrocytic Insulin Signaling Couples Brain Glucose Uptake with Nutrient Availability. *Cell* **166**, 867–880 (2016).
5. Molofsky, A. V. *et al.* Astrocyte-encoded positional cues maintain sensorimotor circuit integrity. *Nature* **509**, 189–194 (2014).
6. Lioy, D. T. *et al.* A role for glia in the progression of Rett's syndrome. *Nature* **475**, 497–500 (2011).
7. Wang, X. *et al.* Astrocytic Ca2+ signaling evoked by sensory stimulation in vivo. *Nat. Neurosci.* **9**, 816–823 (2006).
8. Sabelström, H. *et al.* Resident Neural Stem Cells Restrict Tissue Damage and Neuronal Loss After Spinal Cord Injury in Mice. *Science* **342**, 637–640 (2013).
9. Liddelow, S. A. *et al.* Neurotoxic reactive astrocytes are induced by activated microglia. *Nature* **541**, 481–487 (2017).
10. Hasel, P., Rose, I. V. L., Sadick, J. S., Kim, R. D. & Liddelow, S. A. Neuroinflammatory astrocyte subtypes in the mouse brain. *Nat. Neurosci.* **24**, 1475–1487 (2021).
11. Zuchero, J. B. *et al.* CNS Myelin Wrapping Is Driven by Actin Disassembly. *Dev. Cell* **34**, 152–167 (2015).
12. Steadman, P. E. *et al.* Disruption of Oligodendrogenesis Impairs Memory Consolidation in Adult Mice. *Neuron* **105**, 150-164.e6 (2020).
13. Wilkins, A., Majed, H., Layfield, R., Compston, A. & Chandran, S. Oligodendrocytes Promote Neuronal Survival and Axonal Length by Distinct Intracellular Mechanisms: A Novel Role for Oligodendrocyte-Derived Glial Cell Line-Derived Neurotrophic Factor. *J. Neurosci.* **23**, 4967–4974 (2003).
14. Knowles, J. K. *et al.* Maladaptive myelination promotes generalized epilepsy progression. *Nat. Neurosci.* **25**, 596–606 (2022).
15. Zhang, P. *et al.* Senolytic therapy alleviates Aβ-associated oligodendrocyte progenitor cell senescence and cognitive deficits in an Alzheimer's disease model. *Nat. Neurosci.* 1 (2019) doi:10.1038/s41593-019-0372-9.
16. Boisvert, M. M., Erikson, G. A., Shokhirev, M. N. & Allen, N. J. The Aging Astrocyte Transcriptome from Multiple Regions of the Mouse Brain. *Cell Rep.* **22**, 269–285 (2018).
17. Endo, F. *et al.* Molecular basis of astrocyte diversity and morphology across the CNS in health and disease. *Science* **378**, eadc9020 (2022).
18. Yao, Z. *et al.* A high-resolution transcriptomic and spatial atlas of cell types in the whole mouse brain. 2023.03.06.531121 Preprint at https://doi.org/10.1101/2023.03.06.531121 (2023).
19. Hodge, R. D. *et al.* Conserved cell types with divergent features in human versus mouse cortex. *Nature* **573**, 61–68 (2019).
20. Chen, Z.-P. *et al.* Lipid-accumulated reactive astrocytes promote disease progression in epilepsy. *Nat. Neurosci.* **26**, 542–554 (2023).

21. Wang, C. *et al.* Selective removal of astrocytic APOE4 strongly protects against tau-mediated neurodegeneration and decreases synaptic phagocytosis by microglia. *Neuron* (2021) doi:10.1016/j.neuron.2021.03.024.
22. Monje, M. *et al.* Hedgehog-responsive candidate cell of origin for diffuse intrinsic pontine glioma. *Proc. Natl. Acad. Sci. U. S. A.* **108**, 4453–4458 (2011).
23. Alcantara Llaguno, S. *et al.* Malignant Astrocytomas Originate from Neural Stem/Progenitor Cells in a Somatic Tumor Suppressor Mouse Model. *Cancer Cell* **15**, 45–56 (2009).
24. Deverman, B. E. *et al.* Cre-dependent selection yields AAV variants for widespread gene transfer to the adult brain. *Nat. Biotechnol.* **34**, 204–209 (2016).
25. Chan, K. Y. *et al.* Engineered AAVs for efficient noninvasive gene delivery to the central and peripheral nervous systems. *Nat. Neurosci.* **20**, 1172–1179 (2017).
26. Nonnenmacher, M. *et al.* Rapid evolution of blood-brain-barrier-penetrating AAV capsids by RNA-driven biopanning. *Mol. Ther. - Methods Clin. Dev.* **20**, 366–378 (2021).
27. De, A., El-Shamayleh, Y. & Horwitz, G. D. Fast and reversible neural inactivation in macaque cortex by optogenetic stimulation of GABAergic neurons. *eLife* **9**, e52658 (2020).
28. El-Shamayleh, Y., Kojima, Y., Soetedjo, R. & Horwitz, G. D. Selective Optogenetic Control of Purkinje Cells in Monkey Cerebellum. *Neuron* **95**, 51-62.e4 (2017).
29. Mendell, J. R. *et al.* Single-Dose Gene-Replacement Therapy for Spinal Muscular Atrophy. *http://dx.doi.org/10.1056/NEJMoa1706198* https://www.nejm.org/doi/10.1056/NEJMoa1706198?url_ver=Z39.88-2003&rfr_id=ori%3Arid%3Acrossref.org&rfr_dat=cr_pub%3Dwww.ncbi.nlm.nih.gov (2017) doi:10.1056/NEJMoa1706198.
30. Dimidschstein, J. *et al.* A viral strategy for targeting and manipulating interneurons across vertebrate species. *Nat. Neurosci.* **19**, 1743–1749 (2016).
31. Vormstein-Schneider, D. *et al.* Viral manipulation of functionally distinct interneurons in mice, non-human primates and humans. *Nat. Neurosci.* 1–8 (2020) doi:10.1038/s41593-020-0692-9.
32. Hrvatin, S. *et al.* A scalable platform for the development of cell-type-specific viral drivers. *eLife* **8**, e48089 (2019).
33. Mich, J. K. *et al.* Functional enhancer elements drive subclass-selective expression from mouse to primate neocortex. *Cell Rep.* **34**, 108754 (2021).
34. Graybuck, L. T. *et al.* Enhancer viruses for combinatorial cell-subclass-specific labeling. *Neuron* **109**, 1449-1464.e13 (2021).
35. Ben-Simon, Y. *et al.* A suite of enhancer AAVs and transgenic mouse lines for genetic access to cortical cell types. *Cell* (2025) doi:10.1016/j.cell.2025.05.002.
36. Johansen, N. J. *et al.* Evaluating methods for the prediction of cell-type-specific enhancers in the mammalian cortex. *Cell Genomics* 100879 (2025) doi:10.1016/j.xgen.2025.100879.
37. Kussick, E. *et al.* Enhancer AAVs for targeting spinal motor neurons and descending motor pathways in rodents and macaque. *Cell Rep.* 115730 (2025) doi:10.1016/j.celrep.2025.115730.
38. Hunker, A. C. *et al.* Enhancer AAV toolbox for accessing and perturbing striatal cell types and circuits. *Neuron* **113**, 1507-1524.e17 (2025).
39. Furlanis, E. *et al.* An enhancer-AAV toolbox to target and manipulate distinct interneuron subtypes. *Neuron* **113**, 1525-1547.e15 (2025).

1307 40. Li, L. *et al.* Identification and application of cell-type-specific enhancers for the macaque
1308 brain. *Cell* **0**, (2025).
1309 41. Jüttner, J. *et al.* Targeting neuronal and glial cell types with synthetic promoter AAVs in
1310 mice, non-human primates and humans. *Nat. Neurosci.* **22**, 1345–1356 (2019).
1311 42. Lin, C.-H. *et al.* Identification of cis-regulatory modules for adeno-associated virus-
1312 based cell-type-specific targeting in the retina and brain. *J. Biol. Chem.* **298**, (2022).
1313 43. Gleichman, A. J., Kawaguchi, R., Sofroniew, M. V. & Carmichael, S. T. A toolbox of
1314 astrocyte-specific, serotype-independent adeno-associated viral vectors using microRNA
1315 targeting sequences. *Nat. Commun.* **14**, 7426 (2023).
1316 44. Wang, L.-L. *et al.* Revisiting astrocyte to neuron conversion with lineage tracing in vivo.
1317 *Cell* **184**, 5465-5481.e16 (2021).
1318 45. Xie, Y., Zhou, J. & Chen, B. Critical examination of Ptbp1-mediated glia-to-neuron
1319 conversion in the mouse retina. *Cell Rep.* **39**, 110960 (2022).
1320 46. Le, N., Appel, H., Pannullo, N., Hoang, T. & Blackshaw, S. Ectopic insert-dependent
1321 neuronal expression of GFAP promoter-driven AAV constructs in adult mouse retina. *Front.*
1322 *Cell Dev. Biol.* **10**, (2022).
1323 47. Borden, P. M. *et al.* A fast genetically encoded fluorescent sensor for faithful in vivo
1324 acetylcholine detection in mice, fish, worms and flies. 2020.02.07.939504 Preprint at
1325 https://doi.org/10.1101/2020.02.07.939504 (2020).
1326 48. Fröhlich, D. *et al.* Dual-function AAV gene therapy reverses late-stage Canavan disease
1327 pathology in mice. *Front. Mol. Neurosci.* **15**, 1061257 (2022).
1328 49. Hillen, A. E. J. *et al.* In vivo targeting of a variant causing vanishing white matter using
1329 CRISPR/Cas9. *Mol. Ther. - Methods Clin. Dev.* **25**, 17–25 (2022).
1330 50. Hagemann, T. L. *et al.* Antisense therapy in a rat model of Alexander disease reverses
1331 GFAP pathology, white matter deficits, and motor impairment. *Sci. Transl. Med.* **13**, eabg4711
1332 (2021).
1333 51. Lister, R. *et al.* Global Epigenomic Reconfiguration During Mammalian Brain
1334 Development. *Science* **341**, 1237905 (2013).
1335 52. Luo, C. *et al.* Single-cell methylomes identify neuronal subtypes and regulatory
1336 elements in mammalian cortex. *Science* **357**, 600–604 (2017).
1337 53. Lee, D.-S. *et al.* Simultaneous profiling of 3D genome structure and DNA methylation in
1338 single human cells. *Nat. Methods* **16**, 999–1006 (2019).
1339 54. Liu, H. *et al.* DNA methylation atlas of the mouse brain at single-cell resolution. *Nature*
1340 **598**, 120–128 (2021).
1341 55. Fullard, J. F. *et al.* Open chromatin profiling of human postmortem brain infers functional
1342 roles for non-coding schizophrenia loci. *Hum. Mol. Genet.* (2019) doi:10.1093/hmg/ddy229.
1343 56. Li, Y. E. *et al.* An atlas of gene regulatory elements in adult mouse cerebrum. *Nature*
1344 **598**, 129–136 (2021).
1345 57. Lee, Y., Messing, A., Su, M. & Brenner, M. GFAP promoter elements required for
1346 region-specific and astrocyte-specific expression. *Glia* **56**, 481–493 (2008).
1347 58. Sun, W. *et al.* SOX9 Is an Astrocyte-Specific Nuclear Marker in the Adult Brain Outside
1348 the Neurogenic Regions. *J. Neurosci.* **37**, 4493–4507 (2017).
1349 59. Gow, A., Friedrich, V. L., Jr & Lazzarini, R. A. Myelin basic protein gene contains
1350 separate enhancers for oligodendrocyte and Schwann cell expression. *J. Cell Biol.* **119**, 605–
1351 616 (1992).

1352 60. Bin, J. M., Harris, S. N. & Kennedy, T. E. The oligodendrocyte-specific antibody 'CC1'
1353 binds Quaking 7. *J. Neurochem.* **139**, 181–186 (2016).
1354 61. Bailey, T. L. *et al.* MEME Suite: tools for motif discovery and searching. *Nucleic Acids*
1355 *Res.* **37**, W202–W208 (2009).
1356 62. Hume, M. A., Barrera, L. A., Gisselbrecht, S. S. & Bulyk, M. L. UniPROBE, update
1357 2015: new tools and content for the online database of protein-binding microarray data on
1358 protein–DNA interactions. *Nucleic Acids Res.* **43**, D117–D122 (2015).
1359 63. Kulakovskiy, I. V. *et al.* HOCOMOCO: towards a complete collection of transcription
1360 factor binding models for human and mouse via large-scale ChIP-Seq analysis. *Nucleic Acids*
1361 *Res.* **46**, D252–D259 (2018).
1362 64. Castro-Mondragon, J. A. *et al.* JASPAR 2022: the 9th release of the open-access
1363 database of transcription factor binding profiles. *Nucleic Acids Res.* **50**, D165 (2022).
1364 65. Furushima, K., Murata, T., Kiyonari, H. & Aizawa, S. Characterization of Opr deficiency
1365 in mouse brain: Subtle defects in dorsomedial telencephalon and medioventral forebrain. *Dev.*
1366 *Dyn.* **232**, 1056–1061 (2005).
1367 66. Inoue, T., Ota, M., Ogawa, M., Mikoshiba, K. & Aruga, J. Zic1 and Zic3 Regulate Medial
1368 Forebrain Development through Expansion of Neuronal Progenitors. *J. Neurosci.* **27**, 5461–
1369 5473 (2007).
1370 67. Hornig, J. *et al.* The Transcription Factors Sox10 and Myrf Define an Essential
1371 Regulatory Network Module in Differentiating Oligodendrocytes. *PLOS Genet.* **9**, e1003907
1372 (2013).
1373 68. Turnescu, T. *et al.* Sox8 and Sox10 jointly maintain myelin gene expression in
1374 oligodendrocytes. *Glia* **66**, 279–294 (2018).
1375 69. Hinderer, C. *et al.* Severe Toxicity in Nonhuman Primates and Piglets Following High-
1376 Dose Intravenous Administration of an Adeno-Associated Virus Vector Expressing Human
1377 SMN. *Hum. Gene Ther.* **29**, 285–298 (2018).
1378 70. Zhang, K. *et al. A Cell Atlas of Chromatin Accessibility across 25 Adult Human Tissues*.
1379 2021.02.17.431699 https://www.biorxiv.org/content/10.1101/2021.02.17.431699v1 (2021)
1380 doi:10.1101/2021.02.17.431699.
1381 71. Goertsen, D. *et al.* AAV capsid variants with brain-wide transgene expression and
1382 decreased liver targeting after intravenous delivery in mouse and marmoset. *Nat. Neurosci.* **25**,
1383 106–115 (2022).
1384 72. Martín-Suárez, S., Abiega, O., Ricobaraza, A., Hernandez-Alcoceba, R. & Encinas, J.
1385 M. Alterations of the Hippocampal Neurogenic Niche in a Mouse Model of Dravet Syndrome.
1386 *Front. Cell Dev. Biol.* **8**, (2020).
1387 73. Madisen, L. *et al.* A robust and high-throughput Cre reporting and characterization
1388 system for the whole mouse brain. *Nat. Neurosci.* **13**, 133–140 (2010).
1389 74. Hartung, M. & Kisters-Woike, B. Cre Mutants with Altered DNA Binding Properties*. *J.*
1390 *Biol. Chem.* **273**, 22884–22891 (1998).
1391 75. Wang, S. *et al.* The Endothelial-Specific MicroRNA miR-126 Governs Vascular Integrity
1392 and Angiogenesis. *Dev. Cell* **15**, 261–271 (2008).
1393 76. Sayeg, M. K. *et al.* Rationally Designed MicroRNA-Based Genetic Classifiers Target
1394 Specific Neurons in the Brain. *ACS Synth. Biol.* **4**, 788–795 (2015).
1395 77. Cho, F. S. *et al.* Enhancing GAT-3 in thalamic astrocytes promotes resilience to brain
1396 injury in rodents. *Sci. Transl. Med.* **14**, eabj4310 (2022).

78. Hasel, P., Aisenberg, W. H., Bennett, F. C. & Liddelow, S. A. Molecular and metabolic heterogeneity of astrocytes and microglia. *Cell Metab.* **35**, 555–570 (2023).
79. Aida, T. *et al.* Astroglial glutamate transporter deficiency increases synaptic excitability and leads to pathological repetitive behaviors in mice. *Neuropsychopharmacol. Off. Publ. Am. Coll. Neuropsychopharmacol.* **40**, 1569–1579 (2015).
80. Li, Z. *et al.* Cell-Type-Specific Afferent Innervation of the Nucleus Accumbens Core and Shell. *Front. Neuroanat.* **12**, (2018).
81. Beier, K. T. *et al.* Circuit Architecture of VTA Dopamine Neurons Revealed by Systematic Input-Output Mapping. *Cell* **162**, 622–634 (2015).
82. Ren, J. *et al.* Anatomically Defined and Functionally Distinct Dorsal Raphe Serotonin Sub-systems. *Cell* **175**, 472-487.e20 (2018).
83. Ren, J. *et al.* Single-cell transcriptomes and whole-brain projections of serotonin neurons in the mouse dorsal and median raphe nuclei. *eLife* **8**, e49424 (2019).
84. Gabitto, M. I. *et al.* Integrated multimodal cell atlas of Alzheimer's disease. 2023.05.08.539485 Preprint at https://doi.org/10.1101/2023.05.08.539485 (2023).
85. Kamath, T. *et al.* Single-cell genomic profiling of human dopamine neurons identifies a population that selectively degenerates in Parkinson's disease. *Nat. Neurosci.* **25**, 588–595 (2022).
86. Pagès, Hervé. BSgenome: Software infrastructure for efficient representation of full genomes and their SNPs. R package version 1.62.0. (2021).
87. Kim, J.-Y., Grunke, S. D., Levites, Y., Golde, T. E. & Jankowsky, J. L. Intracerebroventricular Viral Injection of the Neonatal Mouse Brain for Persistent and Widespread Neuronal Transduction. *JoVE J. Vis. Exp.* e51863 (2014) doi:10.3791/51863.
88. Ragan, T. *et al.* Serial two-photon tomography for automated ex vivo mouse brain imaging. *Nat. Methods* **9**, 255–258 (2012).
89. Tasic, B. *et al.* Shared and distinct transcriptomic cell types across neocortical areas. *Nature* **563**, 72 (2018).
90. Traag, V. A., Waltman, L. & van Eck, N. J. From Louvain to Leiden: guaranteeing well-connected communities. *Sci. Rep.* **9**, 5233 (2019).
91. Choi, J.-H. *et al.* Optimization of AAV expression cassettes to improve packaging capacity and transgene expression in neurons. *Mol. Brain* **7**, 17 (2014).
92. Bari, B. A. *et al.* Stable Representations of Decision Variables for Flexible Behavior. *Neuron* **103**, 922-933.e7 (2019).
93. Akam, T. & Walton, M. E. pyPhotometry: Open source Python based hardware and software for fiber photometry data acquisition. *Sci. Rep.* **9**, 3521 (2019).
94. Fullard, J. F. *et al.* An atlas of chromatin accessibility in the adult human brain. *Genome Res.* **28**, 1243–1252 (2018).